NBS TECHNICAL NOTE 1075

U.S. DEPARTMENT OF COMMERCE / National Bureau of Standards

Electromagnetic-Acoustic-Transducer/Synthetic-Aperture System for Thick-Weld Inspection

NATIONAL BUREAU OF STANDARDS

The National Bureau of Standards[1] was established by an act of Congress on March 3, 1901. The Bureau's overall goal is to strengthen and advance the Nation's science and technology and facilitate their effective application for public benefit. To this end, the Bureau conducts research and provides: (1) a basis for the Nation's physical measurement system, (2) scientific and technological services for industry and government, (3) a technical basis for equity in trade, and (4) technical services to promote public safety. The Bureau's technical work is performed by the National Measurement Laboratory, the National Engineering Laboratory, and the Institute for Computer Sciences and Technology.

THE NATIONAL MEASUREMENT LABORATORY provides the national system of physical and chemical and materials measurement; coordinates the system with measurement systems of other nations and furnishes essential services leading to accurate and uniform physical and chemical measurement throughout the Nation's scientific community, industry, and commerce; conducts materials research leading to improved methods of measurement, standards, and data on the properties of materials needed by industry, commerce, educational institutions, and Government; provides advisory and research services to other Government agencies; develops, produces, and distributes Standard Reference Materials; and provides calibration services. The Laboratory consists of the following centers:

Absolute Physical Quantities[2] — Radiation Research — Chemical Physics — Analytical Chemistry — Materials Science

THE NATIONAL ENGINEERING LABORATORY provides technology and technical services to the public and private sectors to address national needs and to solve national problems; conducts research in engineering and applied science in support of these efforts; builds and maintains competence in the necessary disciplines required to carry out this research and technical service; develops engineering data and measurement capabilities; provides engineering measurement traceability services; develops test methods and proposes engineering standards and code changes; develops and proposes new engineering practices; and develops and improves mechanisms to transfer results of its research to the ultimate user. The Laboratory consists of the following centers:

Applied Mathematics — Electronics and Electrical Engineering[2] — Manufacturing Engineering — Building Technology — Fire Research — Chemical Engineering[2]

THE INSTITUTE FOR COMPUTER SCIENCES AND TECHNOLOGY conducts research and provides scientific and technical services to aid Federal agencies in the selection, acquisition, application, and use of computer technology to improve effectiveness and economy in Government operations in accordance with Public Law 89-306 (40 U.S.C. 759), relevant Executive Orders, and other directives; carries out this mission by managing the Federal Information Processing Standards Program, developing Federal ADP standards guidelines, and managing Federal participation in ADP voluntary standardization activities; provides scientific and technological advisory services and assistance to Federal agencies; and provides the technical foundation for computer-related policies of the Federal Government. The Institute consists of the following centers:

Programming Science and Technology — Computer Systems Engineering.

[1]Headquarters and Laboratories at Gaithersburg, MD, unless otherwise noted;
mailing address Washington, DC 20234.
[2]Some divisions within the center are located at Boulder, CO 80303.

Electromagnetic-Acoustic-Transducer/ Synthetic-Aperture System for Thick-Weld Inspection

C. M. Fortunko[†]
R. E. Schramm
J. C. Moulder
J. D. McColskey

Fracture and Deformation Division
Center for Materials Science
National Bureau of Standards
U.S. Department of Commerce
Boulder, Colorado 80303

[†]Present address: Aerojet Ordnance, Tustin, California 92680

Funded by:
Ames Laboratory
Energy and Mineral Resources Research Institute
Iowa State University
Ames, Iowa 50011

U.S. DEPARTMENT OF COMMERCE, Malcolm Baldrige, Secretary

NATIONAL BUREAU OF STANDARDS, Ernest Ambler, Director

Issued May 1984

National Bureau of Standards Technical Note 1075
Natl. Bur. Stand. (U.S.), Tech Note 1075, 130 pages (May 1984)
CODEN: NBTNAE

U.S. GOVERNMENT PRINTING OFFICE
WASHINGTON: 1984

For sale by the Superintendent of Documents, U.S. Government Printing Office, Washington, DC 20402

CONTENTS

Appendices		Page

LIST OF FIGURES

LIST OF TABLES

ELECTROMAGNETIC-ACOUSTIC-TRANSDUCER/ SYNTHETIC-APERTURE SYSTEM FOR THICK-WELD INSPECTION

C. M. Fortunko*, R. E. Schramm,
J. C. Moulder, J. D. McColskey
Fracture and Deformation Division
National Bureau of Standards
Boulder, Colorado 80303

ABSTRACT

This report describes a system based on electromagnetic-acoustic transducers (EMATs) as an approach to automated nondestructive evaluation of thick weldments ($\geq$25 mm). Good signal-to-noise ratios, often a problem with EMATs, were possible through careful design of the transducers and associated electronic circuits and the use of signal averaging. At 454 kHz, the transducers produce shear-horizontal waves of approximately 7-mm wavelength in steel. The long wavelength permits determination of through-thickness flaw depth from the amplitudes of scattered ultrasonic waves. A minicomputer controlled transducer positioning and acquired the digitized ultrasonic waveforms for synthetic aperture processing. The synthetic aperture technique further improved signal quality and yielded flaw localization through the weld thickness. Measurements on artificial flaws demonstrated a detectability threshold of 0.5 mm (through thickness) and sizing ability up to 2.5 mm, in agreement with theoretical predictions. Details include the design of the transducers and electronics, as well as the mechanical positioner, signal processing algorithms, and complete computer program listing.

Key words: electromagnetic-acoustic transducer; flaw detection; nondestructive evaluation; S-H waves; synthetic aperture; ultrasonics; weld inspection

*Present Address: Aerojet Ordnance, Tustin, California 92680

Chapter 1

INTRODUCTION

Rapid advances in automated welding and increased demands for reliable weld-quality inspection tools have created a need for new ultrasonic inspection systems. In particular, new systems capable of operation at elevated temperatures and rapid scan rates are in demand in fully and semi-automated welding applications to complement radiographic and conventional ultrasonic inspection techniques. In such applications, radiographic techniques are fundamentally limited because of their inability to detect and dimension most sharp flaws, and possible exposure of fabrication and inspection personnel to potential health hazards. On the other hand, conventional ultrasonic techniques are limited because they tend to be difficult to automate, require fluid couplants that are incompatible with many welding environments, and are often operator-dependent.

This report describes progress on a new weld inspection system currently under development at the National Bureau of Standards for the U.S. Navy. This system traces its origins to earlier ones developed at the Rockwell International Science Center (Fortunko, 1979) and a girth-weld inspection system developed at the National Bureau of Standards (Fortunko and Schramm, 1983). It incorporates many of the features of the earlier systems. For example, all three systems utilize novel, noncontacting ultrasonic transducers that can operate on the surfaces of most weldments. In addition, the new transducers are able to generate and detect special ultrasonic probing signals, shear waves polarized parallel to the surface of a plate (SH-waves). These are easier to interpret than the longitudinal waves and shear waves polarized in the sagittal plane of the plate that are usually generated and detected by conventional piezoelectric transducers. The present inspection system also incorporates recent improvements in electromagnetic-acoustic transducer (EMAT) technology and improved digital signal processing routines that compensate for many hardware-related shortcomings of the earlier systems. It is also more flexible than the earlier systems since it incorporates digitally controlled scanning mechanisms that permit the execution of a wide variety of inspection protocols.

This report contains eight chapters and five appendixes.

Chapter 2 presents an overview of the inspection process concept, including a perspective on other ultrasonic inspection approaches. This chapter enumerates the main benefits of using SH-wave EMATs with emphasis on the special problems of detecting and characterizing weld flaws. Also included in Chapter 2 is a discussion of the benefits and shortcomings of operating in the long wavelength region (with respect to the principal flaw dimensions). Chapter 3 presents an overview of the system with a block-diagram approach to describe all the main functional elements of the system as implemented at the National Bureau of Standards for a feasibility demonstration in laboratory environments. Chapters 2 and 3 familiarize the reader with the four main themes of this report: 1. use of rapidly scanned, non-contacting transducers (EMATs); 2. use of special ultrasonic probing signals (SH-waves); 3. operation in the long-wavelength scattering region; 4. extensive use of digital synthetic aperture and other special signal processing techniques to improve the overall signal-to-noise performance of the new inspection system. Details of these special features of the system are described in detail in the remaining chapters and appendixes forming the main body of the report.

Chapter 4 includes an extensive description of a new SH-wave EMAT element specially developed to increase the longitudinal resolution of the inspection system and reduce the contamination of the ultrasonic signals by unwanted electromagnetic and ultrasonic interferences. In this context, the radiation patterns of the new transducer and details of the calibration procedures are discussed. (The development of a new EMAT was necessary because existing designs could not be adapted to the inspection of thick plate weldments at in the 400-800 kHz range which allows flaw sizing in the range of interest.) It is noted that the new transducer design also incorporates a mechanical face-plate that very effectively protects it from damage by abrasion while causing only a very small loss in efficiency.

Chapter 5 is devoted entirely to EMAT electronics, with special emphasis on the design and optimization of analog subsystems that determine sensitivity. Separate sections describe the principles of operation of a very efficient, high-power amplifier for driving EMAT-like electrical loads and very low-noise preamplifiers needed to establish the low noise-figures, essential to overcome the inherently low transduction efficiencies of EMATs. Examples of several important systems, including detailed circuit diagrams are provided.

The details of the three main signal processing schemes (signal averaging, digital filtering, and synthetic aperture reconstruction) used to acquire and process the ultrasonic signals are treated in Chapter 6. This chapter includes three separate sections, which are devoted to signal averaging, synthetic aperture reconstruction, and overall software summary. The synthetic aperture section emphasizes the use of signal processing in the frequency-domain via the use of digital FFT algorithms. This approach allows for the full use of the dynamic range of a 16-bit minicomputer to avoid spatial sidelobe problems associated with time-quantization errors. A detailed logic diagram illustrates the main steps involved in the gathering and processing of ultrasonic data. Also included are specific examples of unprocessed and processed waveforms.

The details of the mechanical apparatus used to move the EMATs on the surface of the work-piece are given in Chapter 7. This chapter describes a unique way of mounting the transducer package in a flexible gimbal-derived enclosure that allows for conformal tracking of the EMATs on the surface. This feature is particularly important in the inspection of weldments, which are often deformed in the vicinity of welds by the action of residual stresses. Also included is a description of the mechanical scanner that transports the EMATs in a preprogrammed manner while maintaining adequate phase coherence of the many ultrasonic beams used in synthetic aperture reconstruction. Although the particular hardware implementation described in this report is suitable only for laboratory use, the principles are directly applicable to a scaled-up prototype version that would be suitable for further evaluation of the system in a technology demonstration phase.

Chapter 8 is a discussion of the experimental results from a laboratory version of the new SH-wave inspection system used on a calibration specimen containing well characterized model flaws. Chapter 8 describes the calibration specimen and the experimental procedures used to collect the ultrasonic data. Then follows a discussion and analysis of the experimental results summarized in terms of a flaw length vs. flaw depth diagram that is compatible with a fitness-for-purpose approach to weld quality validation. A large number of figures illustrate the principal parametric performance limits (including transverse and longitudinal resolution) of an SH-wave EMAT system operating at 454 kHz. Because suitable calibration specimens containing well characterized interior flaws were unavailable, the discussion is limited to surface flaws. However, the system's performance limitations with respect to interior flaws can now be extrapolated from the surface flaw case on the basis of a wealth of closed-form and finite-element analytical treatments (Datta, 1983).

The report ends with a short summary, Chapter 9, on the highlights of the just completed work and an outline of several ideas for future work. Appendixes provide detailed listings of the software, illustrate a typical operator-system interactive session, give a list of several technical papers that have resulted from the work covered in the present report, and acknowledge those who have helped us along the way.

References

Datta, S. K., 1983, University of Colorado, private communication.

Fortunko, C. M., 1979, Ultrasonic inspection of weldments with frequency scanned SH waves, in: "Proceedings of the IEEE Ultrasonics Symposium,:" B. R. McAvoy, ed., IEEE, New York.

Fortunko, C. M., and Schramm, R. E., 1983, Evaluation of pipeline girth welds using low-frequency horizontally polarized waves, J. NDE, 3:155.

Chapter 2

INSPECTION CONCEPT

Ultrasonic Principles

Nondestructive evaluation techniques are often necessary to verify the integrity of ferritic butt weldments. They must reliably detect longitudinal and transverse planar flaws that exhibit a significant projected depth along the through-thickness direction. As an example, Fig. 2-1 shows two longitudinal flaws of the planar variety (i.e. flaws whose principal length dimensions lie along the welding direction). This figure also illustrates the concept of detecting longitudinal flaws using low-frequency shear waves polarized along the direction parallel to the surfaces of the butt weldment (SH-waves). The two planar flaws in Fig. 2-1 are inadequate penetration (IP) of the weld preparation groove and incomplete (sidewall) fusion (IF) between the weld deposit and the base metal. A transverse flaw (not shown) would be largely normal to the welding direction, i.e., the flaw would be in the plane of Fig. 2-1.

In most cases of practical interest, it is not possible to interrogate the flaw region ultrasonically along a direction that is normal to the surfaces of a butt weldment because the weld crowns (shown in Fig. 2-1) are generally not removed after welding. For this reason, it is usually necessary to inspect the weld deposit and the fusion zone using a transducer located on the surface of the base metal. When SH-waves are used for detection of planar flaws, it is normally advantageous to inspect the region of the weld deposit and fusion zone at a near-grazing angle with respect to the surfaces of a butt weldment, as shown in Fig. 2-1, because, in this mode, the flaw presents the largest obstacle to the illuminating ultrasonic signal.

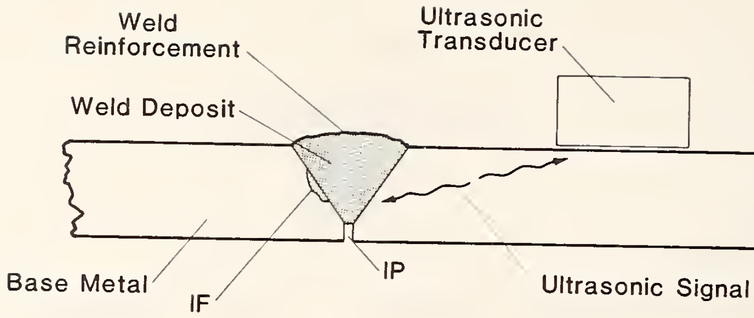

Figure 2-1: SH-wave detection of planar flaws in a weld.

Recent theoretical and experimental investigations have shown that planar flaws and open cracks in butt welds are detectable with low-frequency SH-wave techniques (Fortunko, King, and Tan, 1982, and Fortunko and Schramm, 1982). This technique differs from conventional ultrasonic techniques in three important respects. First, shear waves that are polarized parallel to the surface of a plate weldment (SH-waves) fill the weld region. Second, the probing ultrasonic signals are generated and detected using novel electromagnetic-acoustic transducers (EMATs) that do not require the application of grease or fluid couplants to the surfaces of the inspected part and can operate in adverse environments. Third, the ultrasonic frequency of operation used by the new inspection technique is typically 500 kHz, an order of magnitude lower than the principal frequencies of conventional systems (2.25, 5, and 10 MHz).

Setting the frequency of operation at approximately 500 kHz is highly beneficial when the principal goal of an inspection is the reliable detection of major flaws. At low frequencies, when the ultrasonic wavelength is comparable to or larger than the principal flaw dimensions, the effect of certain flaw parameters on the scattered signal amplitude can be substantially reduced. In particular, if the frequency of operation is sufficiently low, the effects of surface roughness, branching, and departure from planarity are reduced and the amplitude of the scattered ultrasonic signals can be unambiguously related to certain principal flaw dimensions (Budiansky and Rice, 1978; Doyle and Scala, 1978; and Richardson and Elsley, 1979). In addition, at long wavelengths open planar flaws are more detectable than blunt voids of comparable dimensions. This is advantageous from the fitness-for-purpose point of view, which emphasizes the importance of principal flaw dimensions and assumes that sharp flaws are inherently more critical than blunt flaws (Lundin, 1976; Reed, McHenry, and Kasen, 1979; and British Standards Institution, 1980). Another advantage of long wavelengths is a substantial reduction in the need to maintain precise equipment alignments.

Figure 2-2 illustrates the qualitative differences between scattering of ultrasonic waves in the long (low-frequency) and short (high-frequency) wavelength regions. (The flaw is assumed planar and relatively long in the direction of the normal to the plane of the figure.) At high frequencies, Fig. 2-2a, most of the incident ultrasonic energy reflects specularly from the front face of the flaw; i.e., the angle of reflection with respect to the face normal equals the angle of incidence. Also, a significant portion of the incident signal diffracts from the tips of the flaw, which act like ultrasonic line sources. If the surface of the flaw exhibits some roughness, a significant portion of the incident signal can also scatter incoherently (not shown). Furthermore, depending on the orientation of the flaw with respect to the incident signal and the type of ultrasonic signal used (i.e., shear vs. longitudinal), significant mode conversions may occur. As a result, the scattered ultrasonic field at high frequencies is very complicated and difficult to interpret.

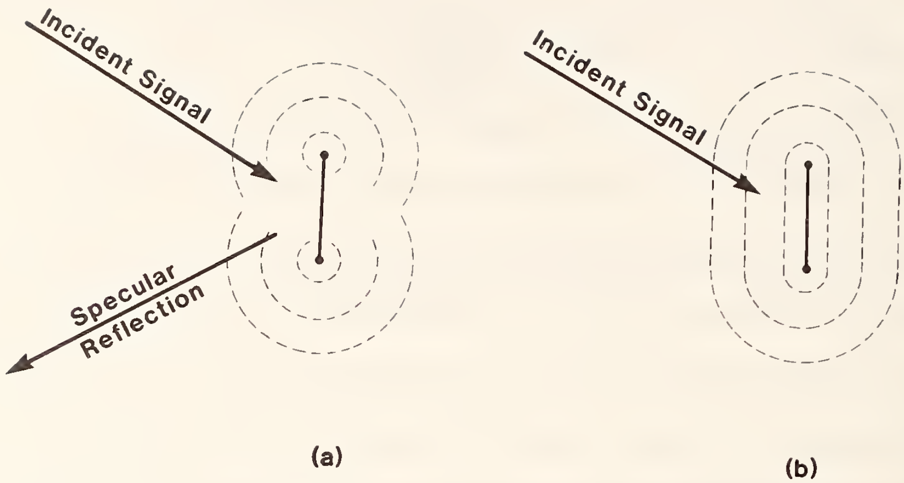

Figure 2-2: Ultrasonic scattering by two-dimensional defects. (a) Short wavelength. (b) Long wavelength.

At low ultrasonic frequencies (Fig. 2-2b), in the long wavelength scattering region, the scattered ultrasonic signals are usually easier to interpret because the specular reflection component becomes negligible and the tip-diffracted signals merge. As a consequence, the scattered ultrasonic signals are much less sensitive to flaw orientation and detail. In addition, the amplitudes of the scattered ultrasonic fields increase monotonically with flaw dimensions. This useful phenomenon can improve the ability of an ultrasonic inspection system to discriminate between flaws of different sizes and types (Datta, 1977, and Richardson and Elsley, 1979).

Signal Processing

In the past, the use of low-frequency SH-wave EMAT inspection systems has been considered in the context of nondestructive evaluation of pipeline girth welds in conjunction with acceptance criteria (Reed, Kasen, McHenry, and Fortunko, 1983). In that case it was convenient to represent the spatial distribution and strength of the illuminating and scattered ultrasonic fields in terms of modal expansions. However, in the present context it is more convenient to employ a ray representation that is very closely related to techniques used in seismology and ocean acoustics (Officer, 1958). The different approach is justified by the fact that the present SH-wave EMAT system uses ultrasonic tone-bursts of shorter duration than those in Fortunko and Schramm (1983), and that the plate weldments are thick relative to the ultrasonic wavelength.

At low ultrasonic frequencies, flaw detectability in butt welded plates may be significantly degraded by multipath propagation effects and ultrasonic clutter caused by multiple reflections and mode conversion of the incident and scattered ultrasonic fields by the free surfaces. At high frequencies this phenomenon is less important because it is much easier to collimate the ultrasonic signals and remove unwanted signals by time-gating.

Figure 2-3 illustrates the two different physical situations. In both cases, the probing SH-wave signals are generated and detected by an EMAT pair. However, Fig. 2-3a illustrates the case when the thickness of the plate under inspection is sufficiently large compared to the ultrasonic wavelength so that ultrasonic signals arriving at the receiver EMAT following a reflection from the bottom surface can be gated-out in the time domain. Effectively, the case shown in Fig. 2-3a corresponds to that of a flaw embedded near the surface of a half-space. Figure 2-3b illustrates the case when the signals from the opposite surface can no longer be obscured by means of signal-gating techniques because the ultrasonic signals, arriving via different paths, overlap in the time-domain.

Figure 2-3 does not show the paths of signals generated by mode conversion effects at the free surfaces of the plate and by the flaw.

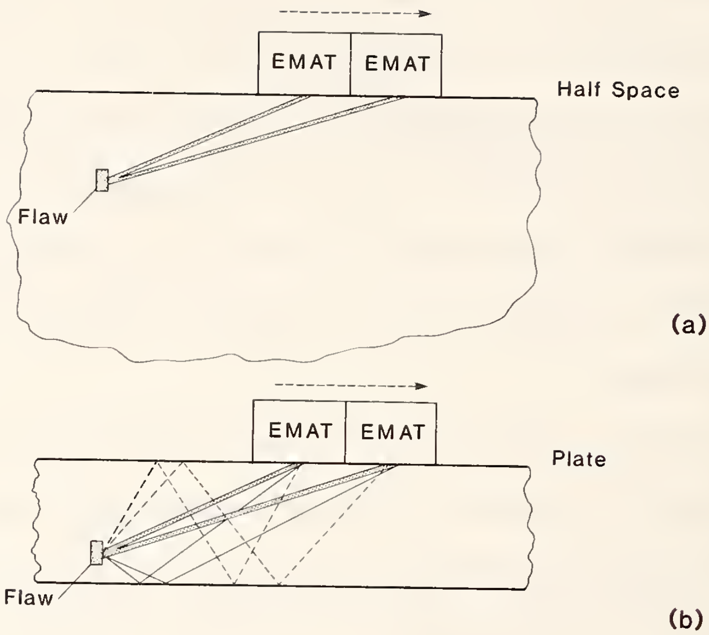

Figure 2-3: Ultrasonic signal paths. (a) Semi-infinite half-space. (b) Multiple paths in finite thickness plate.

Physically, this simplification is justified by the mode-selective properties of SH-wave EMATs that significantly de-emphasize the detection of signals of unwanted polarization: Rayleigh waves, shear vertical (SV), and longitudinal (L) waves.

Figure 2-4 illustrates the effect of the multipath propagation phenomenon on the appearance of SH-wave signals received at the free surface of a 25-mm-thick ferritic plate containing a planar, surface flaw 6.8-mm deep and 25-mm long. Relatively short, 4-RF-cycle, current bursts at a center frequency of 500 kHz generated the ultrasonic signals. The top trace shows the appearance of the received SH-wave signals when the mean distance along

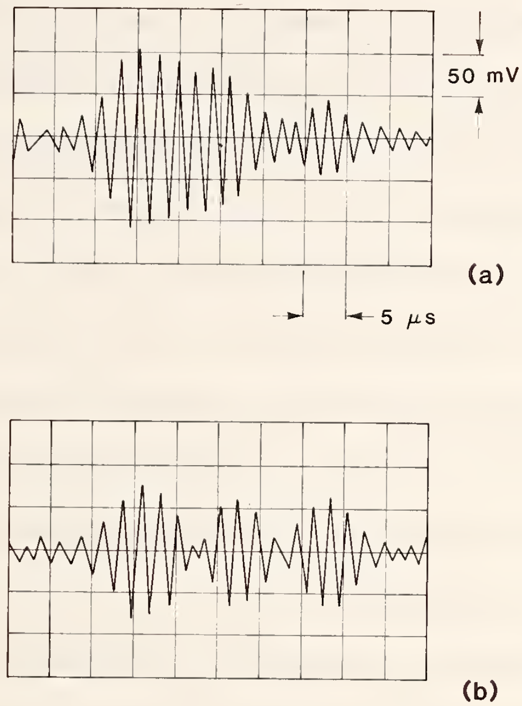

Figure 2-4: SH-wave reflection signals. (a) EMAT-flaw distance about 55 mm. Signal interference. (b) EMAT-flaw distance about 65 mm. Signal separation.

the surface between the EMATs and the flaw was approximately 50 mm. Here the first two arrivals are not separated in the time domain and interfere strongly. These interferences resulted in considerable variations in the maximum amplitude of this signal due to beating and deconvolution and would be highly uncertain. The bottom trace shows the same signals when the mean distance between the EMATs and the flaw was approximately 65 mm and the several signals present are more clearly separated and measurable. (The beginning of the frame, showing a remnant from the input drive signal is not shown.)

An additional major task in the design of ultrasonic inspection systems that operate at low frequencies involves the elimination of the unwanted ultrasonic and electromagnetic signals that may mask the presence of a flaw. Such signals may result from electromagnetic and acoustic reverberations of the transducers, direct electromagnetic leakage between the receiver and transmitter EMATs, and grain noise, as well as multipath and end effects. Obviously, the elimination of such unwanted signals is essential to improving the reliability of the detection process. In the present application we decided that digital signal processing techniques, including signal averaging, subtraction, and synthetic aperture, can effectively increase inspection reliability and diminish the effect of unwanted signals and clutter on the detectability of flaws (Chapter 6).

Digital signal averaging is important, particularly in an in-process inspection application, because it can be used to enhance the electronic sensitivity of the EMATs and, most importantly, reduce the contamination of the ultrasonic signals by asynchronous electromagnetic and ultrasonic interferences. However, because the time-average values of multipath, end-effect and grain-noise signals are nonzero, digital subtraction and synthetic aperture techniques must also be employed. The effectiveness of such techniques can be greatly increased by proper design of the EMATs and other analog components of the inspection system that contribute to the generation of the unwanted electromagnetic and ultrasonic signal.

Figure 2-3b shows the preferred inspection configuration for butt welds, which takes the full advantage of signal enhancement by digital signal processing. The transmitter and receiver EMATs are designed to aim the ultrasonic beam in the direction of the flaw and minimize direct ultrasonic cross-talk. The ultrasound beams are aimed at the grazing angle, but spread rapidly by diffraction to fill the entire thickness of the plate. As a consequence, the presence of a flaw causes several signals to arrive at the receiver EMAT at different times. These signals are shown in Fig. 2-5.

For simplicity, in constructing Fig. 2-5 we assumed that the same transducer generates and receives the probing and scattered ultrasonic signals (pulse-echo mode). The flaw is located a distance below the top surface of the plate. The same surface also supports the transducer, which is at the observation point O. Two families of rays are shown. The first family, Fig. 2-5a, is all the rays reflecting first from the top surface of the plate. The second family, Fig. 2-5b, is all the rays reflecting first from the bottom surface. The actual experimental situation, as exemplified by the configuration shown in Fig. 2-3b, is much more complicated in that separate EMATs are necessary to generate and receive the ultrasonic signals (pitch-catch mode). A consequence of this arrangement is two additional families of rays. (For a comprehensive discussion of this phenomenon the interested reader shown consult Brekhovkikh (1980).) It is evident that this complicated situation causes the receiver-EMAT to detect many signals. Physically, these additional signals correspond to the multiple rays connecting the two EMATs with the flaw. Because at long wavelengths it is impractical to generate highly collimated ultrasonic beams, especially using end-fire transducers such as the EMAT, an alternative procedure is needed to reduce the received ultrasonic signal complexity.

A practical way to improve the flaw-signal quality is synthetic aperture processing. In this technique, the transmitter and receiver EMATs are moved together along a scan line that lies on the top surface of the plate. As a result, the principal flaw signal, depicted by a solid line in Fig. 2-3, arrives slightly later in each successive measurement as the two EMATs are

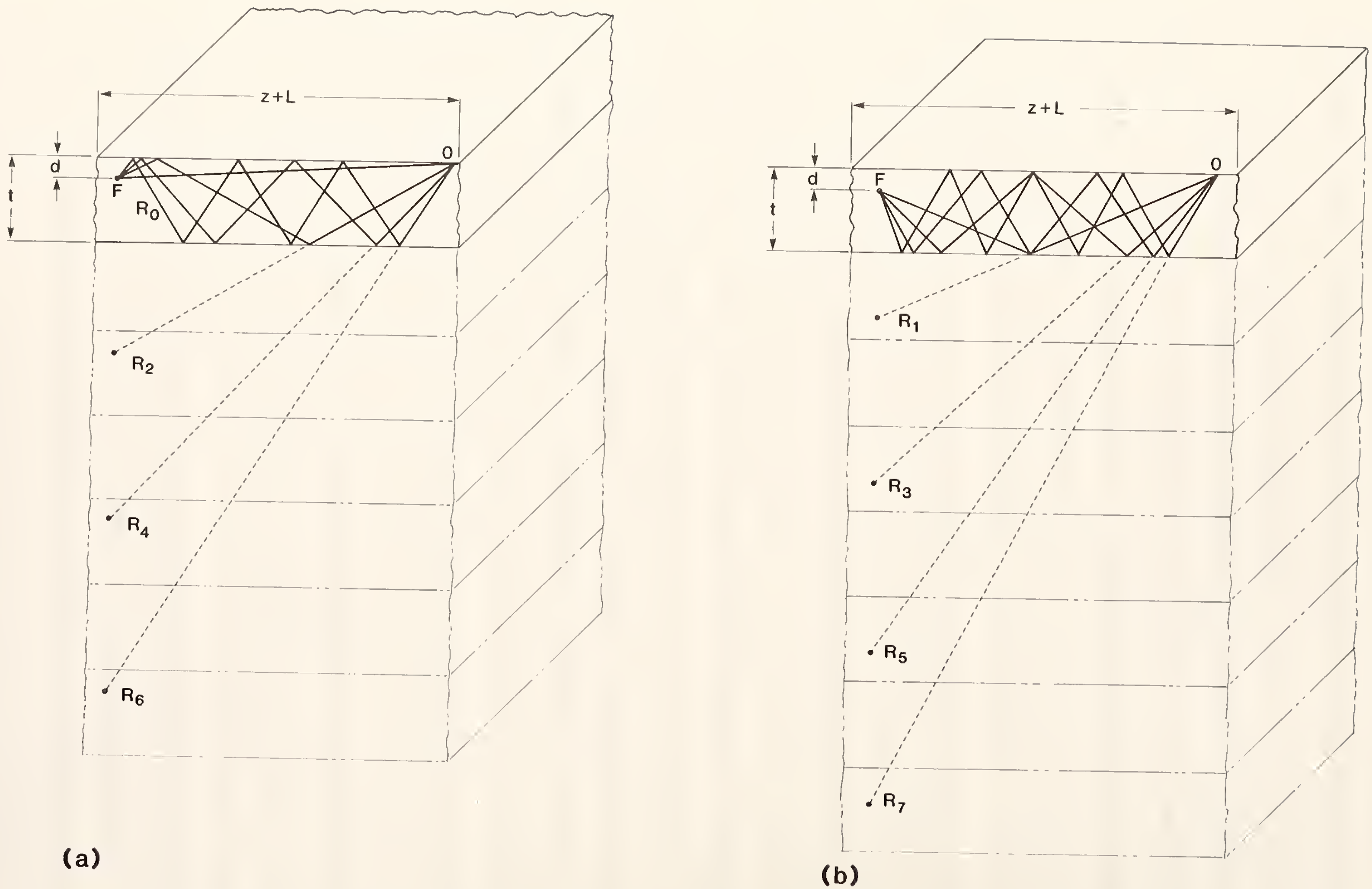

Figure 2-5: Multipath propagation of ultrasonic pulses in a plate and the equivalent path length. (a) Even number of surface reflections. (b) Odd number of surface reflections.

moved away from the flaw. The timing of the other flaw signals is shifted correspondingly. On the other hand, the timing of all electromagnetic and ultrasonic interferences remains unchanged or undergoes changes in the opposite direction. This phenomenon can be exploited to significantly enhance the principal flaw-signal quality with respect to all other signals.

In the synthetic aperture technique, the flaw signals from a given direction are processed by shifting each received waveform by a time increment that compensates for the change in arrival time of signals from that direction and then adding the signals together. This reduces the signals from all other directions and reinforces the flaw signal.

Figure 2-6 shows the appearance of signals received from a deep surface flaw in a 25-mm-thick steel plate as the spacing between both EMATs and the flaw is increased in 2.1-mm steps. The successive waveforms (labeled 1-10) contain residual electromagnetic interference (A) and ultrasonic cross-talk signals (B) in addition to the principal flaw signal and those that have propagated via the alternate paths (C). The reconstructed waveform is shown at the bottom.

Figure 2-6 shows very substantial improvement in the quality of the flaw signal by elimination of the electromagnetic and ultrasonic interferences from the display. In addition, the flaw is represented by a single waveform with a nearly triangular envelope. This decontaminated signal is much more desirable for processing by any detection algorithm than any of the 10 unprocessed waveforms.

Summary

The inspection system described in the present report takes advantage of improvements in SH-wave EMAT design resulting in better collimation of the sound beams in the flaw direction. The system is operated at relatively low

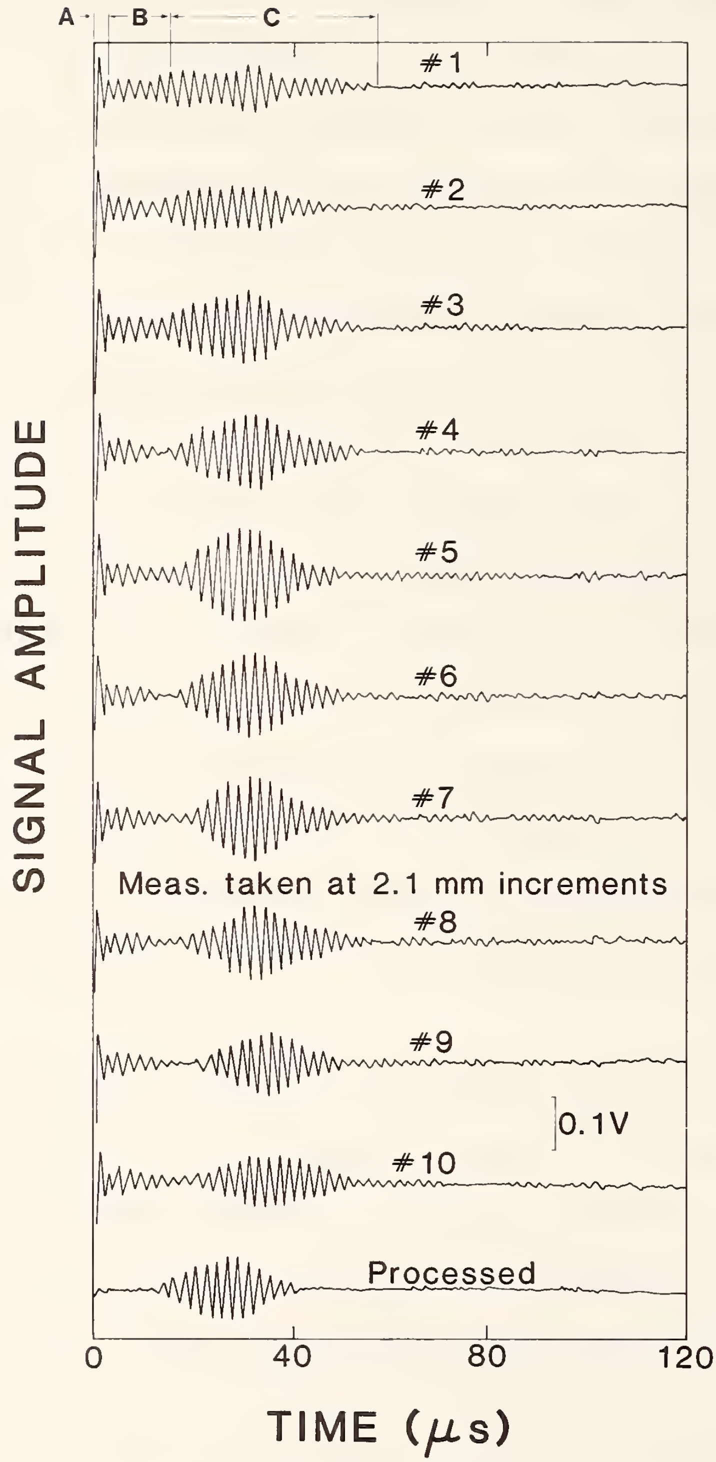

Figure 2-6: Synthetic aperture processing of a reflection echo from a saw cut in the surface of a 25-mm thick plate. Signals #1 to #10 are raw data taken at incremental increases of 2.1 mm between EMATs and cut. The processed waveform is at the bottom.

ultrasonic frequencies (typically 450 kHz) to reduce sensitivity to flaw orientation and surface detail. Finally, the quality of the flaw signals is substantially improved by employing advances in digital signal processing, including digital background subtraction, synthetic aperture focusing, and time-averaging. The following sections of this report describe the technical details of the above features of the SH wave EMAT inspection system.

References

Brekhovkikh, L. M., 1980, "Waves in Layered Media," Academic Press, New York.

British Standards Institution, 1980, Guidance on some methods for the derivation of acceptance levels for defects in fusion welded joints, PD 6493, British Standards Institution, London.

Budiansky, B., and Rice, J. R., 1978, On the estimation of a crack fracture parameter by long wavelength scattering, J. Appl. Mech., 45:453.

Datta, S.K., 1977, Diffraction of plane elastic waves by ellipsoidal inclusions, J. Acous. Soc. Amer., 61:1432.

Doyle, P. A., and Scala, C. M. , 1978, Crack depth measurement by ultrasonics: a review, Ultrasonics, 16:164.

Fortunko, C. M. , King, R. B., and Tan, M., 1982, Nondestructive evaluation of planar defects in plates using low-frequency shear horizontal waves, J. Appl. Phys., 53:3450.

Fortunko, C. M., and Schramm, R. E., 1982, Ultrasonic nondestructive evaluations of butt welds using electromagnetic-acoustic transducers, Weld. J., 61:39.

Fortunko, C. M., and Schramm, R. E., 1983, Evaluation of pipeline girth welds using low-frequency horizontally polarized waves, J. NDE, 3:155.

Lundin, C. D., 1976, The significance of weld discontinuities - a review of current literature, WRC Bulletin 222, Welding Research Council, New York.

Officer, C. B., 1958, "Introduction to the Theory of Sound Transmission." McGraw-Hill Book Co., Inc., New York.

Reed, R. P., Kasen, M. B., McHenry, H. I., and Fortunko, C. M., 1984, Fitness-for-service criteria for pipeline girth weld quality, WRC Bulletin (in press), Welding Research Council, New York.

Reed, R. P., McHenry, H. I., and Kasen, M. B., 1979, A fracture mechanics evaluation of flaws in pipeline girth welds, WRC Bulletin 245, Welding Research Council, New York.

Richardson, J.M. and Elsley, R.K., 1979, Extraction of low-frequency properties from scattering measurements, in: "Proceedings of the IEEE Ultrasonics Symposium," B. R. McAvoy, ed., IEEE, New York.

Chapter 3

SYSTEM CONCEPT - OVERVIEW

This chapter presents an overview of a specific implementation of the inspection concept described in Chapter 2. Specifically, block-diagrams describe the architecture of a laboratory-scale system, including hardware and software components. This configuration demonstrates the technology and establishes the inherent performance limits of our SH-wave EMAT inspection concept. Additional discussion includes various methods of employing the system to dectect and characterize different flaw categories in weldments, as well as factors limiting the overall resolution. Our emphasis here is on an overview. The functional details of the components, including circuit diagrams, EMAT-assembly drawings and software listings, are given in the following chapters and appendixes.

Figures 3-1 and 3-2 show the main functional blocks of the SH-wave technology demonstration system. The operation of the system is centrally controlled by a 16-bit minicomputer (block 1 in Fig. 3-1) that uses a high-level (BASIC language) operating environment. The programs, inspection parameters, and data are stored by two floppy-disk drives (2). The operator initiates all commands through a keyboard (3) which is a part of a video display terminal (VDT) equipped with medium-resolution graphics capability. A dot-matrix printer (4) can provide a hardcopy of system perameters and plots of signal waveforms and processed data. The minicomputer directs the operation of several peripheral devices through a standard interface bus. The system is capable of fully automated data collection followed by signal processing. During data collection, the minicomputer controls the operation of the mechanical scanners (5 and 6), which move the EMAT search-head (7) on

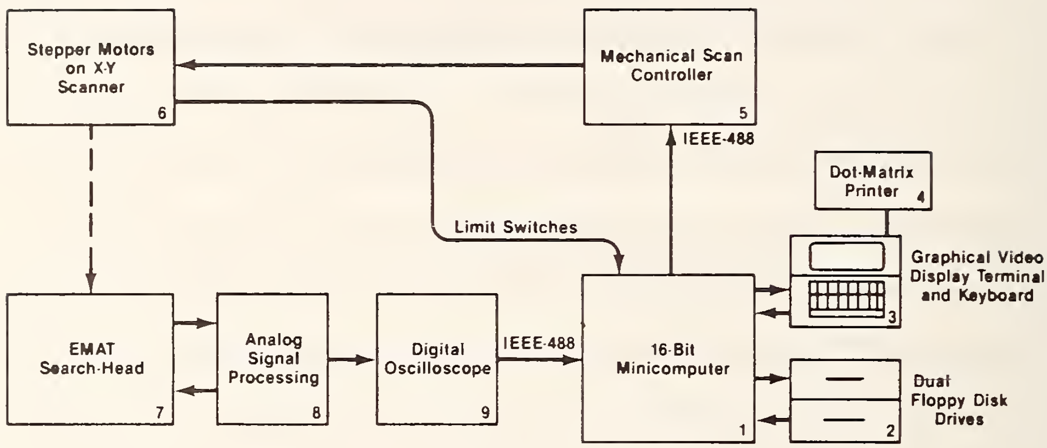

Figure 3-1: Block-diagram of SH-wave-EMAT weld inspection system.

the surface of the weldment. After analog signal processing (8), a digital oscilloscope (9) displays the data and transfers it to the computer on the IEEE-488 bus. Limit switches on the lead-screw mechanisms signal the computer of any overscanning so it can remove power from the stepper motors and prevent mechanical damage. (The operation of the mechanical scanners and their controllers is described in detail in Chapter 7.)

The minicomputer does not directly operate the analog circuits (8), which generate the high-power electrical signals (typically 1000 watts-peak) driving the transmitter-EMATs and preamplify the low-level signals detected by the receiver-EMATs. This portion of the inspection system operates asynchronously with respect to the mincomputer clock circuit to reduce electromagnetic interference levels. The analog receiver signal reaches the computer through a digitizing oscilloscope (9).

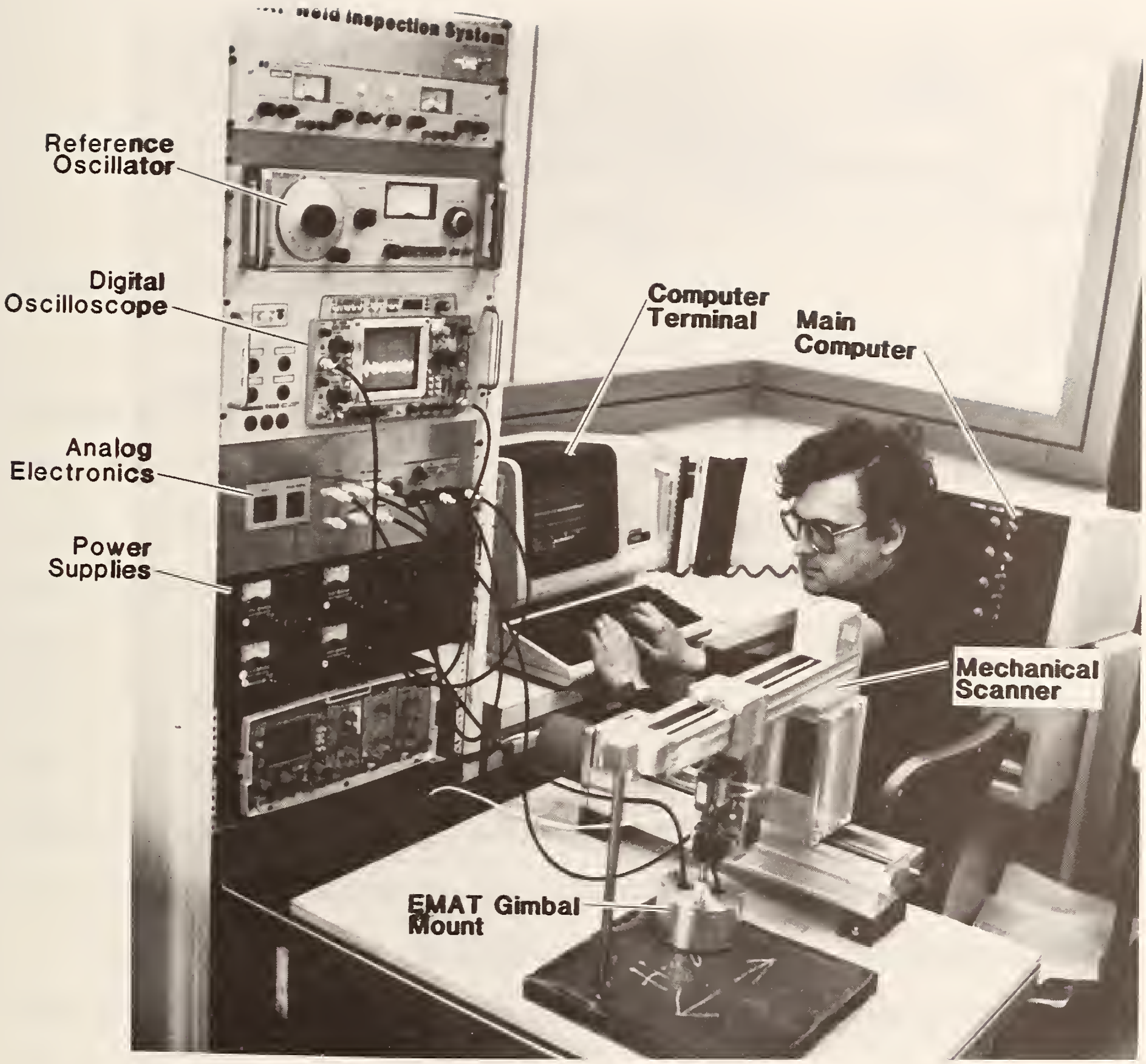

Figure 3-2: Photograph of laboratory SH-wave-EMAT weld inspection system.

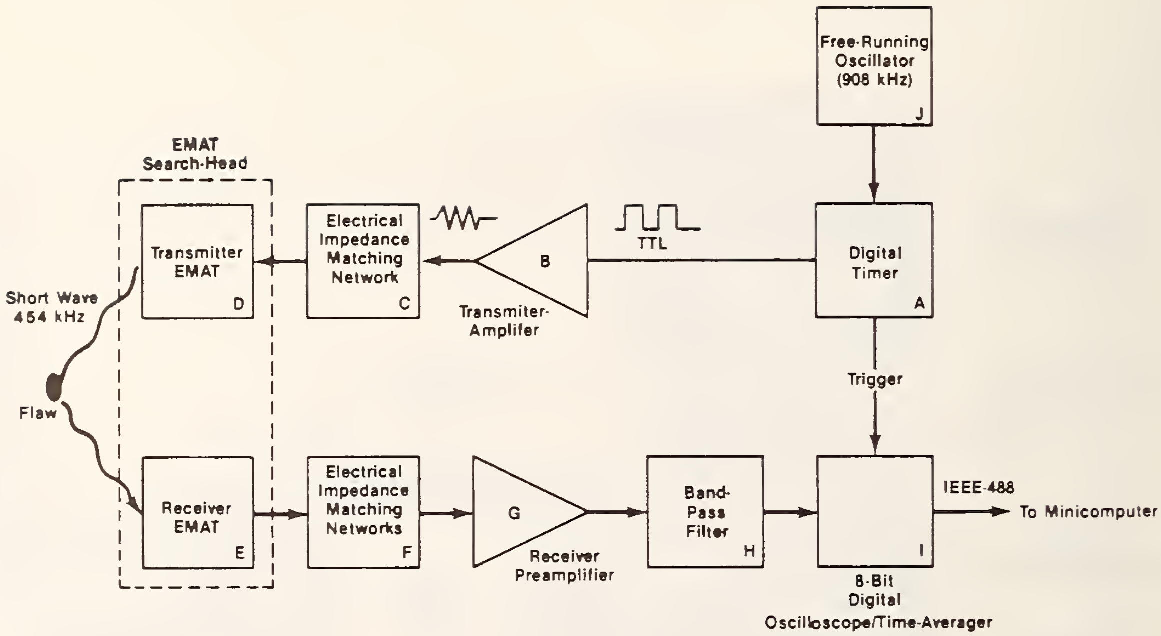

Figure 3-3: Block-diagram of the analog electronics section.

Figure 3-3 is a block-diagram for sections 7, 8, and 9 of the inspection system. To avoid confusion with Fig. 3-1, the individual components are marked by letter codes (A-I). (The construction of the EMATs and other specially constructed electrical subsystems are described in Chapters 4 and 5.)

The analog section can be functionally subdivided into the "transmitter" side and the "receiver" side. On the "transmitter" side, the key role is played by a digital timer circuit (A) that generates a unipolar TTL-compatible (TTL stands for the transistor-transistor-logic family of digital circuits) train of pulses whose period is synchronized to the period of a free-running oscillator (J). The timer, which uses digital counting circuits, also generates a trigger pulse for an 8-bit digital oscilloscope (I) serving as an

A/D converter, and establishes the pulse-repetition-frequency (PRF). The length-of-burst and PRF parameters are manually selectable using switches located on the front panel of the timer. Typical PRFs are two thousand times slower than the frequency of the free-running oscillator (908 kHz). The TTL-level output of the timer goes directly to the input of a class-D transmitter-amplifier (B) that drives the transmitter-EMAT (D) through a special impedance-matching network (C).

On the "receiver" side, the output of the receiver-EMAT (E) is first preamplified by a specially designed, low-noise amplifier (G), passed through a band-pass filter (H) and, then, digitized by the oscilloscope (I). The digital oscilloscope also computes a time-average of up to 256 individual waveforms. Normally, 16 time-averages are used. This capability is needed to compensate for the low transduction efficiencies of SH-wave EMATs and to reduce the influence of implusive and other electromagnetic interferences. An impedance-matching network (F) is used to minimize the noise figure of the receiver-preamplifier. The digital oscilloscope transfers the time-averaged output waveform to the minicoputer over the IEEE-488 data bus.

As configured in Fig. 3-2, with both EMATs located on the same side of the weld and aligned along a plane normal to the welding direction, the SH-wave EMAT system is mainly intended to detect longitudinal flaws in butt weldments. This category includes elongated slag, inadequate penetration (IP), incomplete fusion (IF), and certain cracks. By definition, longitudinal flaws are aligned with the welding direction, as shown in Fig. 3-4a. Because the wavelength of the ultrasonic signal is large (7.4mm) in relation to conventional ultrasonic systems, small concentrations of weld porosity cannot normally be detected. In the noramal inspection mode, the weld region is interrogated by moving the EMAT search unit in a pattern on the surface of the

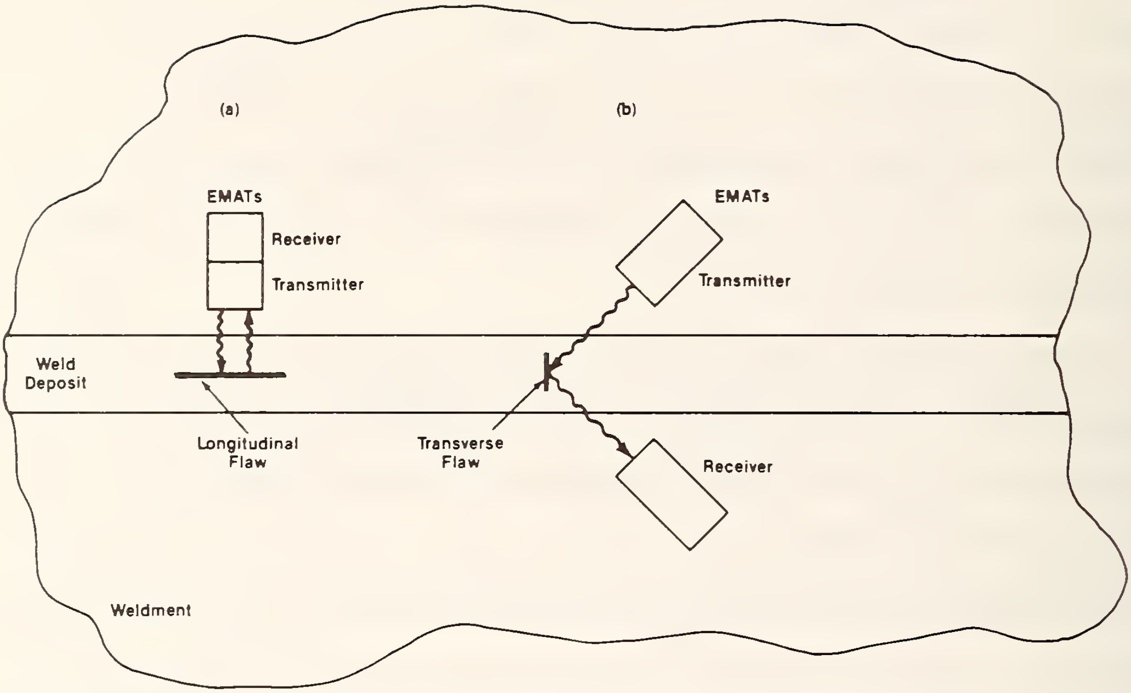

Figure 3-4: Concept for detecting and characterizing weld flaws. (a) Longitudinal. (b) Transverse.

weldment such as shown in Fig. 8-2. To obtain better transverse and longitudinal resolution, extensive use is made of digital signal processing, including synthetic aperture reconstruction. (The details of the digital signal processing procedures are treated separately in Chapter 6.)

The inspection configuration of Fig. 3-4a is not suitable for detecting the important category of transverse weld flaws. Figure 3-4b illustrates this category of weld flaw along with a possible inspection approach. In contrast to Fig. 3-4a, the two EMATs in Fig. 3-4b are positioned on opposite sides of the weld and aligned symmetrically with respect to the welding direction to exploit the phenomenon of specular reflection. Implementation of the inspection concept shown in Fig. 3-4b would require a substantially different and more complicated mechanical arrangement than that shown in Fig. 3-2. For this reason, detection of transverse weld flaws is not included in the present report.

Although the laboratory-scale demonstration system shown in Fig. 3-2 does not allow very long scan distances, it is believed that the SH-wave inspection concept is inherently suitable for the in-process inspection role in many shipyard applications with very long machine-welded joints. Of course, a different arrangement for moving the EMAT search-heads on the surface would be necessary. Perhaps, already existing mechanisms can be adapted to fill this role (de Sterke, 1981). Although no provisions were made to ruggedize and shield the laboraory set-up for field use, industrial or military-quality versions of all components, except for the specially made EMATs and portions of the analog electronics section, are available commercially.

<u>Reference</u>

de Sterke, A., 1981, Automated Ultrasonic Inspection of Circumferential Welds in Pipelines, <u>Met. Constr.</u>, 12:42.

Chapter 4

DESIGN OF EFFECTIVE SH-WAVE EMATS

In the inspection of plate butt weldments it is desirable to maximize the collimation of the ultrasonic beam in the direction of the flaw. There are two ways to accomplish this: 1) using synthetic aperture processing, and 2) designing an SH-wave electromagnetic-acoustic transducer (EMAT) with the desired beam shape. In practice, to satisfy system design requirements, a combination of the above two techniques yields the desired beam collimation. This section emphasizes the details of SH-wave EMAT design necessary to obtain the desired beam shape characteristics and, simultaneously, reduce the effect of unwanted ultrasonic and electromagnetic interference.

Operational Principles

Figure 4-1 shows a primitive EMAT element composed of a wire conductor carrying a dynamic current I_ω and a source of strong magnetic bias field H_0. The current I_ω induces dynamic eddy currents J_ω in the metal conductor surface. The strong magnetic bias field, H_0, causes the deflection of the moving electrons in a direction defined by the cross-product of the direction vectors associated with J_ω and H_0. The resultant Lorentz body forces, T, generate ultrasonic signals that propagate radially into the bulk of the metal conductor, away from the wire. The signal polarization depends on the direction of the static bias field H_0 with respect to the free surface (this report does not discuss the subject of generating ultrasonic signals using magnetostrictive transduction mechanisms). Waves with particle displacements parallel to the free surface are called SH-waves.

The primitive transducer element in Fig. 4-1 is not very useful in a practical application. First, it is not very efficient, because of the

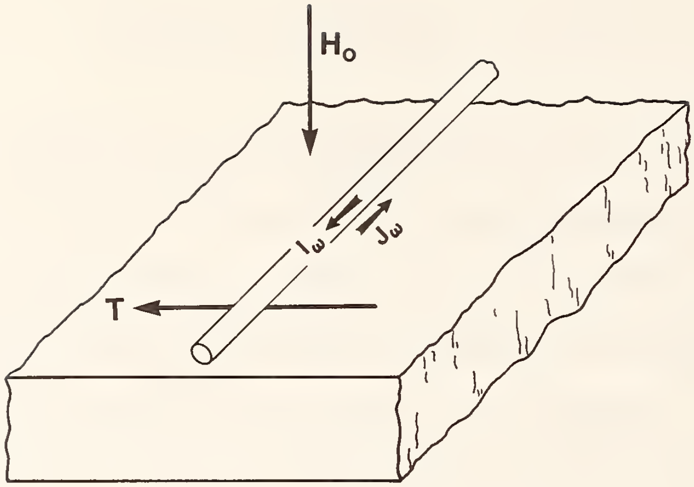

Figure 4-1: Primitive EMAT element. The eddy current J_ω produced by I_ω in a wire at the surface interacts with the external magnetic field H_o to produce traction force T.

practical difficulties of efficiently matching isolated wire radiators to transmitter-amplifiers and receiver-preamplifiers in the frequency band used in flaw detection (450 kHz typically). Second, the radiation pattern exhibits cylindrical symmetry when generating SH-waves. Cylindrical radiation patterns are not useful for inspecting butt welds in plates, because as much energy is aimed at the opposite surface of the plate as at the flaw (Fig. 4-2). Because the opposite surface presents a greater obstacle to the ultrasonic signal than the flaw, detection may be difficult. Clearly, a practical EMAT must be able to generate most of the signal in the general direction of the flaw, i.e. along the surface, and discriminate against signals that can propagate along directions near the normal to the plate.

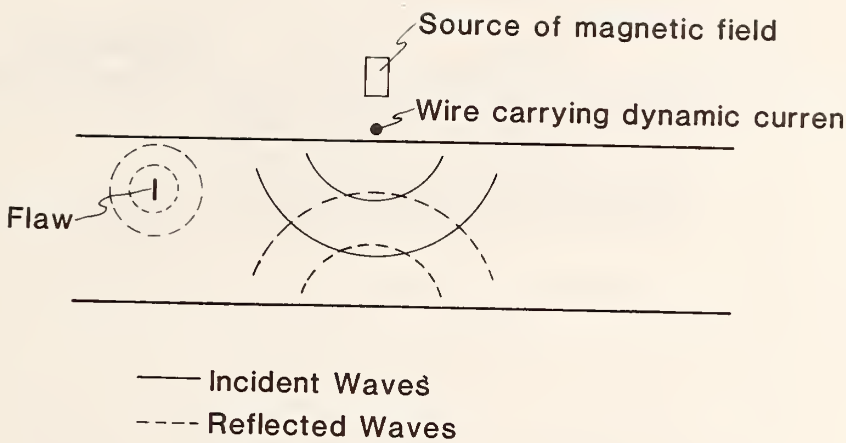

Figure 4-2: The radiation pattern of the simple EMAT in Fig. 4-1 produces a stronger reflection from the plate back surface than does a flaw.

Practical Configurations

In the past, a number of different EMAT configurations have been proposed. The majority of applications involving the use of SH-waves made extensive use of the periodic-permanent-magnet (PPM) EMATs of the general type depicted in Fig. 4-3. It is easily seen that the EMAT shown in Fig. 4-3 can be constructed by superposing a number of the primitive EMATs shown in Fig. 4-1. However, in Fig. 4-3 the sources of the static magnetic field range symetrically along the conductor carrying the dynamic current I_{ω}. To confine the eddy current distribution to the region directly below the periodic-permanent-magnet array, there are two oppositely polarized rows of magnets and the conductor is in the form of an elongated spiral coil.

Detailed factors governing the beam-forming characteristics (e.g., directivity) of periodic-permanent-magnet EMATs are in Fortunko and Schramm

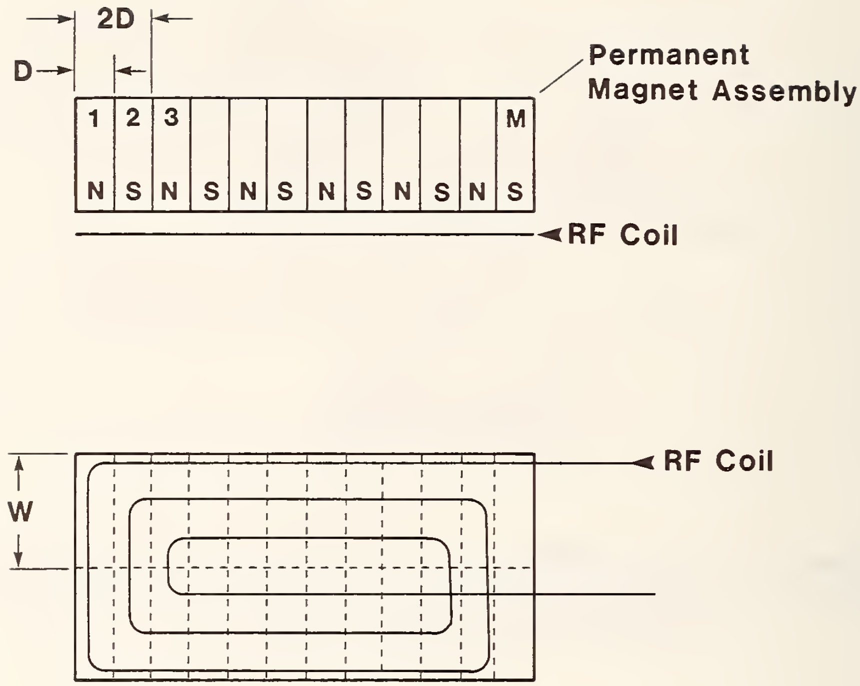

Figure 4-3: Schematic of a periodic-permanent-magnet (PPM) EMAT containing M pairs of magnets.

(1983), while Thompson (1973, 1977, 1978) discusses the principles of the transduction mechanisms. In the sagittal plane (i.e., the plane normal to the surface of the plate and parallel to the principal propagation direction), the directivity pattern of a PPM EMAT can be determined approximately from the relation (Vasile and Thompson, 1979, and Fortunko, King and Tan, 1982):

$$DF(\emptyset) = \left\{ \frac{\pi}{2} \frac{\sin\left(\frac{\pi D}{\lambda} \sin \emptyset\right)}{\left(\frac{\pi D}{\lambda} \sin \emptyset\right)} \right\} \cdot \left\{ \frac{\sin\left[\frac{MD}{2}\left(\frac{2\pi}{\lambda} \sin \emptyset - \frac{\pi}{D}\right)\right]}{\sin\left[\frac{D}{2}\left(\frac{2\pi}{\lambda} \sin \emptyset - \frac{\pi}{D}\right)\right]} \exp\left(-jM\pi/4\right) \right\} \qquad \text{Eq. 4-1}$$

where the angle $\emptyset$ is defined by the ray from the PPM EMAT center to an observation point and the normal to the plate surface. As shown in Fig. 4-3, the PPM EMAT is a periodic array of M permanent magnets (usually made from high-strength samarium-cobalt) with a period L=2D and half-width W, and a spiral-wire coil placed between the magnet assembly and the plate surface. In practice, a spacer of thickness δ (not shown in Fig. 4-3) is inserted between the magnets to reduce eddy current losses. Then, L becomes $2(D+\delta)$. In Eq. 4-1, λ is the bulk ultrasonic wavelength ($\lambda = v_s/f$).

The PPM EMAT of Fig. 4-3 is M essentially independent cells. The cells are connected in-parallel acoustically and in-series electrically. As a consequence, the PPM EMAT can be viewed as an ultrasonic equivalent of an electromagnetic end-fire antenna. This fact is reflected in Eq. 4-1, which can be interpreted as a product of element-structure and array-form factors. For clarity, braces isolate the element and array factors. Narrow beam widths can be realized only when the EMAT is driven electrically by a tone-burst at least M cycles long. Then, the principal beam direction is:

$$\emptyset = \arcsin\left[\lambda/2(D+\delta)\right] \qquad \text{Eq. 4-2}$$

The end-fire properties of the PPM EMAT in Fig. 4-3 can be verified experimentally using the calibration configuration in Fig. 4-4, a 152-mm radius, 203-mm wide aluminum test-block with a semi-cylindrical cross-section. The angles Θ and $\emptyset$ define the coordinates at the observation point. The PPM EMAT under test (in this case, the transmitter EMAT) is placed symmetrically

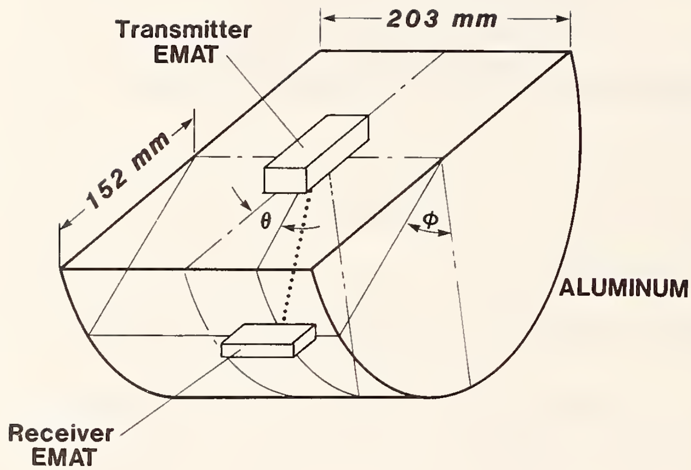

Figure 4-4: Aluminum test block and transducer configuration to measure the angular distribution of ultrasonic energy.

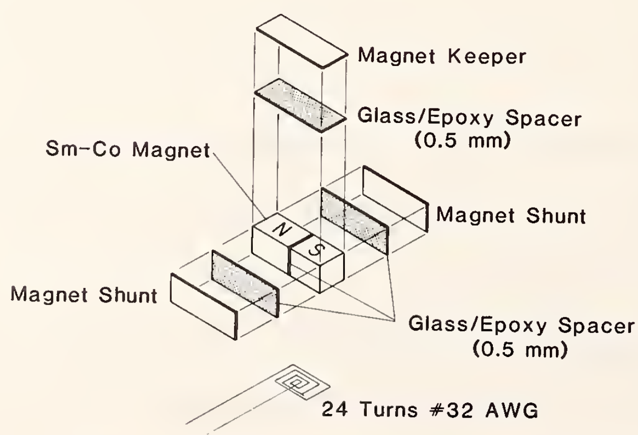

Figure 4-5: Simple EMAT (M=1) with maximum sensitivity to SH waves propagating normal to the surface.

at the intersection of the two symmetry planes. A second EMAT serves as a probe. The simple EMAT of Fig. 4-5 exhibits maximum sensitivity to shear wave signals that propagate along the normal to the surface. (Figure 4-6 shows its theoretical and experimental radiation patterns.) As a result, it is very useful in diagnosing the performance characteristics of the more complicated PPM EMATs.

The experimental and theoretical radiation patterns of the EMAT in Fig. 4-3 are compared in Fig. 4-7. In this case the measurements were taken in the sagittal plane (Θ=0). The EMAT characteristics were: M=16, W=12.5 mm, D=3.2 mm and δ=0.5 mm. The frequency was 410 kHz.

A comparison of the experimental and theoretical results shown in Fig. 4-7 verifies the end-fire characteristics of the EMAT shown in Fig. 4-3 over most of the range of $\emptyset$. In particular, the maximum amplitude of the radiated signal occurs at the grazing angle, $\emptyset$=0°. A discrepancy between the measured and theoretical values exists for $\emptyset$<60°. This is attributed to second-harmonic frequency components and transducer end-effects. It is important to note that the amplitude of the signal transmitted along the surface normal is negligible.

Final Design

Although the SH-wave EMAT shown in Fig. 4-3 exhibits the desired directivity characteristics, it suffers from excessive sensitivity to electromagnetic interference (EMI). A better design in Fig. 4-8 uses two separate RF coils to induce eddy currents at the surface of the metal plate. The coils are symmetrical with respect to the sagittal plane (not shown) and connected in-series electrically to increase the input electrical impedance. However, one of the coils is wound clockwise while the other is wound counterclockwise. This winding arrangement reduces the EMAT sensitivity to EMI and minimizes

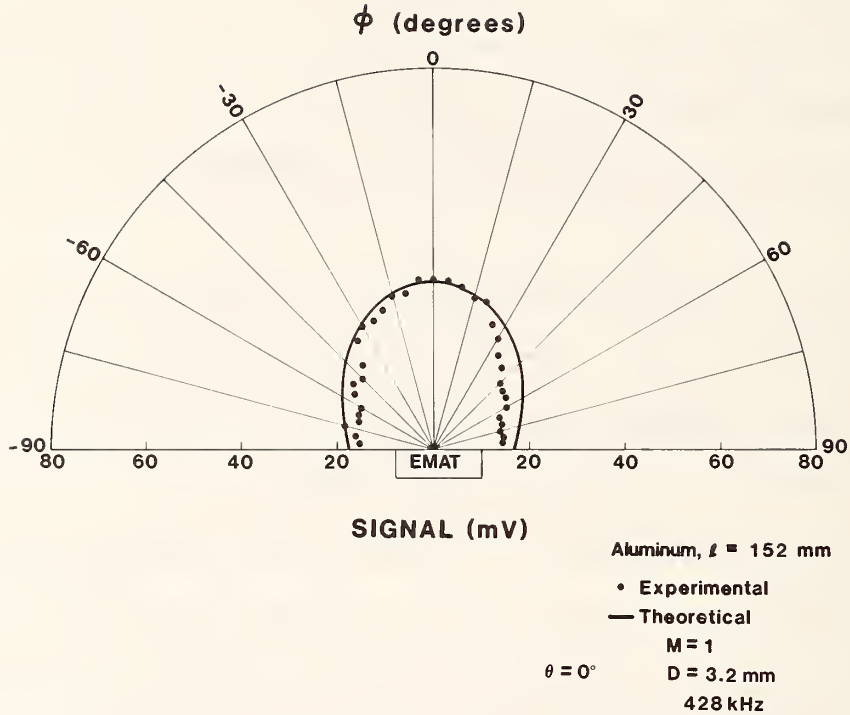

Figure 4-6: Angular radiation pattern of EMAT in Fig. 4-5 (M=1). Maximum amplitude is normal to the surface.

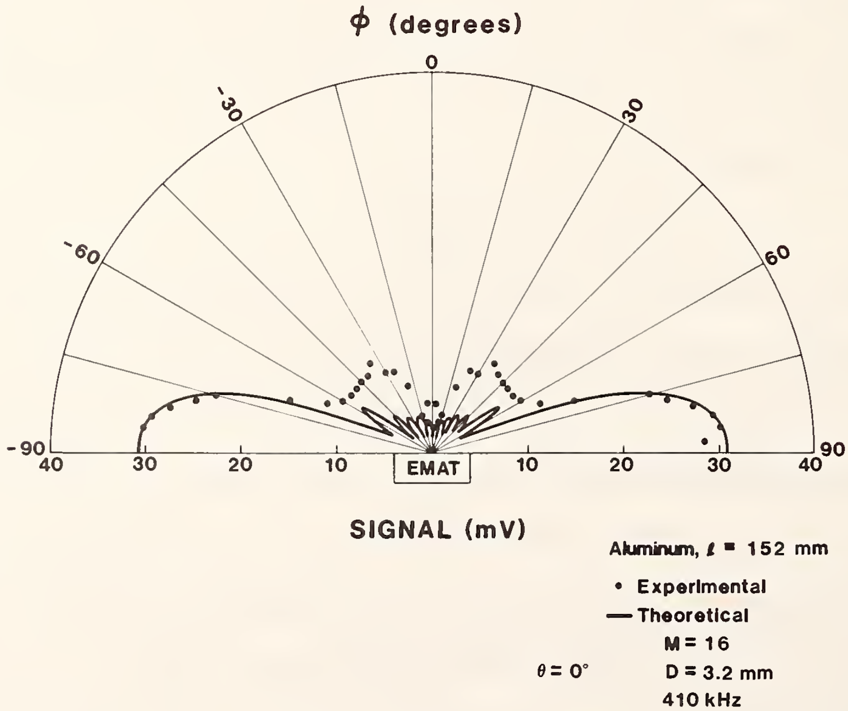

Figure 4-7: Angular radiation pattern of EMAT in Fig. 4-3 (M=16). Maximum amplitude grazes the surface.

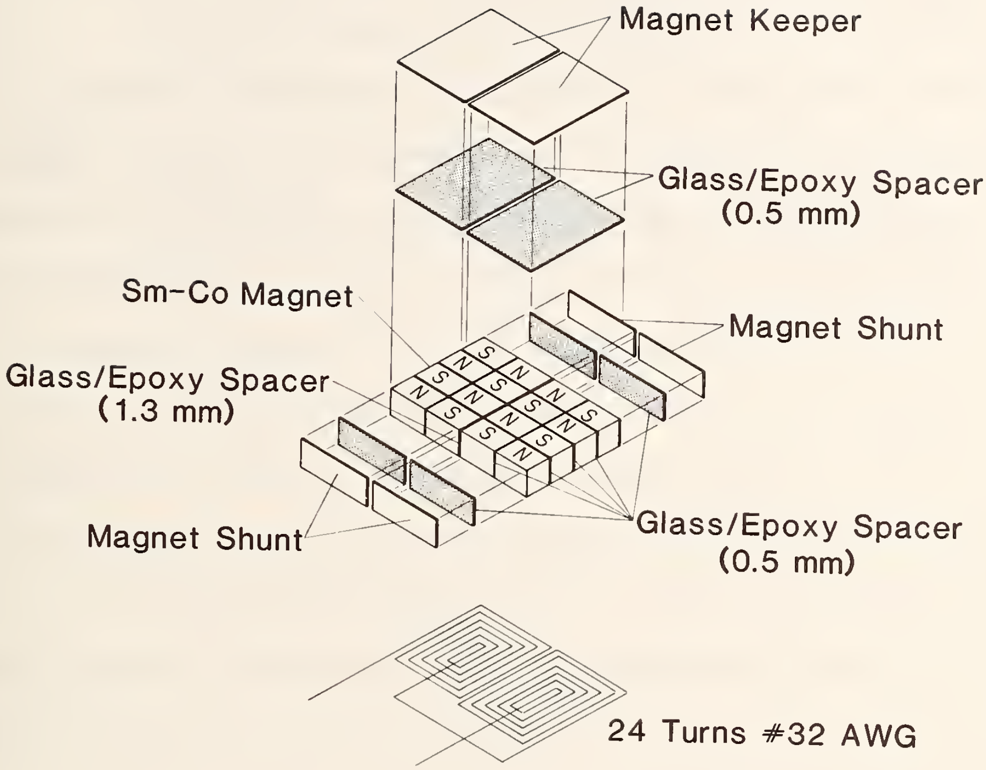

Figure 4-8: Improved EMAT design. The two coils are counter-wound to minimize pickup of EMI.

direct electromagnetic cross-talk between adjacent EMATs. To maintain phase coherence, there are four rows of permanent magnets. The four magnet structures are polarized to maintain mirror symmetry with respect to the sagittal plane.

Figure 4-8 shows all the essential EMAT components, except for a thin (80 μm), 304-type stainless steel face plate protecting the EMAT coils from damage. Fiberglass-epoxy spacers, 0.5 mm thick, separate the individual magnets to reduce eddy current flow in the samiarium-cobalt (Sm-Co) magnets. A central 1.3-mm-thick spacer of the same material separates the magnet assembly into double rows associated with each spiral coil. In addition, 3.7-mm thick soft-iron plates serve as magnet-keepers and shunts.

The SH-wave EMAT in Fig. 4-8 was originally designed to operate in the 440 to 500-kHz region. The magnets are 5-mm deep along the polarization direction, 3.3-mm long along the propagation direction and 8-mm wide along the direction that is normal to the propagation direction. Each elongated spiral coil contains 24 turns of #32 AWG magnet wire. At 500 kHz the input electrical impedence when placed on ferritic steel is (19 + 15.3j) ohms ($j=\sqrt{-1}$). This is a relatively high impedence level that is intermediate between the low impedance levels required by the transmitter amplifier (less than 1 ohm) and the high impedance levels required by the receiver preamplifier (typically 500-1000 ohms). It is convenient to raise or lower this impedance to maximize the electrical efficiency of the system. (Chapter 5 covers this topic extensively.)

It is interesting to examine the radiation patterns of the EMAT design in Fig. 4-8 as a function of frequency and length-of-signal parameters. Figures 4-9 (a) to (d) show measurements at several selected frequencies. The measurements were made in the sagittal plane using the EMAT in Fig. 4-5 as a probe and the semicylindrical test-block in Fig. 4-4 as an experimental range. The radiation patterns are for center frequencies of 400, 441, 500 and 700 kHz with a three-cycle RF tone burst. In addition, Figs. 4-10 (a) and (b) show the radiation patterns at 441 kHz with, respectively, four and eight RF-cycle drive signals. In some of the figures, the actual received waveforms are also shown to better illustrate certain peculiarities of the PPM SH-wave EMATs.

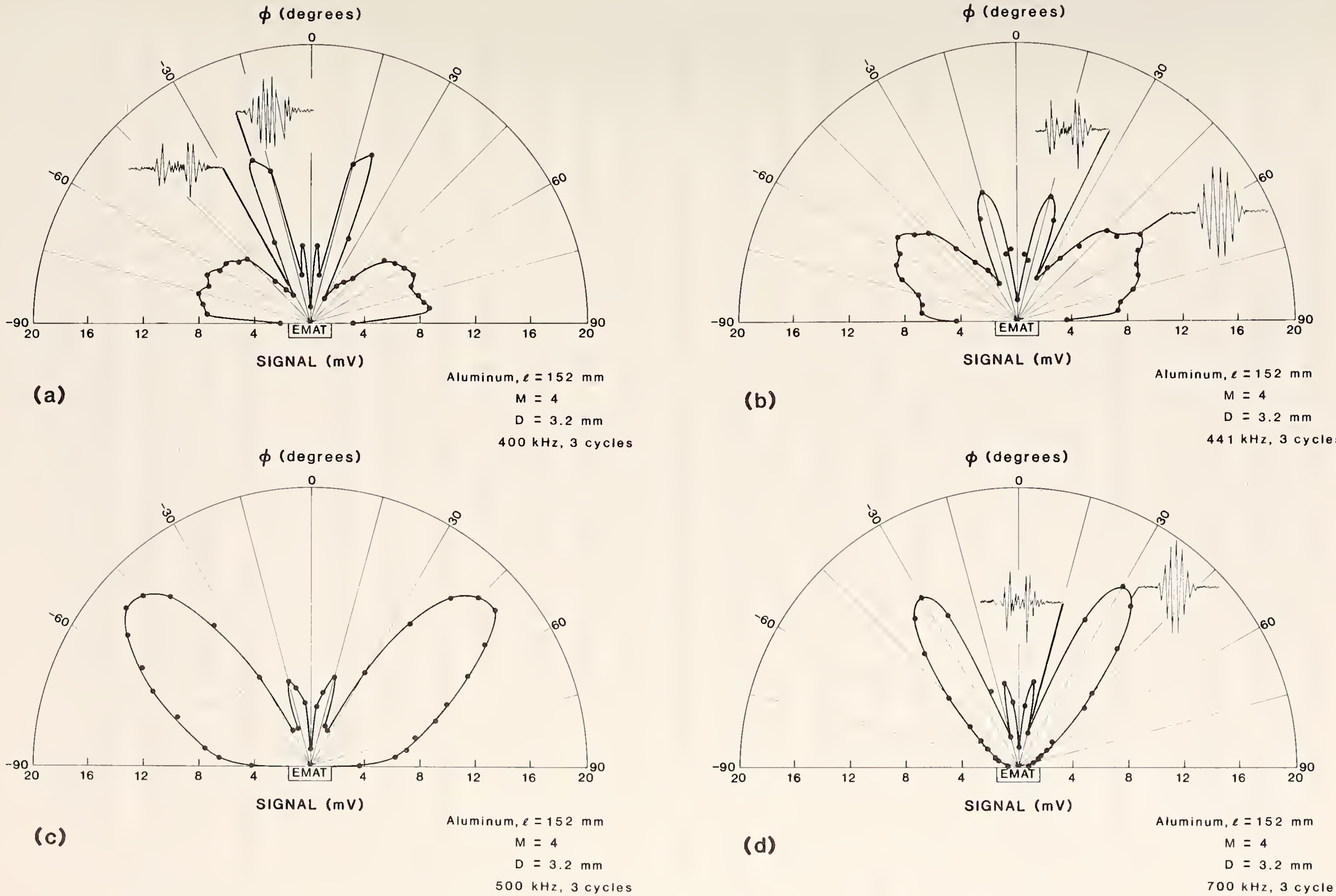

Figure 4-9: Radiation patterns of EMAT in Fig. 4-8. Three cycle tone burst. (a) 400 kHz. (b) 441 kHz. (c) 500 kHz. (d) 700 kHz.

Even a cursory examination of the ultrasonic radiation patterns and shapes reveals several interesting features. For example, in Figs. 4-9 (a) and (b), a three-RF-cycle tone-burst drives the EMAT. Comparing the two figures shows that the major lobes of the two radiation patterns lie in the range 90-45 degrees with respect to the surface normal. However, in addition to the two major lobes, which are distributed symmetrically with respect to the surface normal (PPM EMATs are bidirectional), two additional lobes exist, aimed at approximately 15 degrees with respect to the surface normal. A closer examination of the actual received waveform reveals that the center frequency of the signal transmitted through the two subsidiary lobes is mainly second-harmonic components. (The presence of such signals is not detrimental to the inspection process, because they can be efficiently filtered out by zero-padding the Fourier spectra during synthetic aperature processing.) The major lobes aimed along the surface are the most important aspects of the two radiation patterns in Figs. 4-9 (a) and (b). (At 90 degrees the amplitude of the signal appears to decrease by approximately two-thirds. However, this is due to the M=1 receiver EMAT near the corner formed by the cylindrical and flat surfaces of the test-block.) These radiation patterns are very desirable for inspecting butt weldments, because they insure that the flaw remains in the field of view of the transducer over maximum scan distances. This feature aids in realizing long synthetic apertures to help discriminate against unwanted ultrasonic signals.

The radiation patterns in Figs. 4-9 (c) and (d) exhibit major lobes aimed into the material at 47 and 30 degrees with respect to the surface normal. We have included the two figures for completeness, to illustrate the fact that the direction of the SH-wave signals can be smoothly varied by simple changing the center frequencies. These radiation patterns are useful in angle-beam inspections and as a means of localizing the flaw with respect to the plate through-thickness direction by triangulation. (At grazing incidence the transverse resolution of an ultrasonic inspection system is very poor (Fortunko and Schramm, 1983).

Finally, it is interesting to compare the radiation pattern in Fig. 4-9(b) with those Figs. 4-10 (a) and (b). The three patterns were generated by the same EMAT when driven by three, four and eight RF-cycles, respectively. The pattern for four RF-cycles appears to be smoother than the patterns for three and eight RF-cycles. However, the quantitative differences in the three radiation patterns are very minor. For this reason, to increase the longitudinal resolution of the SH-wave inspectin system, we have used the shortest pulse, three cycles.

For completeness, we also show typical transverse distributions of an ultrasonic beam generated by a SH-wave EMAT. In particular we show the transverse distributions at 520 kHz in Fig. 4-11 of the M=1 EMAT shown in Fig. 4-5. The measurements used an identical EMAT as a probe. (The results were corrected to account for the fact that the signal passes through two identical transducers.) An examination of the radiation patterns at zero and 45 degrees with respect to the surface normal shows that the two patterns are nearly identical and can be accurately predicted by simple theory. The close adherence of the two patterns also demonstrates the great repeatability of the measurements, a very desirable feature for synthetic aperture systems. (We have also shown that the EMATs preserve not only the amplitude, but also the phase of the received signals (King and Fortunko, 1983).) The above results demonstrate that the radiation properties of the PPM SH-wave EMATs are very well understood and can be custom-tailored to specific applications.

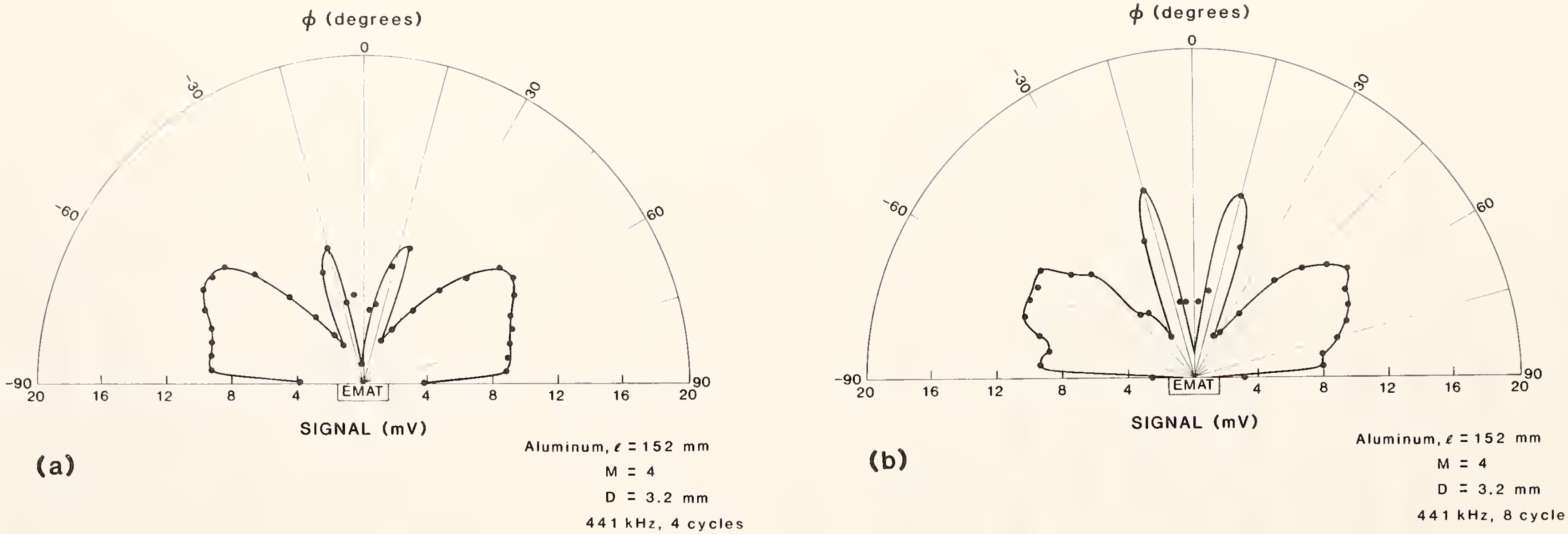

Figure 4-10: Radiation patterns of EMAT in Fig. 4-8. 441 kHz. (a) Four cycle tone burst. (b) Eight cycle tone burst.

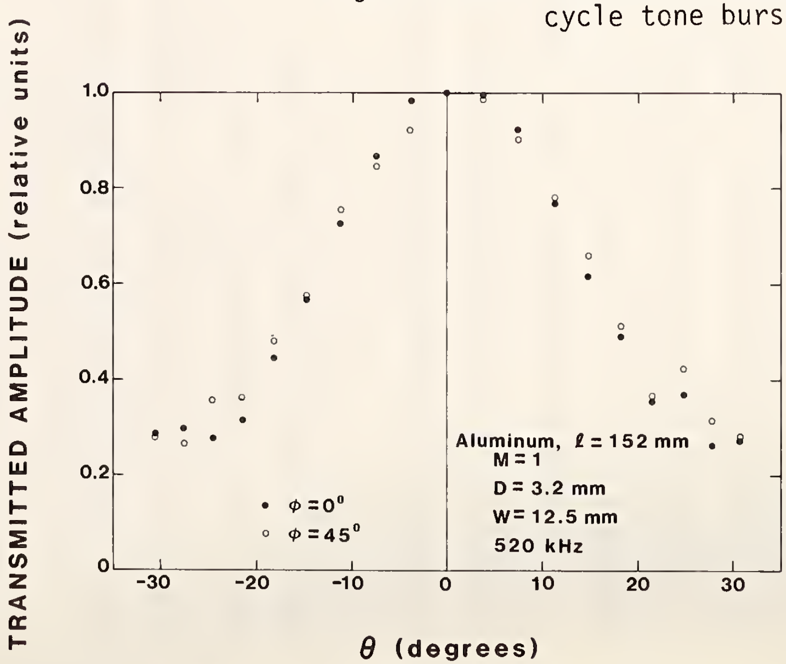

Figure 4-11: Transverse radiation distribution of M=1 EMAT (Fig. 4-5).

References

Fortunko, C.M., King, R.B. and Tan, M., 1982, Nondestructive evaluation of planar defects using low-frequency shear horizontal waves, J. Appl. Phys., 53: 3450.

Fortunko, C.M. and Schramm, R.E., 1983, An analysis of electromagnetic acoustic transducer arrays for nondestructive evaluation of thick metal sections and weldments, in: "Review of Progress in Quantitative Nondestructive Evaluation, Vol. 2," D.O. Thompson and D.E. Chimenti, eds., Plenum Press, New York.

King, R.B. and Fortunko, C.M., 1983, Determination of in-plane residual stress states in plates using horizontally polarized shear waves, J. Appl. Phys., 54: 3027.

Thompson, R.B., 1973, A model for the electromagnetic generation of Raleigh and Lamb waves, IEEE Trans. Sonics-Ultrasonics, 20: 340.

Thompson, R.B., 1977, Mechanism of electromagnetic generation and detection of ultrasonic Lamb waves in iron-nickel alloy polycrystals, J. Appl. Phys., 48: 4942.

Thompson, R.B., 1978, A model for the electromagnetic generation of guided waves in ferromagnetic metal polycrystal, IEEE Trans. Sonics-Ultraonsics 25: 7.

Vasile, C.F., and Thompson, R.B., 1979, Excitation of horizontally polarized elastic waves by electromagnetic transducers with periodic magnets, J. Appl. Phys., 50: 2583.

Chapter 5

TRANSDUCER ELECTRONICS

Design of Low-Noise Receiver Amplifiers for EMATs

The principal challenge facing the designer of an EMAT-based ultrasonic inspection system is the need to design an optimal receiver-EMAT to preamplifier interface. In particular, extreme care is necessary to ensure use of an efficient electrical impedance-matching network to minimize the preamplifier noise-figure. (The preamplifier converts the low-level output of an EMAT to a high level signal and drives a length of transmission line feeding the rest of the signal-processing chain.) Although this subject is treated in great detail in a number of specialized texts (Ott, 1976; Krauss, Bostian, and Raab, 1980; Clarke and Hess, 1971), it is useful to outline the impedance matching techniques that are particularly useful for matching SH-wave EMATs in the 400 to 1500 kHz region. It has been the authors' experience that these techniques are simple to implement and verify experimentally without sophisticated instrumentation.

Thermal noise generated by the random motions of electrons within the EMAT ultimately limits the sensitivity of the EMAT-based ultrasonic inspection system. However, in most cases of practical importance this ultimate sensitivity is not attainable because of other sources of electrical noise and ultrasonic and external electromagnetic interferences. Chapter 4 addresses limiting the influences of ultrasonic and electromagnetic interferences through proper SH-wave EMAT design. This chapter specifically addresses the problems associated with minimizing the amount of excess electrical noise that can exist due to improper design or implementation of the impedance-matching network connecting the receiver-EMAT to the receiver-preamplifier. In the present context, the term excess noise refers to all active and passive sources of electrical noise that contribute to a larger-than-one noise-figure in the receiver-preamplifier chain.

Figure 5-1 illustrates a very useful way of characterizing the noise performance of a receiver-EMAT/receiver-amplifier combination. A resistive sensor R_S is connected to a noisy amplifier represented by a noise-free amplifier and two equivalent noise sources I_N and V_N. The quantities I_N and V_N represent the current and voltage excess noise generated within the amplifier. An equivalent voltage source, V_S, represents the Johnson noise associated with R_S. Using the circuit shown in Fig. 5-1, it is straightforward to show that the noise-figure is minimized when the value of the resistor R_S is set equal to the ratio V_N/I_N. This ratio is in the range of 50 ohms for bipolar transistors and 500-1000 ohms for junction field-effect transistors (J-FETs), which are typically used as the front-ends of low-noise receiver-preamplifiers. Both types of transistors can be used in the 400 to 1500 kHz region. In our designs we have used J-FETs because of their biasing simplicity. Since the electrical impedance levels of our SH-wave EMATs are in

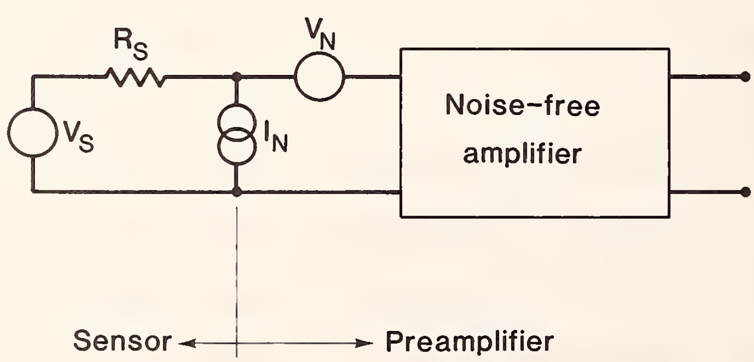

Figure 5-1: Idealized schematic of a receiver-amplifier system.

the range 5-15 ohm, an appropriate impedance transformer is necessary to obtain a 500-1000 ohm impedance level at the input to the receiver-preamplifier. Fortunately, this large transformation ratio is possible with properly designed transmission-line transformers (Krauss, Bostian, and Raab, 1980). This technique is preferred to resonant matching because it offers superior efficiencies and bandwidths compatible with the acoustic bandwidths of the SH-wave EMATs described in Chapter 4.

An example of a transmission-line transformer/J-FET receiver-amplifier chain is shown in Fig. 5-2. In this particular design, a chain of four transmission-line transformers, with 1:4 impedance-transformation ratios, matches the SH-wave EMAT to the input of the receiver-amplifier. The transformers are approximately 18 turns of #30 AWG bifilar wire on two 13-mm diameter toroidal ferrite cores with an initial permeability of 1000 (Krauss, Bostian and Raab, 1980). (It is interesting to note that the efficiency of the fourth transformer in the chain is degraded substantially because its magnetizing reactance is comparable to the optimum value of the source resistance R_S.)

In Fig. 5-2, the receiver-preamplifier is a two-stage design. The J-FET device in the first stage conditions the noise figure of the preamplifier while the second device acts as an active impedance transformer to the low-impedance (200 ohm) twisted-wire-pair transmission line that connects to the remaining signal processing chain. The overall voltage gain of this amplifier is approximately 12. Two sets of back-to-back diodes limit high-voltage signals that can exist when the transmitter-amplifier is active or when impulsive noise interferences are present. This is useful primarily when the receiver-amplifier can be located in close physical proximity to the receiver-EMAT and the output transmission line is very short (less than 1 meter).

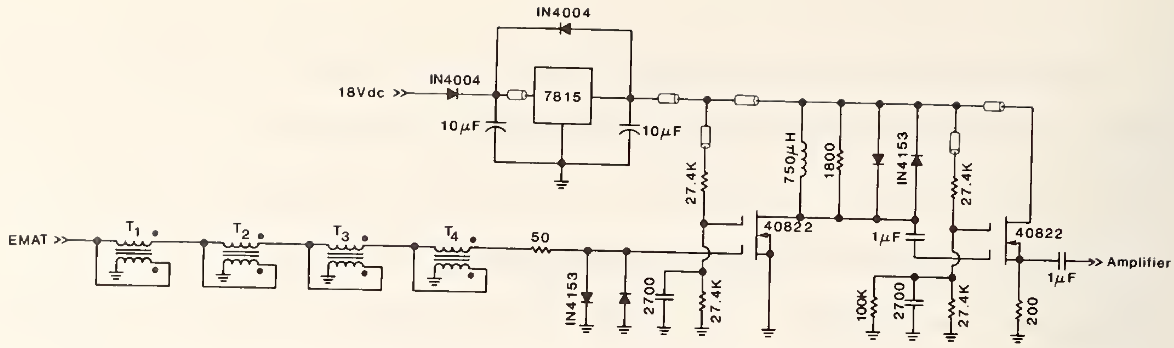

All resistors metal film, 1%

All resistances in Ω

All capacitances in pF unless otherwise noted

T_1, T_2, T_3, T_4 : 15 turns #30 AWG bifilar wire on two 13mm dia., 3D3 cores

Ferrite Beads

EMAT PREAMPLIFIER AND LINE DRIVER

Figure 5-2: Schematic of the transmission-line transformers and J-FET preamplifier used in the current work with a transmission line < one meter long.

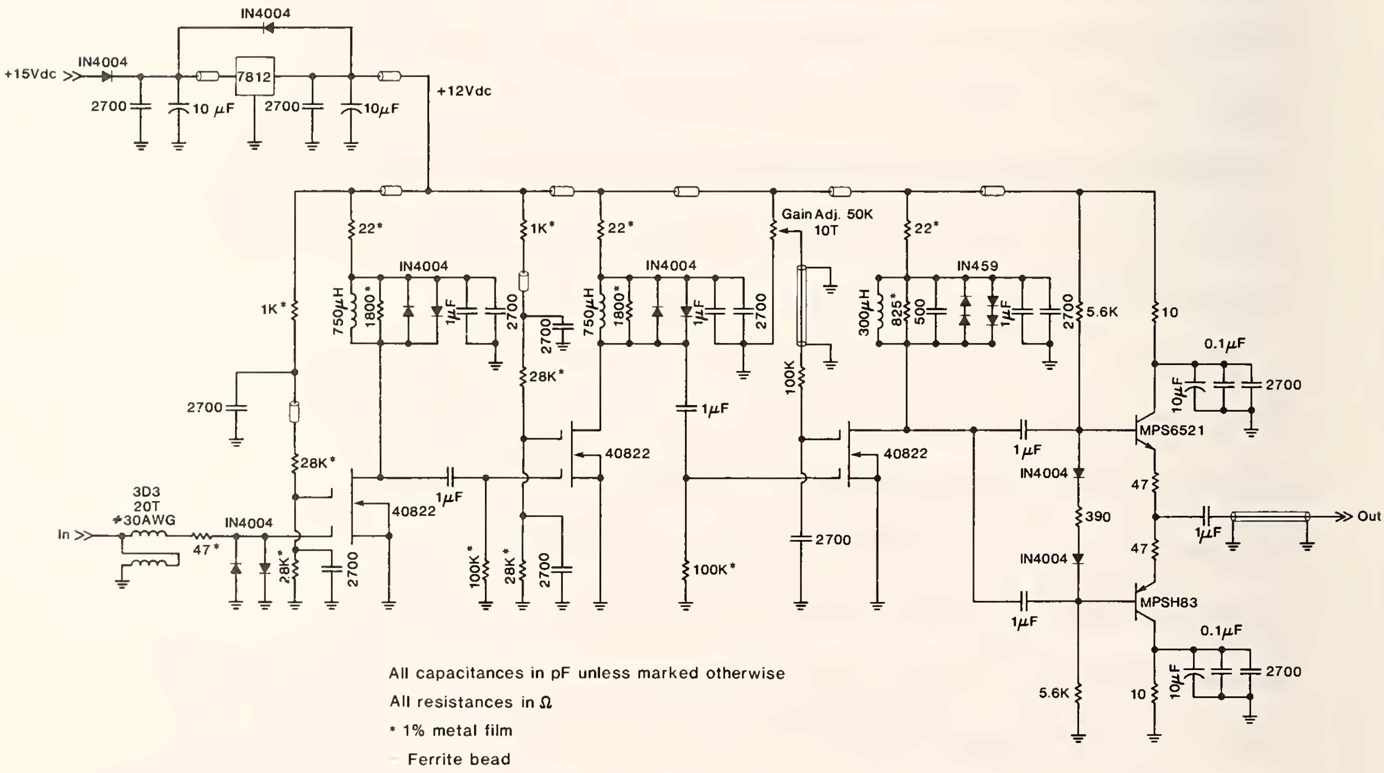

500 kHz EMAT PREAMPLIFIER

Figure 5-3: Preamplifier schematic. Useful for longer transmission lines.

A higher-gain receiver-preamplifier design useful for driving very long 50-ohm transmission lines is shown in Fig. 5-3. In this case only one input transformer is shown in the Figure, because the remaining three transformers are usually integrated directly within the EMAT housing. The individual mid-stages are tuned to a center frequency of approximately 500 kHz. Typical voltage gains are in the range of 500-1000.

Both amplifiers include an on-board voltage-regulated power supply and ferrite beads that help to minimize electromagnetic interferences. Metal-film resistors at the input stages in both designs reduce shot noise. In addition, good soldering practices eliminate contact noises. It is believed that both amplifier designs offer noise-figures in the range 3-4 dB when transformer losses are taken into account.

It should be noted that although the receiver-preamplifier designs shown in Figs. 5-2 and 5-3 utilize overload protection features, they are not well suited for operation in the pulse-echo mode in which the same EMAT acts as a transmitter and receiver of elastic waves. The transformers impose the principal limitation because they store a very substantial portion of the transmitter output energy. In spite of repeated efforts, we have not been able to devise a satisfactory scheme for designing a functional transmit-receive (T/R) switch for EMAT systems operating below 1 MHz. This remains one of the main obstacles to designing more compact, low-frequency, SH-wave-EMAT systems.

Design of Efficient Power Amplifiers for EMAT Applications

To maximize the conversion efficiencies for generating acoustic waves, both EMATs and piezoelectric transducers must be appropriately matched to their power amplifiers to ensure optimum utilization of the available transmitter power output. However, because piezoelectric transducers are generally much more efficient than EMATs and produce higher open-circuit voltages for a given surface displacement, the design philosophy of pulsers for driving piezoelectric transducers has been traditionally guided by spectral considerations and the voltage breakdown characteristics of semiconductor components used in capacitance-discharge circuits. (The possibility of depoling the piezoelectric drive elements traditionally sets the high-voltage limits.) As a consequence, resonant matching of piezoelectric transducers has not been widely used to maximize generation efficiencies.

The electrical characteristics of most EMATs, as viewed from the electrical input port, are significantly different from those of piezoelectric transducers designed primarily for NDE applications. Electromagnetic transducers generally behave as inductive loads, while the bulk capacitance of the piezoelectric crystal or ceramic drive element dominates the electrical input impedances of most piezoelectric transducers. (Reactances caused by mechanical motion of the elements themselves are generally smaller than the bulk capacitive reactance.) As a consequence, to maximize transduction efficiencies and optimize temporal responses, different electrical circuit configurations are necessary for EMATs and for piezoelectric transducers.

The conceptual differences between electrical circuits used for driving EMATs and those used for driving most piezoelectric transducer elements can be best illustrated by reference to Fig. 5-4, which shows the basic capacitive discharge circuit used in most commercial pulsers for driving piezoelectric transducer elements. Only six circuit elements comprise the circuit in Fig. 5-4a: 1) dc voltage source, V_C; 2) current limiting resistor, R_C; 3) ideal switch, S; 4) charging capacitor, C; 5) damping resistor, R_D; and 6) piezoelectric transducer, T. In operation, the capacitor C is first

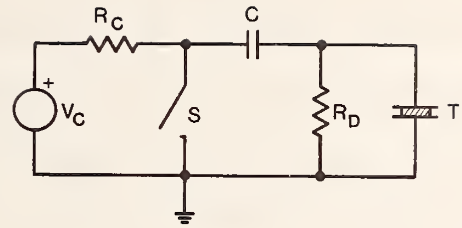

(a)

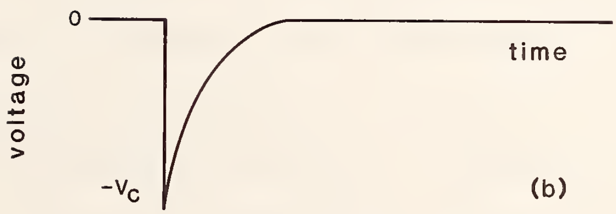

(b)

Figure 5-4: (a) Basic capacitive discharge circuit used in most commercial pulser designs for driving piezoelectric transducer elements. (b) Voltage waveform seen by transducer T.

charged through the resistors R_C and R_D. The maximum voltage is V_C. On closing the switch S, the capacitor discharges through the parallel combination of R_D and T. (It is assumed that $R_C >> R_D$.) The resulting voltage waveform V(t) at the electrical terminals of the transducer T is shown in Fig. 5-4b. V(t) first drops rapidly to a value that is approximately equal to $-V_C$. In practice, the non-ideal behavior of S and series inductances in the circuit determine the initial risetime. Then V(t) increases exponentially to the ground potential, as the charge initially stored by capacitor C discharges through the damping resistor R_D.

The major limitation of the circuit in Fig. 5-4a is that it is useful mainly for producing unipolar signals. As a consequence, the damping resistor R_D and switch S unproductively absorb most of the energy initially stored in the capactior C. Clearly, because of this inherent inefficiency, this circuit is not suitable for EMAT applications.

In many NDE applications using EMATs it is necessary to use gated bursts of RF to drive the transducer. For example, 4 cycles of RF are required to maximize the output of the EMAT in Fig. 4-8 when it is operated in an end-fire mode. (Here, it is assumed that the electrical Q of the EMAT is smaller than the acoustical Q.) Such applications require very efficient power amplifiers. Figure 5-5a shows an example of a circuit configuration that is inherently efficient and easily lends itself to EMAT applications.

Technically, the circuit configuration in Fig. 5-5a is a complementary, voltage-switching, Class-D power amplifier. However, this circuit includes extra components needed in a practical implementation. Those needed to assure Class-D operation are the two constant voltage sources V_B, the two ideal switches S_1 and S_2, and the series tank circuit composed of the EMAT and external capacitor C_4. The waveforms associated with the operation of this basic Class-D amplifier are shown in Fig. 5-5b.

The circuit shown in Fig. 5-5a operates as follows. The switches S_1 and S_2 alternately close and open at a fundamental frequency f_o. Ideally each switch operates at a 50% duty cycle. As a result of this commutating action, a square-wave voltage waveform V(t) (Fig. 5-5b) appears at the output of the amplifier, O. The series tank circuit, composed of the EMAT and series capacitor C_4, acts as a filter that presents the minimum impedance to the

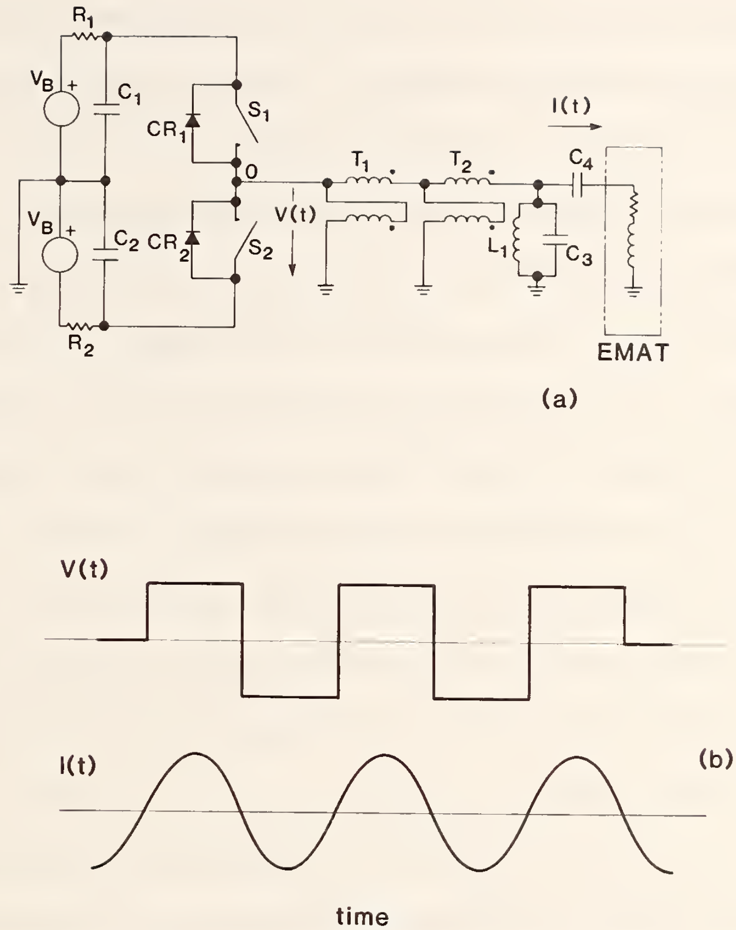

Figure 5-5: (a) Basic schematic of a power amplifier for a transmitter EMAT. (b) Voltage and current waveforms produced by this amplifier.

fundamental-frequency component of the applied voltage waveform. Ideally, the symmetry of the network in Fig. 5-5a ensures that the zeroth (dc) and even-harmonic terms of the Fourier series associated with the driving voltage waveform are not present. The resultant current waveform I(t) is shown in Fig. 5-5b and is nearly sinusoidal and free of even order harmonic components.

This circuit configuration is very efficient since there is no damping resistor and the switches dissipate little power because they drop very little voltage while passing maximum currents. Compared with a classical Class-B amplifier used in many RF transmitter designs, the Class-D can be 27% more efficient at similar maximum current/maximum voltage ratings (Raab, 1974). When implemented with practical switching devices, the performance of the Class-D circuit is, of course, subject to the effects of saturation, parasitics, finite switching times, and device breakdown considerations.

Because of practical considerations associated with the breakdown characteristics of semiconductor switching elements and the input impedance characteristics of typical EMATs, the circuit in Fig. 5-5a includes additional components: current limiting resistors R_1, and R_2, storage capacitors C_1 and C_2, protection diodes CR_1, and CR_2, impedance matching transformers T_1 and T_2, and a parallel tank circuit L_1-C_3.

The capacitor-resistor networks R_1-C_1 and R_2-C_2 provide sufficient energy for short RF bursts at the fundamental frequency f_o. In the event of a short, the resistors R_1, and R_2 limit the output current. The diodes CR_1 and CR_2 provide a path for inductively fed currents when both S_1 and S_2 are in the off position. (Cross-over distortion is used in many designs to reduce the potential of damaging the semiconductor devices used to implement the switches S_1 and S_2.) Finally, the circuit of Fig. 5-5a includes two high-power impedence matching transformers T_1 and T_2 and a parallel tank circuit L_1-C_3 tuned to the fundamental frequency f_o. The two transformers reduce the input impedance of the EMAT (tuned to frequency f_o by C_4) to match the low output impedance levels of the Class-D output stage while the tank circuit L_1-C_3 provides a bypass to ground for higher-than-fundamental harmonics.

Figure 5-6 shows a circuit diagram of a practical power amplifier designed to operate in the 300-600 kHz range. This particular amplifier can produce approximately 1500 W when used in conjunction with the SH-wave EMAT in Fig. 4-8. Figure 5-7 shows the physical construction of the two output power transformers T_1 and T_2. Both transformers are wound using 8 turns of small diameter, flexible coaxial cable (RG-174) on 9.3-mm outside diameter, Q-1-type ferrite cores. The large number of cores (24) prevents saturation. Figures 5-8 a and b are oscilloscope traces of the voltage and current waveforms at the output of the amplifier. The amplifier in Fig. 5-7 consumes approximately 2 W when operated at a 0.4% duty cycle. Figure 5-8b shows that at f_0=450 kHz the current waveform is sinusoidal, as expected, and the peak-to-peak current is 80 amperes. However, the voltage waveform is not square. This results from the finite switching and storage times of the high-power semiconductor devices used to implement the switches S_1 and S_2. (At 250 kHz, the output voltage waveform becomes nearly square.) The amplifier in Fig. 5-6 uses high-power, bipolar switching transistors, because faster devices with comparable breakdown characteristics were not available. Currently, the same amplifier could be implemented using high-power MOS-FET devices.

References

Clarke, K. E. and Hess. D.T., 1971, "Communication Circuits: Analysis and Design," Addison-Wesley, Reading, PA.

Krauss, H. L., Bostian, C.W., and Raab, F.H., 1980, "Solid State Radio Engineering," Wiley, New York.

Ott, H.W., 1976, "Noise Reduction Techniques in Electronic Systems," Wiley-Interscience, New York.

Raab, F. H., 1974, High efficiency RF power amplifiers, Ham Radio, 7:8.

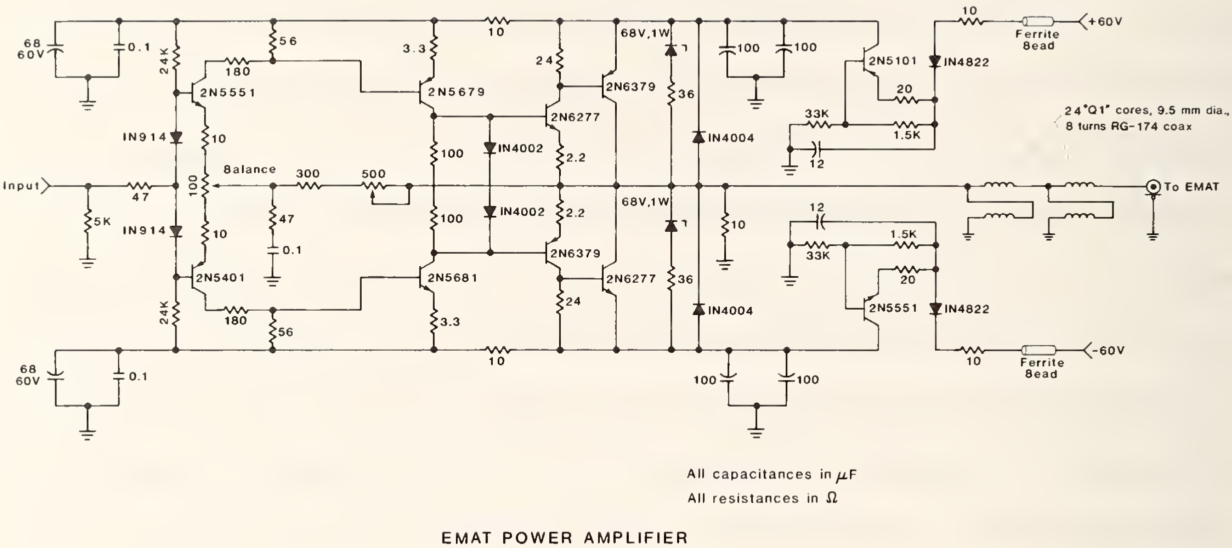

Figure 5-6: Schematic of amplifier for 300-600 kHz used in this work.

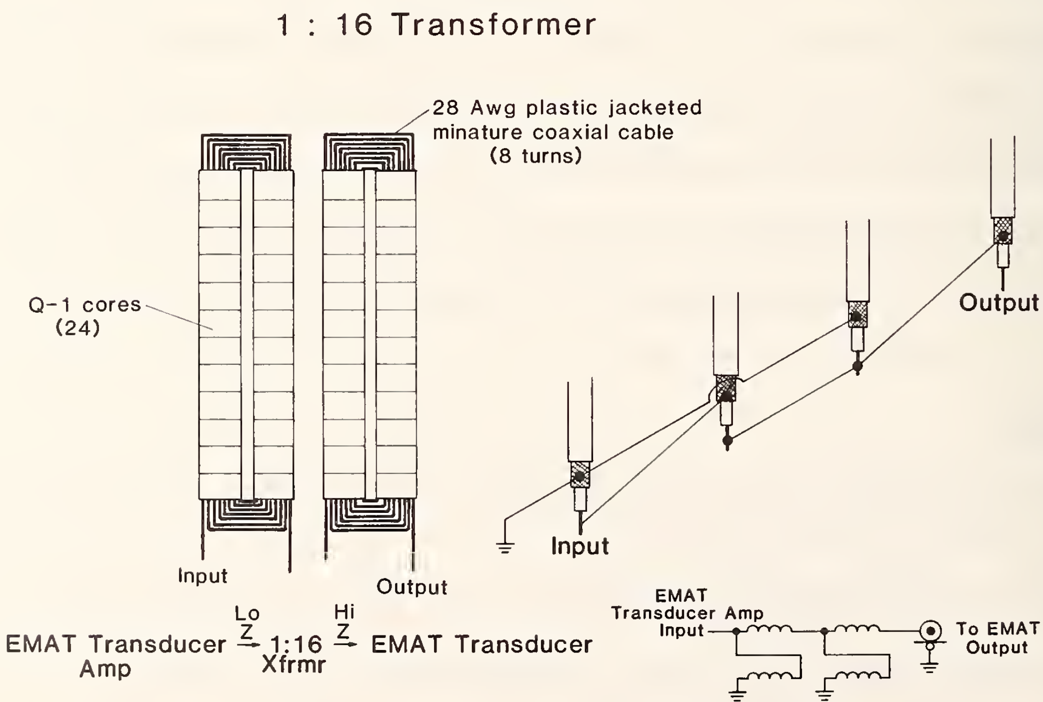

Figure 5-7: Construction of output power transformers used in the amplifier of Fig. 5-6.

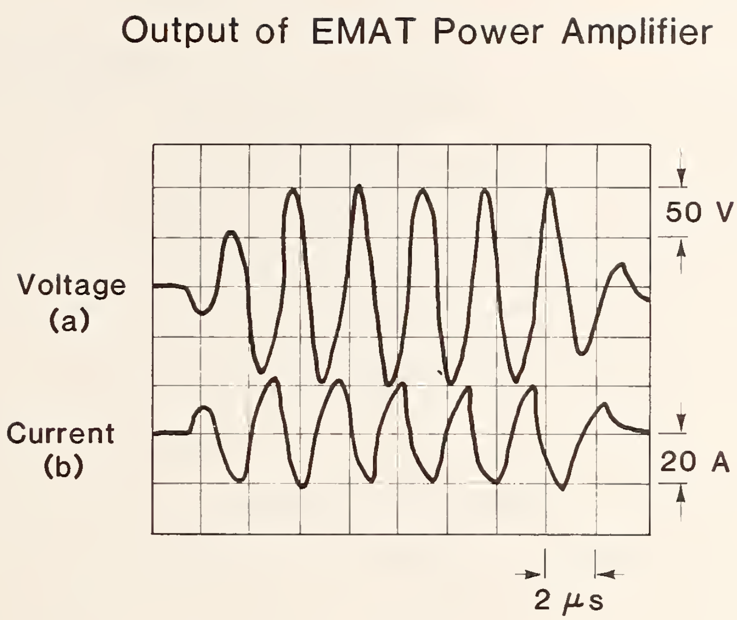

Figure 5-8: Oscilloscope traces of the output of the amplifier in Fig. 5-6. (a) Voltage. (b) Current.

Chapter 6

DIGITAL PROCESSING

Signal Averaging Method

The receiver EMAT signal is displayed on a digital oscilloscope that internally performs the initial time averaging. Since the background noise is mainly electronic and random, an average of 8 to 32 scope traces improves the S/N ratio and reduces the effects of impulsive interference. An IEEE-488 bus transfers the digital data to a minicomputer for storage and analysis.

Synthetic Aperture Method

The synthetic aperture focusing method and its advantages were discussed in Fortunko and Schramm (1983). It requires obtaining data from several locations along a scan line that is approximately normal to the long flaw dimension. From the geometric parameters and sound velocity information, it is possible to time-shift the individual waveforms so they combine coherently. In effect, the sound energy focuses at a particular resolution cell to be examined (Kino, et al., 1980). Subsequently, the same data can be reprocessed to change the location of the focal point (Fig. 6-1). Repetition of this process results in the interrogation of the whole weld in the direction normal to the surface. Only one set of ultrasonic data is necessary.

A practical problem limiting the method is the result of time quantization. Each of the 512 data points in an oscilloscope trace is the signal voltage at a discrete point in time. The time scale on the oscilloscope fixes the amount of time between these points. As a result, an integral number of sampling time intervals will not, in general, give the necessary time-shift. This may cause the appearance of unwanted spatial

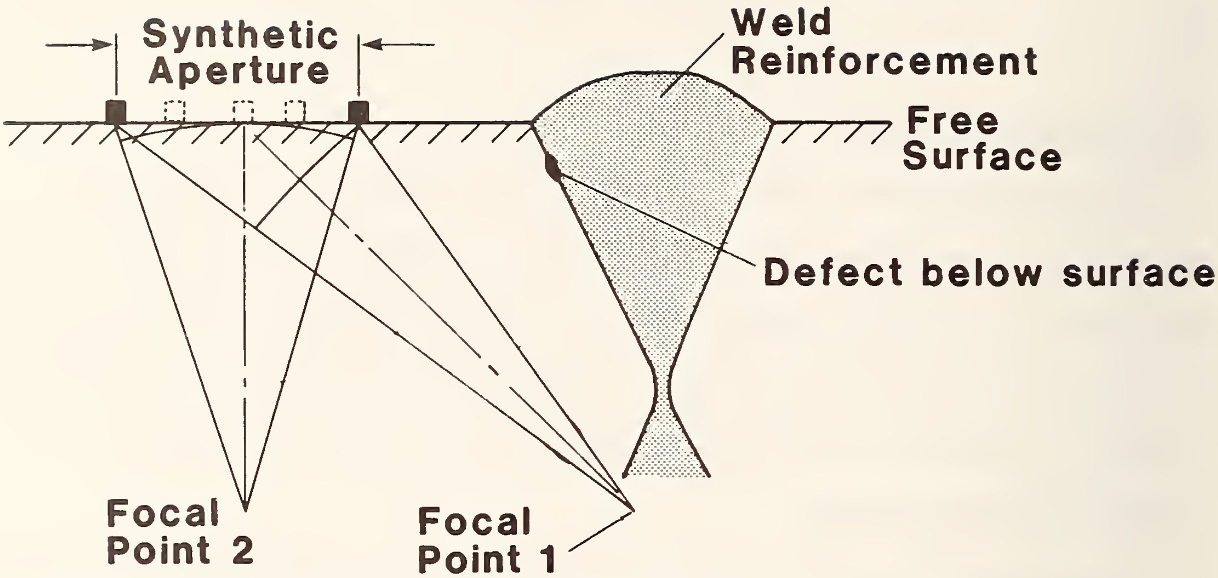

Figure 6-1: By repeated mathematical processing, the same data set can be brought to focus at multiple points.

sidelobes which would have to be eliminated by time-consuming interpolation techniques. Time-shifting in the frequency domain using a Fast Fourier Transform (FFT) overcomes the detrimental effects of time quantization. This takes full advantage of the 16 bit dynamic range of the computer. The transform yields a series of coefficients, $\vec{A}$, composed of real (Re) and imaginary (Im) parts. Multiplying the coefficients, $\vec{A}$, by a complex phase factor gives the effect of time-shifting (indicated by primes). Note Fig. 6-2.

$$\vec{A}' = \vec{A} \exp (j\omega\Delta t) = (Re + jIm)\,(\cos\omega\Delta t + j\sin\omega\Delta t)$$

So that $Re' = Re \cos\omega\Delta t - Im \sin \omega\Delta t$

$$Im' = Im \cos\omega\Delta t + Re \sin\omega\Delta t$$

where $j = \sqrt{-1}$, Δt = change in path length/sound velocity, $\omega = n(2\pi f_o)$, n = harmonic number of Fourier coefficient, and f_o = 1/measurement period (the oscilloscope display sweep time).

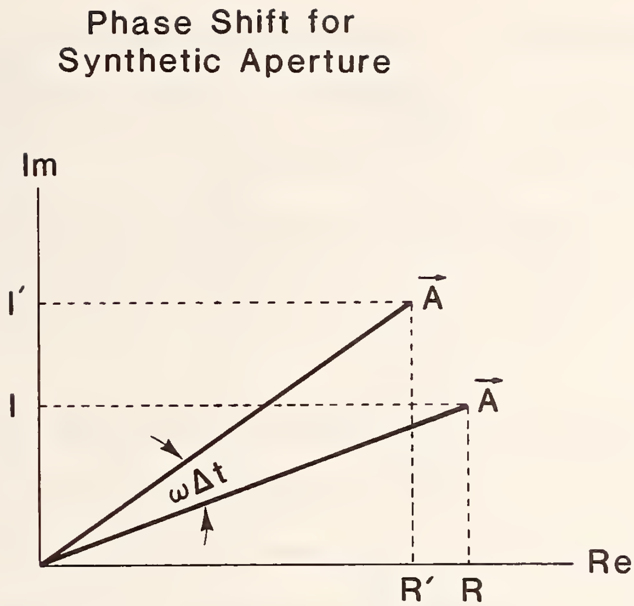

Figure 6-2: Phase shift of Fourier coefficients in the real-imaginary plane.

For convenience, the transducer postion nearest the focal spot usually serves as the reference point (forward shift). Conversely, for a backward shift, the reference becomes the position farthest from the focus. Simple trigonometry determines the change in ultrasound path length at other transducer positons. The oscilloscope produces 512 eight-bit samples for each trace (the values of n range from -256 to 255). Thus, for a typical time scale, the total measurement period is 51.2 μs and the frequency step in the FFT (f_0) is about 19.5 kHz. Since the input data are entirely real, there are FFT symmetry relations that reduce the mathematical manipulations by half (Bergland, 1969).

Examination of the FFT coefficients can reveal electromagnetic noise at other than the operating frequency. The application of suitable windows

(Oppenheim and Schafter, 1975) and other techniques (Taylor, 1983) can minimize this problem. In particular, zero padding the base band can eliminate the effect of dc ground loops.

After time-shifting, the coefficients from each data set are added, and the result is normalized and reverse transformed to produce a reconstructed time signal.

Scanner Control and Ultrasonic Data Collection and Processing

Figure 6-3 is a flowchart of the BASIC computer program used to synchronize the operation. Detailed listings are in Appendix I and an example of typical operator-computer interactions is in Appendix II.

One of the main functions of the computer program is control of the mechanical scanning mechanisms (Chapter 7) that determine the EMAT positions on the surface of the part under inspection. To accomplish this, the computer program transfers appropriate control codes from the main minicomputer to a special, microprocessor controlled, subsystem that directly controls the power supplies of the stepper motors. The master minicomputer transmits the digital codes to the slave microcomputer via an industry-standard IEEE-488 bus.

Another primary function of the computer program involves collecting and processing ultrasonic signals. Because of very high electrical noise levels, the data collection and processing is possible only while the stepper motor power supplies are inactive. When the EMATs are stationary, the computer program executes a data collection and processing sequence.

The first decision block in Fig. 6-3, determines whether to collect and process new ultrasonic data or to recall previously recorded data. The next block allows the console operator to input signal processing and scanner control parameters. Figure 6-4 illustrates the meaning of various geometrical parameters.

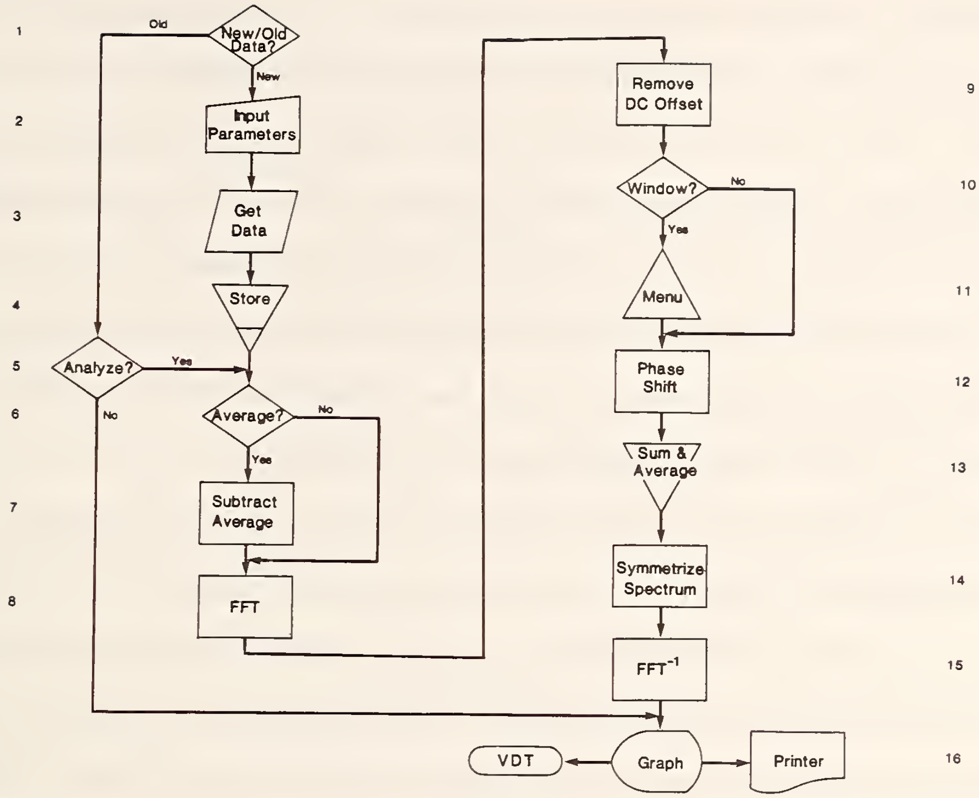

Figure 6-3: Flow chart of computer program used to collect, store, process, and display synthetic aperture data.

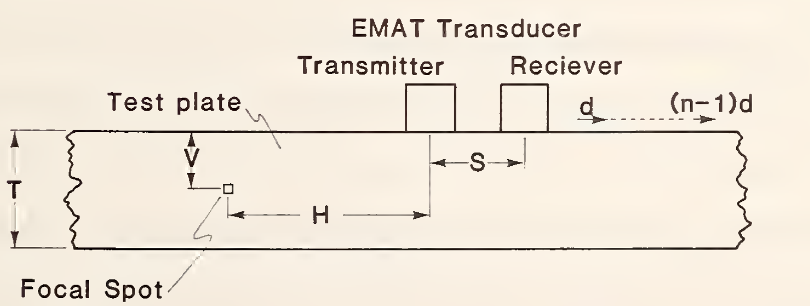

n = number of transducer positions

d = distance between transducer positions

S = separation between transmitter and reciever

T = plate thickness

H = horizontal distance between initial transmitter position and focal spot

V = vertical depth of focal spot

Figure 6-4: Geometrical parameters required for synthetic aperture processing.

The input block (3) in Fig. 6-3 involves reading the output of the digital oscilloscope and transferring it to magnetic memory (standard 8-inch diskette). Since the oscilloscope settings are not externally adjustable via the IEEE-488 bus, manual adjustment of control knobs on the front panel is necessary. Parameters in this category include the trigger time delay, sweep rate, vertical amplifier sensitivity, and the number of time-averages. After storing the data, the program instructs the scanner controls via the IEEE-488 bus to move the EMAT search head to the next location.

The next query (6) allows the operator the option of subtracting a coherent background from the ultrasonic data. Elsley and Fortunko (1981) discuss the rationale for this step in detail. This allows the operator to remove from the new data certain common features such as transducer reverberations and reflections from common geometrical artifacts. It is particularly useful in the inspection of simple weldments whose profile does not vary along the transverse scan direction. The option is implemented by first digitally averaging many sets of data from different EMAT positions and, then, subtracting the average from each of the individual data sets.

If the option in step 6 is not selected, then the program moves directly to the digital computation of the discrete Fourier transform (DFT) of each of the individual data sets in step 8. The DFT is carried out using a library-function fast Fourier transform (FFT) algorithm. At step 9, zero-padding removes the central (dc) coefficient (assuming a two-sided transform). This step helps to remove ground loop and dc offset effects that exist in the analog electronics. The results are stored magnetically along with the original ultrasonic data.

The next query in the program involves a window option in the frequency domain. Several different window are available, including Bartlett and

Hanning (Oppenheim and Schafter, 1975). This option supplements the analog band-pass filters in the receiver EMAT preamplifier chain. However, it is seldom used, and can be bypassed.

Steps 12-14 involve the actual implementation of the synthetic aperture algorithm that is the heart of the computer program. First, the FFTs corresponding to different data sets are phase shifted as determined a-priori from a knowledge of the EMAT positions and details of the scan parameters (e.g., plate thickness, scan length). The phase-shifted FFT's are then added together and renormalized in step 13. The resultant FFT thus represents an ultrasonic data set as obtained by a single array composed of N EMATs that are connected in-parallel acoustically. Because the output waveform from such an array must be real the resultant FFT is symmetrized in step 14 such that the complex conjungate of the negative frequency spectrum is identical to the positive frequency spectrum (Bergland, 1969). After reverse transformation the results are stored magnetically and then are available through the display routines in step 16.

Several forms of output are available, many recorded only to allow a check of the process at this still-experimental stage. Graphical displays include:

1. Original raw data (and averaged data if this option was exercised), as well as the processed result (Fig. 6-5).
2. Fourier coefficients, as transformed, shifted, or averaged (Fig. 6-6).
3. Signal power as a function of frequency (power = $(\text{Real}^2+\text{Imaginary}^2)^{\frac{1}{2}}$), (Fig. 6-7).

All of these graphs can be transferred from a VDT to a printer.

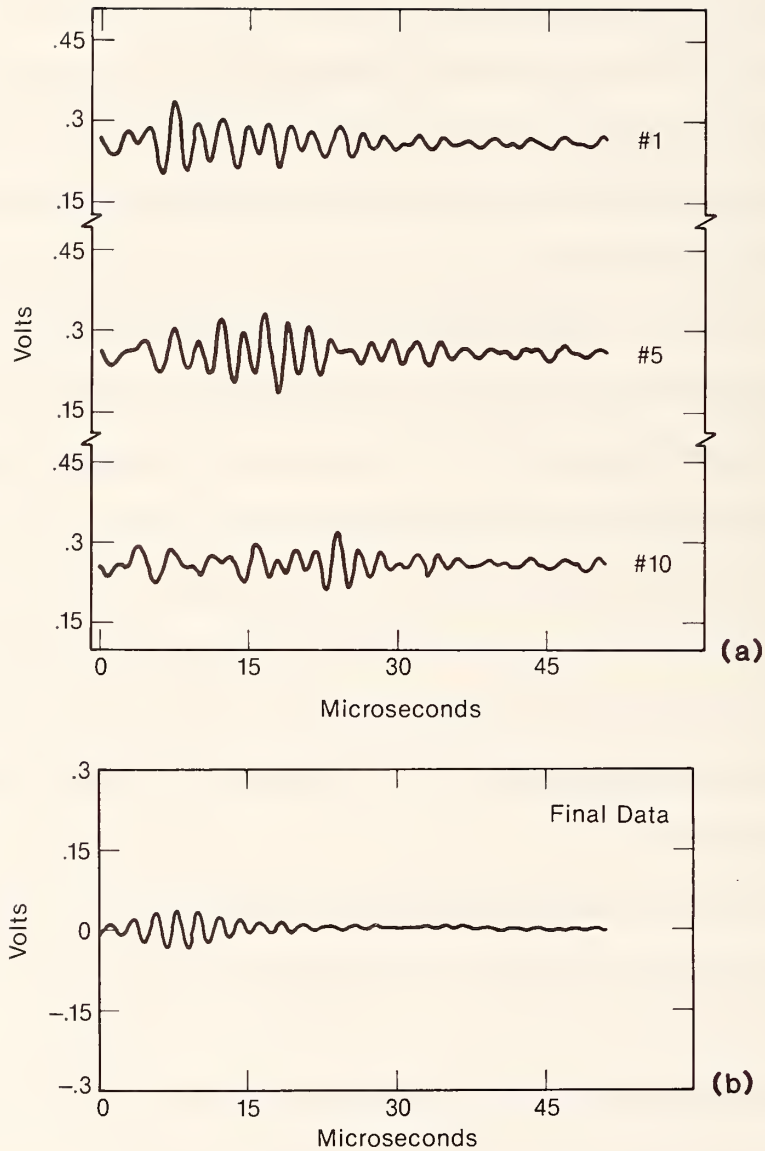

Figure 6-5: (a) Three sets (out of ten) of raw signal data.
(b) Signal after synthetic aperture processing.

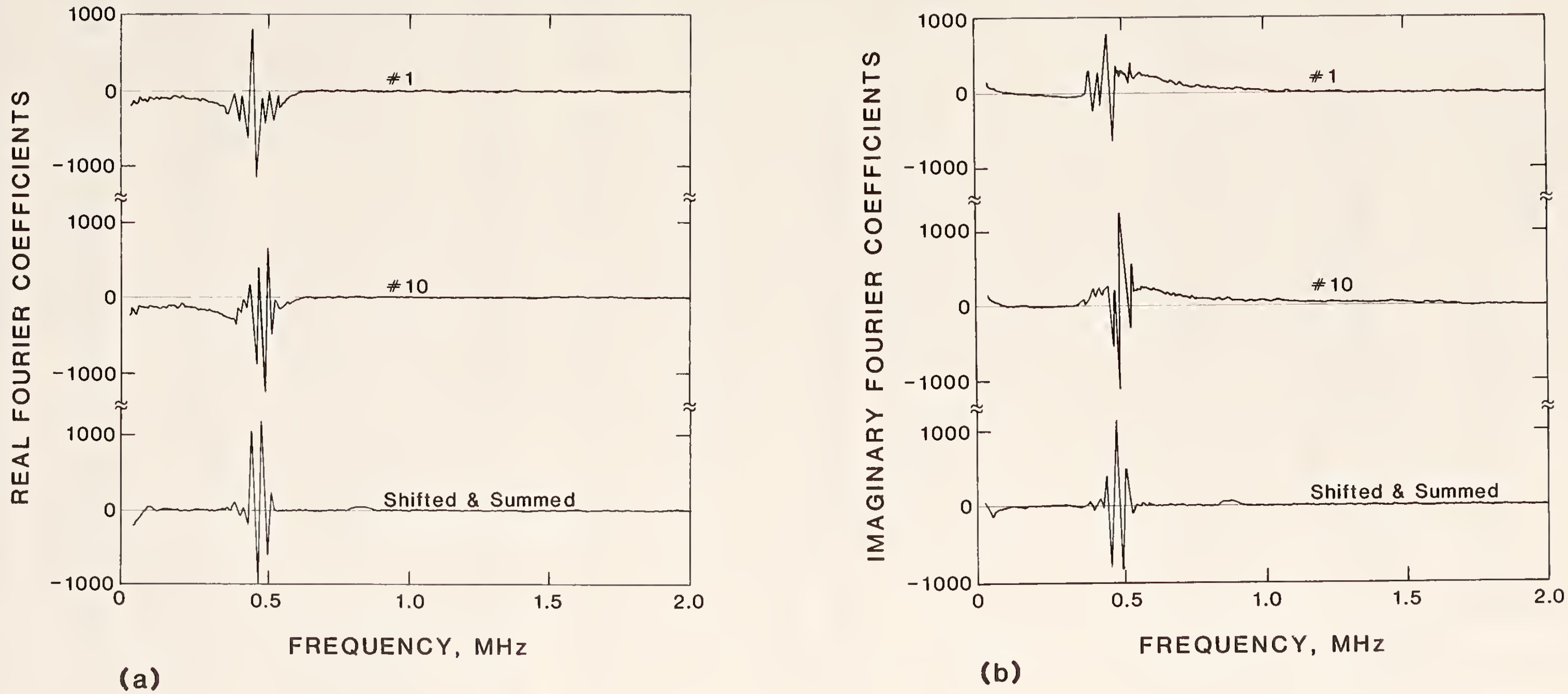

Figure 6-6: Typical Fourier coefficients for some raw data sets and after processing. All the information is centered about the operational frequency of 450 kHz. (a) Real. (b) Imaginary.

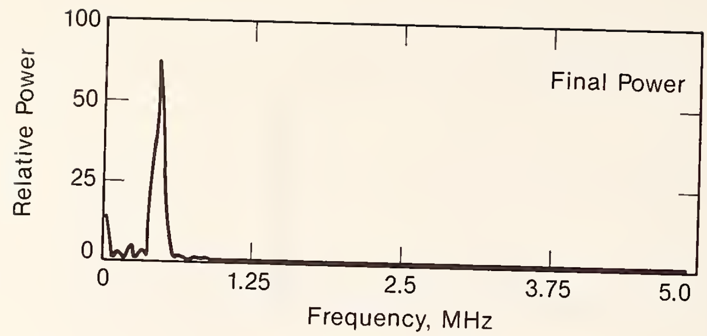

Figure 6-7: Power distribution of processed signal.

Numerical outputs include:

1. Signal amplitude of the raw or processed data.

2. Total relative power represented by any data set.

See Appendix II for a typical run.

References

Bergland, G.D., 1969, A guided tour of the Fourier transform, IEEE Spectrum 6(7):41.

Elsley, R.K., and Fortunko, C.M., 1981, Improvements in flaw detection in austenitic stainless steel weldments, in: "Proceedings of the IEEE Ultrasonics Symposium," B.R. McAvoy, ed., IEEE, New York.

Fortunko, C. M. and Schramm, R. E., 1983, An analysis of electromagnetic acoustic transducer arrays for nondestructive evaluation of thick metal sections and weldments, in: "Reveiw of Progress in Quantitative Nondestructive Evaluation, Vol. 2," D.O. Thompson and D. E. Chimenti, eds., Plenum Press, New York.

Kino, G.S., Corl, D., Bennett, S., and Peterson, K., 1980, Real time synthetic aperture imaging system, in: "Proceedings of the IEEE Ultrasonics Symposium" B. R. McAvoy, ed., IEEE, New York.

Oppenheim, A.V., and Schafter, R.W., 1975, "Digital Signal Processing," Prentice Hall, Englewood Cliffs, NJ.

Taylor, J.S.W., 1983, Digital techniques for enhancing and processing dynamic stress-analysis data, Exp. Tech 7(6):31.

Chapter 7

MECHANICAL APPARATUS

In order to make routine use of the synthetic aperture technique discussed in Chapter 6, it is necessary to have some means of positioning the EMATs accurately and reproducibly, under computer control. Additionally, a rugged transducer housing is required to maintain proper alignment of the transmitter and receiver EMATs on the surface of the weldment and to provide electromagnetic shielding. In this chapter we describe the gimbaled transducer housing and the computer-controlled, two-axis positioner that were designed for the new weld inspection system.

Gimbal-Mounted Transducer Housing

At low frequencies it is difficult to use the same EMAT for both generating and detecting ultrasonic waves, owing to the problems encountered in designing a satisfactory transmit/receive switch (see Chapter 5). It is therefore necessary to use separate EMATs for the transmitter and receiver. The preferred configuration is to position the two transducers symmetrically with respect to a common sagittal plane as in Fig. 6-5. If the transducers are to be mounted in the same housing, some freedom of motion must be provided in the mounting arrangement to allow them both to conform to the surface of the weldment. Often the surface of a weldment is deformed in the vicinity of the weld by the action of residual stresses and the transducer housing must be able to accommodate such deformation without one of the transducers lifting off the surface.

A gimbal mount, shown in Fig. 7-1, provides the freedom of motion necessary to ensure that the EMAT coils and magnet assemblies conform to the surface of the plate under inspection. The gimbals' two axes of rotation are

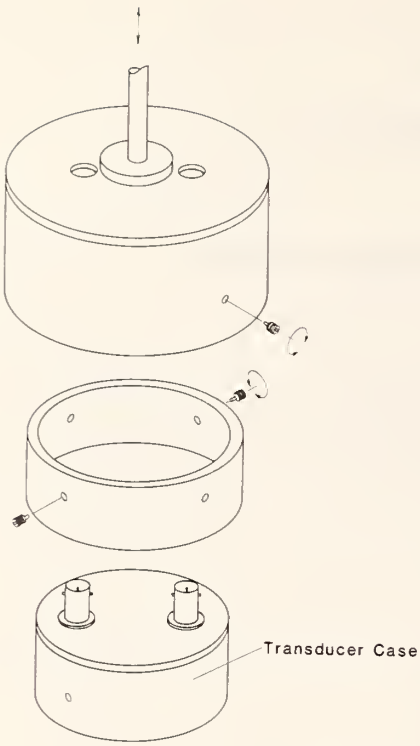

Fig. 7-1: Gimbal-mounted transducer housing for both transmitter and reciever EMATs. The two axes of rotational freedom allow the probe surface to conform to the plane of the plate under inspection.

mutually orthogonal and parallel to the free surface of the plate. A third degree of freedom perpendicular to the plate's surface is provided by attaching the gimbaled transducer case to a pneumatically driven piston that can raise or lower the entire assembly under computer control.

Raising and lowering of the transducers is accomplished by reversing the air pressure supplied to the two sides of the piston with a solenoid-operated valve. Power is supplied to the solenoid valve through a relay controlled by the computer. As the transducer housing is lowered onto the plate, free rotation about the gimbals' axes allows the EMATs to contact the surface uniformly. The pneumatic piston and the transducer housing are shown in Fig. 7-2 mounted on the two-axis positioner. The shaft connecting the piston and the transducer housing passes through a bearing sleeve to ensure that raising and lowering the transducers does not degrade the positional accuracy of the assembly.

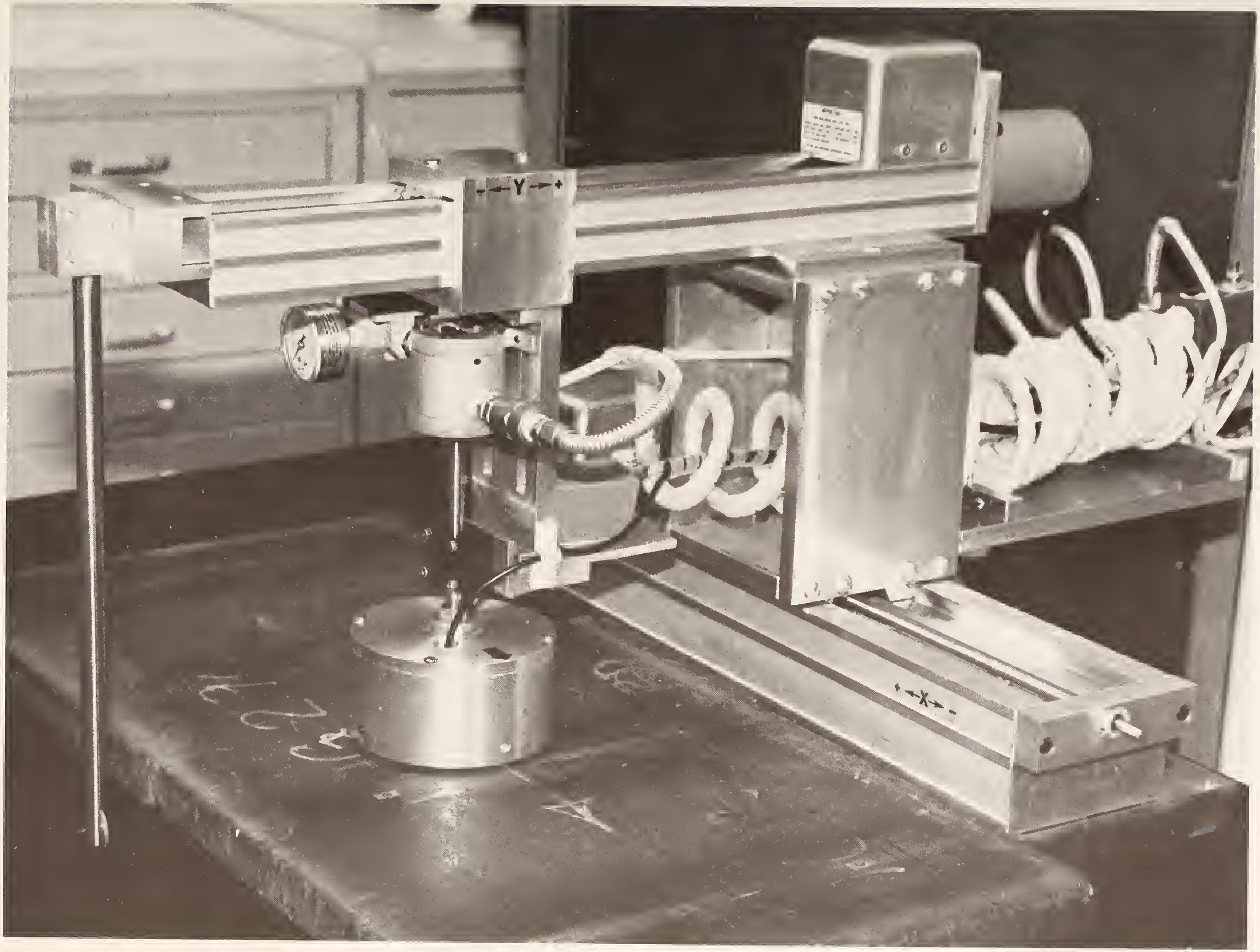

Figure 7-2: Transducer housing attached to pneumatic piston and suspended from the two-axis positioner operated under computer control.

The cylindrical transducer case was machined from mild steel and divided into two compartments by welding a steel plate across the diameter of the cylinder. Rectangular openings were milled into the bottom of each compartment for the EMAT coil and magnet assemblies (Fig. 4-8), which were carefully aligned with each other and then epoxied into place. Dividing the case into two compartments provides a certain degree of electromagnetic shielding of the receiver EMAT from the transmitter EMAT. The bottom of the transducer case is covered with stainless steel tape approximately 0.1 mm-thick. The tape provides excellent protection from abrasion of the EMAT coils when sliding the transducers along the surface of the plate, yet has a minimal effect on the signal strength.

(At the time of this writing, the control logic to operate the pneumatic valve has not been written into the software system in Appendix I. For the work reported here, the transducers have been simply pulled along the plate surface between data collection points. The stainless steel tape over the EMAT coils has proven to be effective wear protection.)

There is sufficient room in the transducer case to permit the impedance-matching components to be mounted in close proximity to the EMATs. The transmitter EMAT is series-tuned with a capacitor so that is presents a purely resistive load to the power amplifier at the frequency of operation. The receiver EMAT has a gang of four 4:1 transformers mounted inside the transducer case to match the impedance of the EMAT to the input impedance of the preamplifier, as discussed in Chapter 5.

Two-Axis Positioner

The two-axis positioner that is used to scan the plate under inspection is shown in Fig. 7-2. It consists of two commercially available precision lead screw translators driven by dc stepping motors. The two lead screws are mounted orthogonally, with the transducer housing and pneumatic piston fixed to the translation stage of one of the lead screws. The total range of travel on either axis is approximately 230 mm, which is adequate for a laboratory system such as this. Adjustable limit switches located at each end of the lead screws provide a means to prevent jamming the drive mechanism. When one of these limit switches is engaged, a dc voltage is applied to a Schmidt-trigger on a module in the minicomputer, activating an interrupt routine (not yet written into the software of Appendix I) that cuts off power to the stepper motor.

The pitch of the lead screws is 1.58 threads/mm (40 threads/in) and the stepping motors provide a resolution of 400 steps per revolution when operated in the "half-step" mode. This results in an overall resolution of 1.6 micrometers. Naturally, the accuracy with which the transducers can be positioned is degraded by hysteresis in the mechanical linkages, but independent measurements indicate that the positioning accuracy is better than ± 0.1 mm. Since the wavelength of the ultrasonic waves is ~ 7 mm, the precision afforded by the positioner is sufficient for the purpose of synthetic aperture processing.

Electronic controls for the two-axis positioner were also obtained commercially. Necessary components include: dc power supplies for each motor and the control electronics, printed circuit driver cards for each motor, indexer cards to provide properly sequenced phase control signals for the driver cards and an IEEE-488 interface card that links the computer to the controller. Actual command sequences used to position the transducers may be found in the software listings in Appendix I.

Chapter 8

MEASUREMENTS

Preparation of Calibration Specimens

To evaluate the intrinsic and operator-dependent sensitivity limits and other performance parameters of the 450-kHz SH-wave EMAT system, we have prepared a special 25.4-mm thick flat-plate calibration specimen, Fig. 8-1, of HY-80 steel supplied by the U.S. Navy. It contains a family of ten 0.25-mm-wide electric-discharge-machined (EDM) slots, all located on the same surface. The plate was used as-received (with protective paint on the surface) without any additional surface preparation. This is very significant since, in a practical application, the SH-wave EMAT system would be expected to operate on similarly unprepared surfaces.

The calibration specimen's width (330 mm) and length (660 mm) eliminate the end-reflection effect on the ultrasonic data. Table 8-1 summarizes the individual calibration-slot dimensions as determined by plastic replica techniques. The letter codes (A through J) denote the slot locations in Fig. 8-1. The slot dimensions span the range of weld flaw sizes that would be of interest from a practical viewpoint (i.e., sharp flaw dimensions typically found at weld root and toe region). These dimensions also correspond to the initial assumptions made in the system design parameters (i.e., EMAT dimensions and operating frequencies). Thus, to separately evaluate the system sensitivity limitations with respect to flaw depth and surface length, the artificial flaws in Table 8-1 form three sets. The first set (A,B,C,D,E,I,and J) has a surface length of approximately 25 mm and depths ranging from 0.48 mm to 6.68 mm. The second set is flaws (C,D,G,H) with a depth of approximately 1.75 mm, but a surface length ranging from 12.8 to

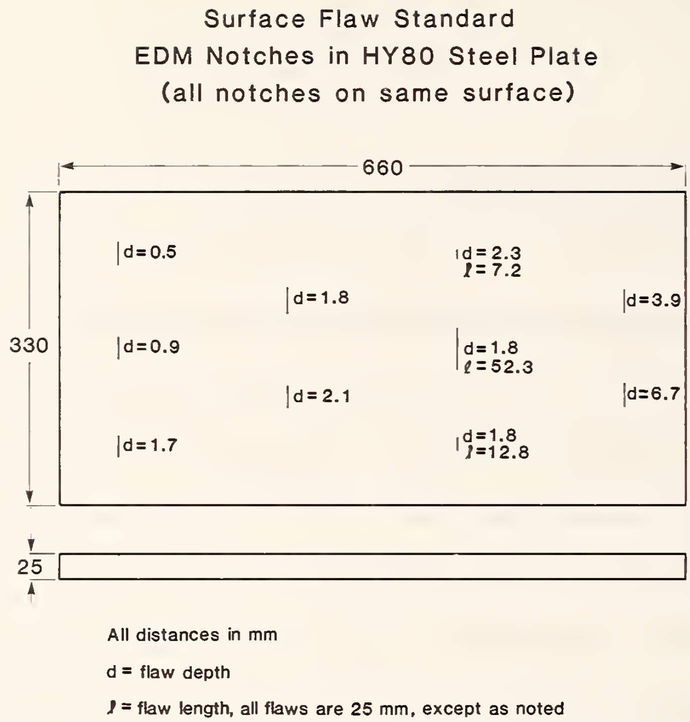

Figure 8-1: Calibration plate with EDM notches.

Table 8-1: Dimensions of EDM notches in calibration plate.

EDM Slot Label	Slot Surface Length, mm	Slot Depth, mm
A	25.7	0.48
B	25.4	0.91
C	25.1	1.68
D	25.7	1.76
E	24.9	2.14
F	7.2	2.29
G	52.3	1.78
H	12.8	1.78
I	26.2	3.94
J	25.2	6.68

52.3 mm. The Third set contains only one flaw (F), which is 2.29 mm-deep and only 7.2-mm long along the surface.

In the design of the calibration specimen shown in Fig. 8-1 considerable attention went into properly choosing the individual flaw positions. For example, note that the slots stagger through the width of the plate to avoid data contamination by end-effects and mutual interferences. In addition, the distances between the slots along the specimen length are sufficiently large to permit SH-wave EMAT-system operation in the synthetic aperture mode, needed to remove the effects of unwanted ultrasonic reverberations and certain electromagnetic phenomena (e.g., direct and impulsive noise) from the processed ultrasonic scattering data.

The surface calibration slots in Table 8-1 are vertically oriented with respect to the plane of the plate. Consequently, they present the maximum cross-section to the ultrasonic beam, aimed parallel to the plane of the plate. Canted slots were not possible because of physical limitations of the EDM equipment. At project inception, provisions were also made to fabricate a representative family of interior flaws by in-welding procedures similar to those described in Fortunko and Schramm (1983). However, such interior flaws were not available because of scheduling difficulties at an independent research laboratory collaborating in the project. Hopefully, the additional tests will be possible in the future using the present SH-wave EMAT system.

Experimental Procedure

The experimental procedure, used to obtain the ultrasonic signals from the calibration plate in Fig. 8-1, was specially designed to take full advantage of the synthetic aperture capabilities of the inspection system. To maximize the number of independent ultrasonic measurements, each slot was illuminated ultrasonically while located on the top and bottom surfaces of the

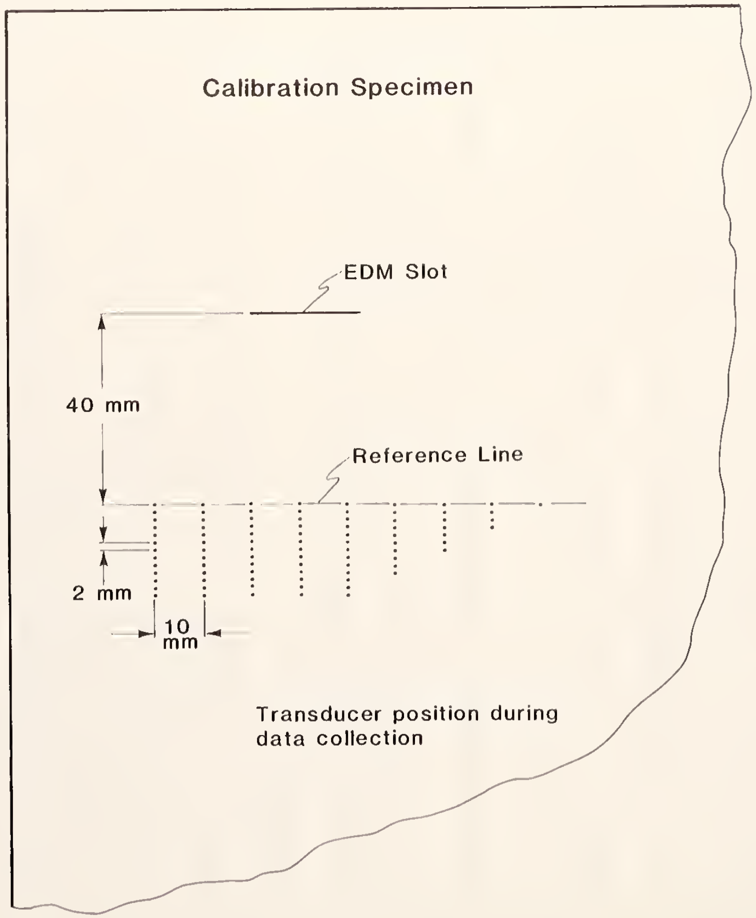

Figure 8-2: Detailed scan pattern used for data collection.

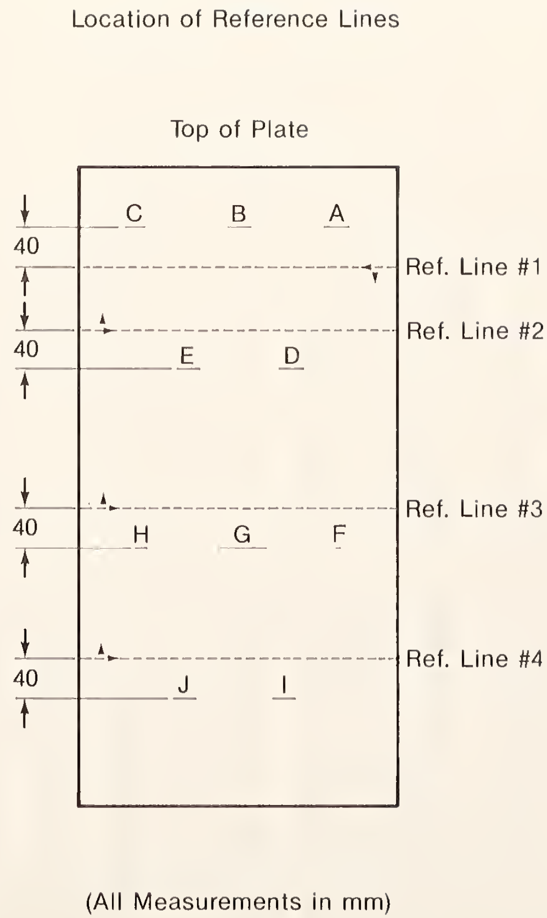

Figure 8-3: Scan pattern used when the slots were on the same side of the plate as the EMATs.

plate (with respect to the EMAT location). In addition, the slots located in the central portion of the calibration specimen were scanned ultrasonically from the right and the left with respect to long slot dimensions. It was possible to scan the slots A,B,C,I, and F from only one side due to an inadequate separation from the specimen ends. Figure 8-2 shows the scan pattern for moving the EMAT-pair ten to fifteen 2-mm steps along the direction normal to the long slot dimensions, and 10-mm steps along the orthogonal direction. The ultrasonic data from each scan-cycle was stored on magnetic media, but not processed. (At each scan location the digital oscilloscope calculated 16 to 32 time-averages before transmitting the data.)

Figure 8-3 shows the detailed scan-pattern used to interrogate slots located on the same surface as the EMAT scanning head. Also shown are the reference lines used in the synthetic aperture reconstruction process as well as the starting points and initial directions of individual scans. (Digital processing details used are given in Chapter 6.) It should be noted that in all cases the reference lines are 40 mm away from the slots, a distance corresponding to the recovery time of the EMAT receiver-amplifier following the transmitter-amplifier pulse. With the plate turned over and the EMATs on the side opposite the slots, the scan pattern and procedures were identical.

Evaluation of Surface Slot Scattering Measurements

Data reduction included the synthetic aperture process and filtering to remove unwanted artifacts caused by electromagnetic interferences (Chapter 6). After this we ploted the peak-to-peak signal voltages and integrated power (computed in the frequency-domain by summing the squares of the Fourier coefficients in the carrier-frequency neighborhood) from the reconstructed signals as a function of position along the scan lines. The results in Figs. 8-4 and 8-5 correspond to the slot-up reference lines in Fig. 8-3. The vertical dotted lines indicate the flaw extremes. It is interesting first to examine the data on a figure-by-figure basis. This is helpful in identifying certain common features and systematic trends in the data that will help later to develop a chart defining the performance limits of the 450-kHz SH-wave inspection system with respect to detection and dimensioning of surface flaws. Of course, similar procedures are equally applicable to defining the system's performance limits with respect to other types of flaws. While examining the data in the figures, it is helpful to refer to Table 8-1, which summarizes the dimensions of the calibration slots. The results for the case of the EMATs and calibration slots located on opposite sides of the plate are very similar and not shown.

Before evaluating the individual data sets in detail, it is important to note the common ultrasonic noise floor in all of the figures. This is probably due to ultrasonic reverberations in the calibration plate and not electronic noise. The fact that the mean level of the noise floor is the same in all the figures is important since it reinforces our claim of high measurement reproducibility for the SH-wave inspection system. The noise floor in Figs. 8-4 and 8-5 determines the minimum detectable flaw sizes. A caution here, however, is that these measurements are on a plate with no surface irregularities. With a weld reinforcement, weld root, etc, present, the noise floor may be higher. The scattering data obtained along reference line 1 (Fig. 8-3) are in the top half of Figs. 8-4a and 8-5a. The three flaws along this line (A, B, and C) are of approximately equal surface length (25 mm), but have depths ranging from 0.48 to 1.68 mm. The voltages and powers of the reflected signals exhibit a monotonic increase with flaw depth. This is an obviously desirable effect, and is a basis for flaw dimensioning in

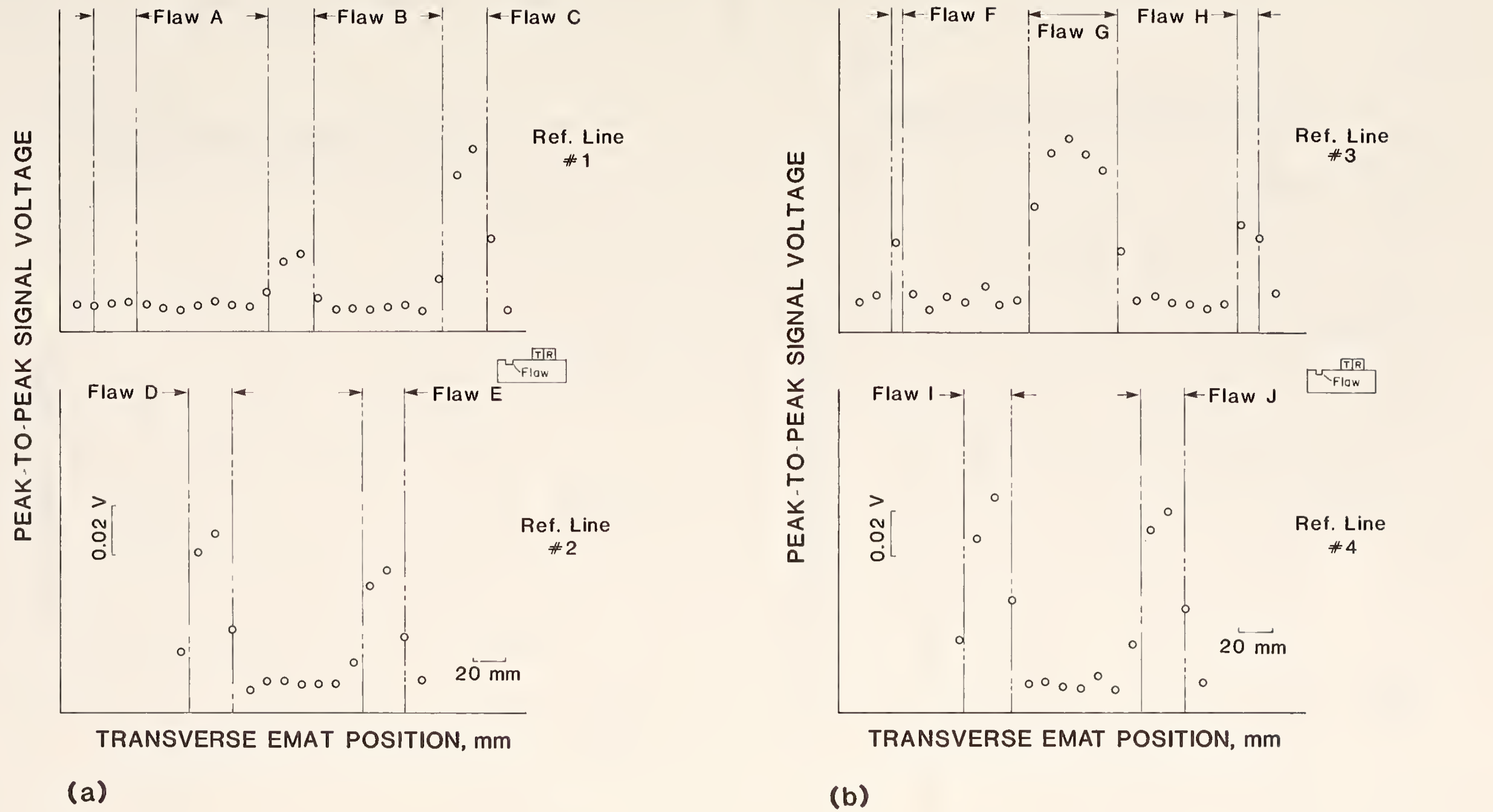

Figure 8-4: Peak-to-peak signal voltage from scan of slots on same side of plate as EMATs. (a) Flaws A-E. (b) Flaws F-J.

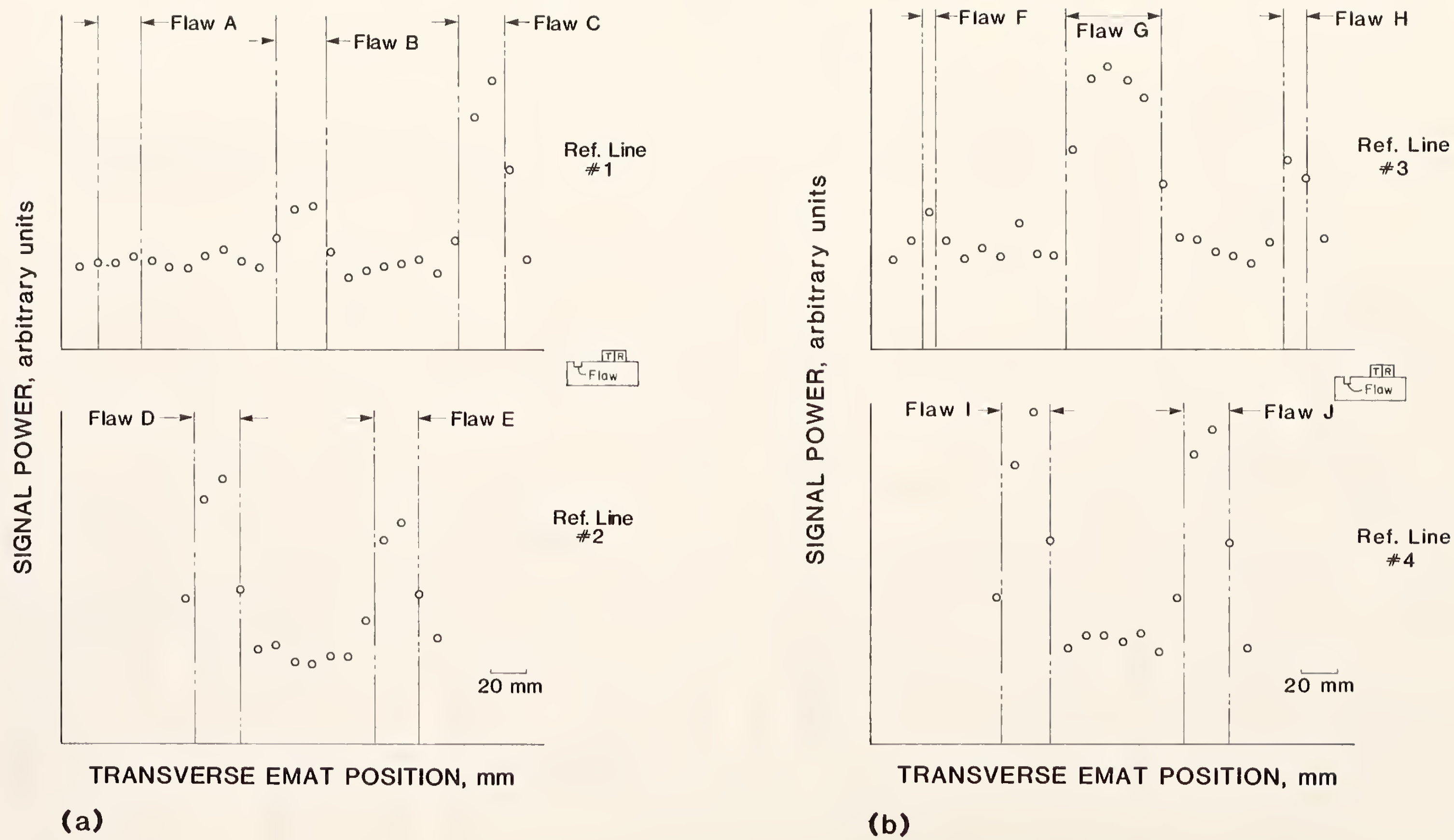

Figure 8-5: Power signal from scan of slots on same side of plate as EMATs. (a) Flaws A-E. (b) Flaws F-J.

the long wavelength region. The presence of flaws B and C is readily discernable, while neither received-signal voltage nor power positively detect flaw A.

The scattering results corresponding to reference line 2 are in the lower half of Figs. 8-4a and 8-5a. There can be no doubt about detecting both slots D and E lying along this reference line. The two flaws are approximately 25 mm long, and 1.76 and 2.14 mm deep, respectively. It is very interesting to observe that the scattering signature of flaw C is nearly identical to that of flaw D. This is not coincidental, since the actual dimensions of the two flaws are nearly identical. Again, this result shows the repeatable nature of the SH-wave EMAT inspection system.

Figures 8-4b and 8-5b depict the ultrasonic scattering data collected along the reference scan lines 3 and 4. Flaws F, G, and H are noteworthy because they are substantially shorter or longer than the 25 mm of the other flaws. Their surface lengths are 7.2, 52.3, and 12.8 mm, respectively. Examining the two figures shows that all three flaws can be positively detected. We believe that the detection of flaw F and not of flaw A is a consequence of the former being substantially deeper than the latter, 2.29 mm vs. 0.48 mm. As with Figs. 8-4a and 8-5a, the flaw signals correspond faithfully to the actual locations. Furthermore, the surface lengths of longer flaws G, I, and J can be resolved. On the other hand, the ultrasonically determined widths of flaws F and H are overestimates. Fortunko and Schramm (1983) discuss this effect as related to the curvature of the phase-front illuminating the planar flaw.

The major feature of flaws I and J is that their through-thickness depths are comparable to a half and full wavelength, respectively. Their reflection signals are nearly identical and indicate system saturation.

To determine the practical flaw detectability limitations and extent of regions where long wavelength flaw sizing may be applicable, we reorganized the experimental results by plotting the reflected signal voltage as a function of flaw length and through-thickness depth. The results are in Figs. 8-6 and 8-7. These include data from both slot-up and slot-down configurations.

In Fig. 8-6 a and b, using peak-to-peak signal voltage and signal power as detection parameters, we plotted the flaw response as a function of flaw through-thickness depth for all flaws with approximately 25 mm surface length. For the top half of Fig. 8-6 the results are for flaws on the same surface as the transducer; for the bottom half, the flaws were on the opposite side of the calibration plate. It is evident that both parameters increase monotonically in the region 0.5 mm < flaw-depth $\leq$ 2.5 mm. The latter dimension corresponds to one third of the ultrasonic wavelength. Above this value the signal amplitude and power exhibit no further increase and remain essentially constant. This is in excellent agreement with theory (Datta, Shah, and Fortunko, 1982).

Figure 8-7 shows the results for flaws approximately 2-mm deep, but whose surface length varies (D, E, F, G, and H). Because of the finite beam width in the plane of the surface, it is not possible to decouple completely the effect of flaw length and depth on the signal voltage. The data collected in Fig. 8-7 demonstrates this effect. The signal voltage increases monotonically in the region 0 < flaw surface-length < $\sqrt{2\lambda z}$, where z denotes the initial transmitter-EMAT-to-flaw separation distance, and then saturates. This effect is also in very close agreement with simple theory. (Fortunko and Schramm, 1983). The calculated value of the quantity $\sqrt{2\lambda z}$ is 24 mm, in very good quantitative agreement with the experimental results of Figs. 8-4 and 8-5.

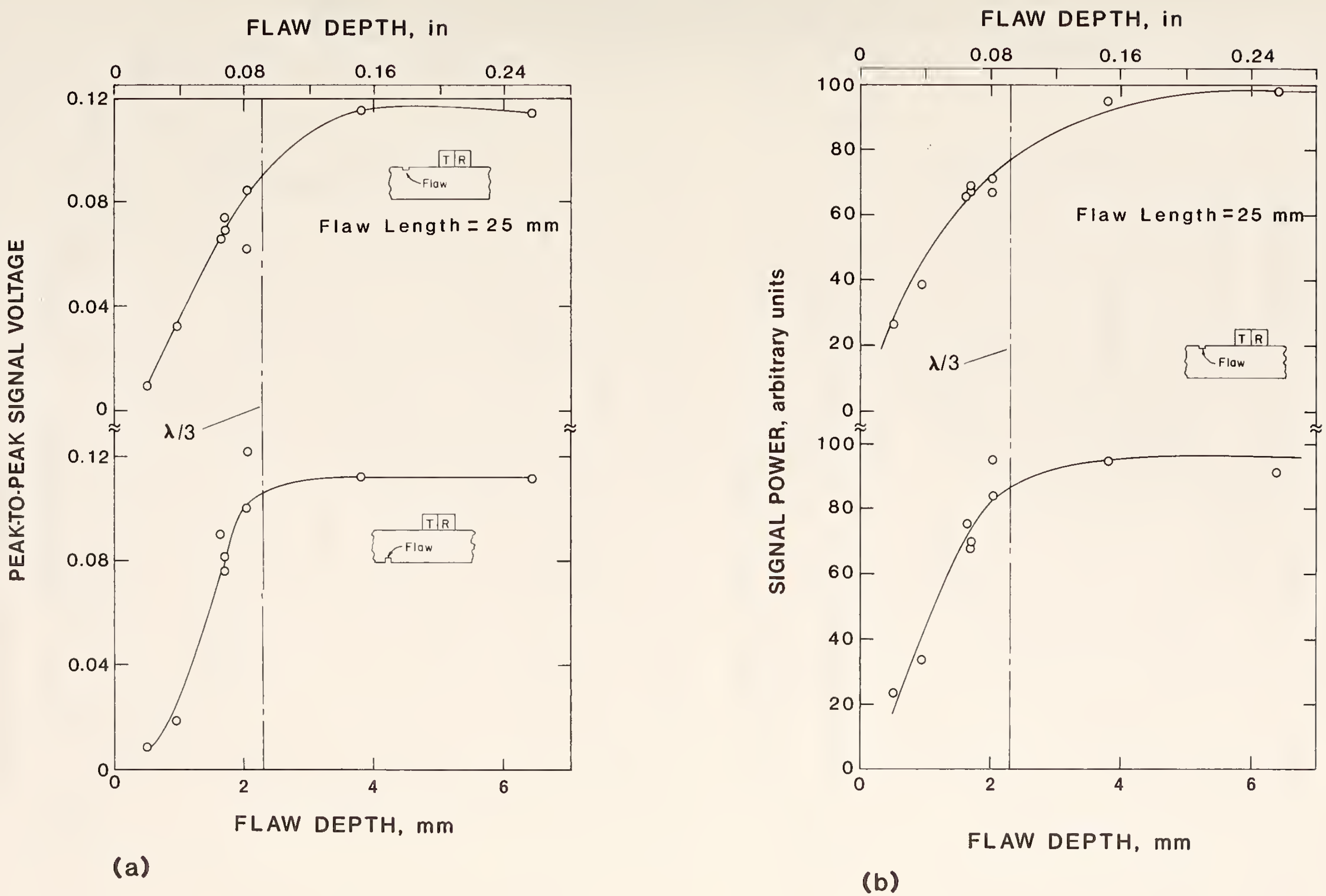

Figure 8-6: Flaw signal as a function of flaw depth for a constant length. The results remain the same for flaws up or down. (a) Peak-to-peak voltage. (b) Power.

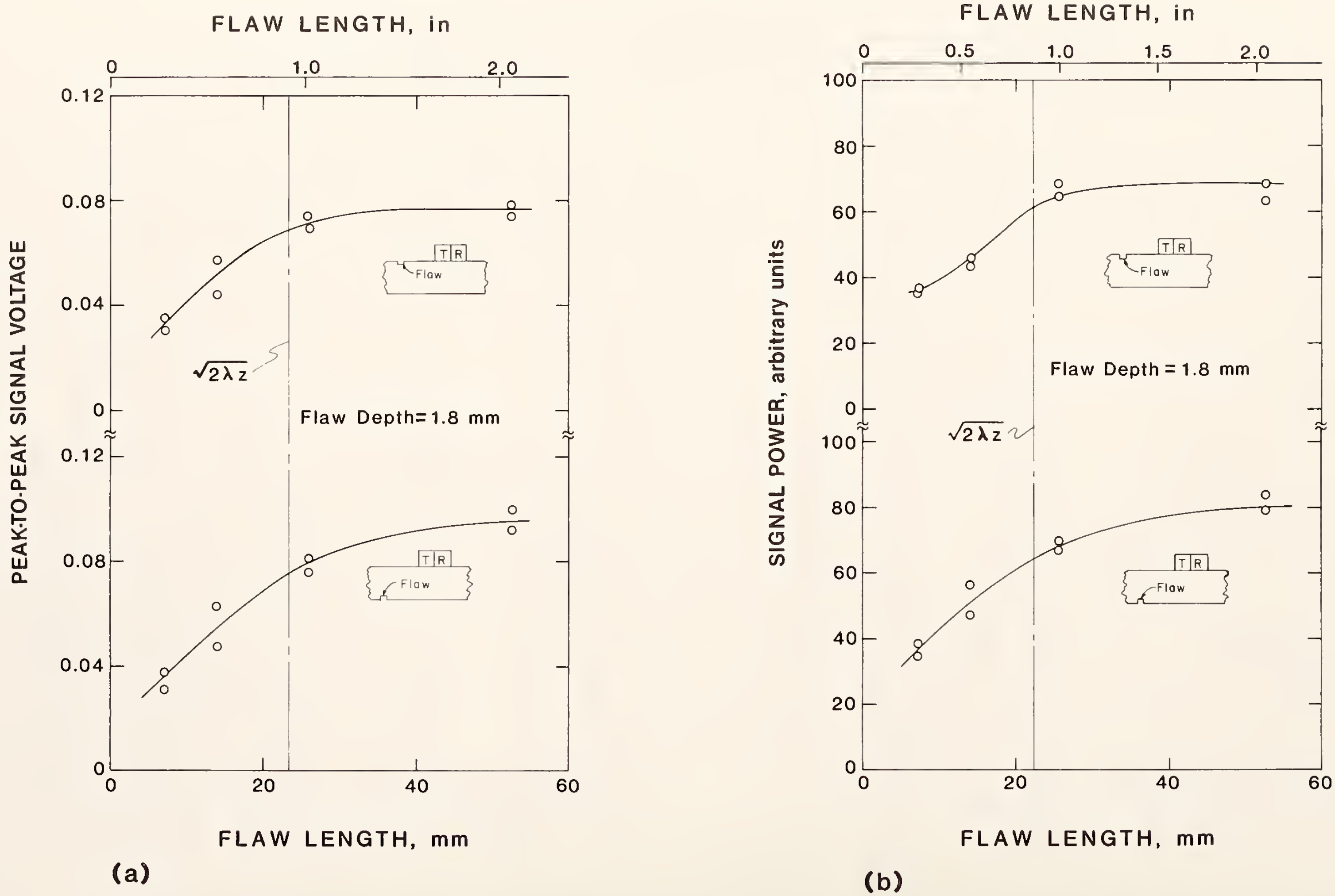

Figure 8-7: Flaw signal as a function of flaw length for a constant depth. The results remain the same for flaws up or down. (a) Peak-to-peak voltage. (b) Power.

Figure 8-7 shows the possibility of resolving the surface length of a planar flaw when its length perpendicular to the axis of the ultrasonic beam exceeds $\sqrt{2\lambda z}$, approximately 24 mm in the present case. Below this value it is no longer possible to estimate the flaw surface length and through-thickness depth separately. Furthermore, Fig. 8-6 shows that the voltage of the reflected signal exhibits a monotonic increase only for a flaw depth less than a third of a wavelength. Hence, it is not possible to estimate flaw depths that are larger than that dimension. Fortunately, the above limitations are not inconsistent with typical flaw sizes that must be reliably detected in conventional inspections of butt welds, which are most often based on the use of comparative reference standards (calibration blocks) (Doyle and Scala, 1978).

In a fitness-for-service approach, it is essential not only to detect flaws with high reliability, but to size them within some region of concern. Figure 8-8 delineates the four regions of flaw-length, flaw-depth combiations: 1.) no detection, 2.) detection only, 3.) detection with depth sizing, and 4.) detection with limited sizing. In the first region, it is not possible to detect the flaw at all. In the second region, the flaws can be reliably detected, but their through-thickness depth is only known to exceed $\lambda/3$. In the third region, the surface length can be estimated from the transverse scan while the depth can be estimated from amplitude (voltage or power) information. In the fourth region, it is still possible to detect the flaw reliably, but the flaw surface-length and depth are not separable. In the last case, it may be necessary to employ other inspection techniques (i.e. conventional ultrasonics or radiography) to estimate the flaw length.

The measurements (Figs. 8-4 through 8-7) on the calibration notches, A through J, of Table 8-1 determined the approximate boundaries in Fig. 8-8.

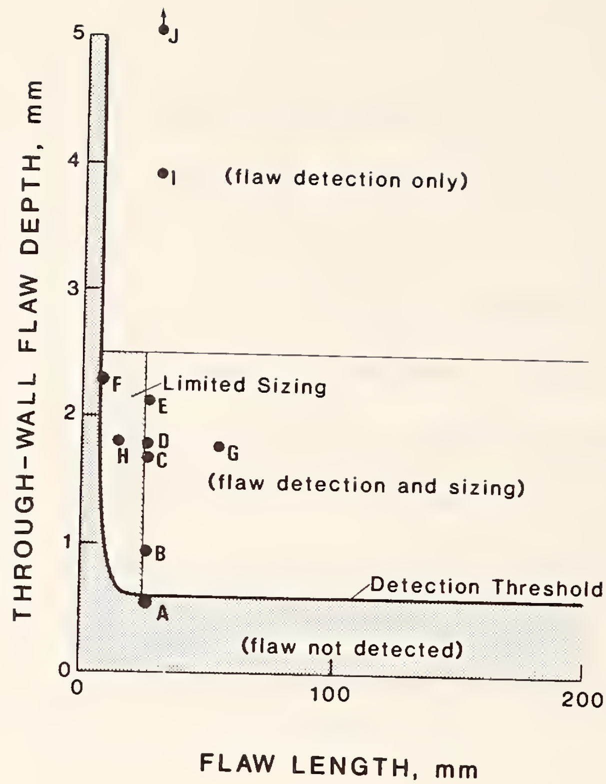

Figure 8-8: Depth and length measurement capabilities and limitations of the present EMAT system. The letters A through J identify the points indicating the dimensions of the calibration notches listed in Table 8-1.

The shallow slot A was essentially undetected (Figs. 8-4 and 8-5) and set the detection threshold. The notches with a 1.8-mm approximate depth, along with the theoretical value, (Fig. 8-7) defined the vertical boundary at about 25 mm. The very short but deep flaw F established a limit to the curve defining the undetected region and indicated its general shape. The flaws with a 25-mm length but various depths, again along with the theoretical value (Fig. 8-6) indicated the upper bound on the ability to correctly size any detectable flaw.

References

Datta, S. K., Shah, A. H., and Fortunko, C. M., 1982, Diffraction of medium and long wavelength horizontally polarized shear waves by edge cracks, J. Appl. Phys., 53:2895.

Doyle, P. A., and Scala, C. M., 1978, Crack depth measurement by ultrasonics: a review, Ultrasonics, 16:164.

Fortunko, C.M., and Schramm, R.E., 1983, Evaluation of pipeline girth welds using low-frequency horizontally polarized waves, J.NDE, 3:155.

Chapter 9

SUMMARY AND RECOMMENDATIONS

In this report we have shown the feasibility of constructing a new type of ultrasonic inspection system for thick, butt welds used in ship construction. (Thick welds are defined for the purposes of this report as those having 12.5-mm and greater thickness.) The system makes use of special ultrasonic probing signals, shear waves that are polarized horizontally with respect to the plate surface (SH-waves). Using these special probing signals is beneficial because they generate fewer unwanted ultrasonic signals. Also, SH-waves can illuminate welds at optimum detection angles because they are able to propagate with equal efficiency at any angle with respect to the free surface. It is believed that, for many types of sharp flaws, ultrasonic illumination at grazing angles with respect to the free surface is advantageous. However, conventional ultrasonic probing signals, SV-waves and L-waves, are not at all suitable for this role.

The experimental results described in this report demonstrate that the new ultrasonic inspection system may be better suited for the role of inspecting thick welds than conventional ultrasonic systems using piezo-electric transducers and operating at 1 to 10 MHz. The new system's advantages are special non-contacting transducers and operation at lower ultrasonic frequencies. The special ultrasonic transducers function on the basis of electromagnetic-acoustic (EMA) coupling, and can preferentially generate and detect the SH-wave probing signals. In addition, because they need not maintain intimate coupling with the surface, the EMA transducers (EMATs) can operate on relatively rough surfaces that may be at elevated temperatures. This characteristic is of considerable importance in weld inspection.

The SH-wave EMAT system is different from conventional ultrasonic systems in two other respects: 1. it operates at relatively long ultrasonic wavelengths (7.4 mm), and 2. it uses synthetic-aperture waveform reconstruction to reduce the contamination of the ultrasonic flaw indications by unwanted ultrasonic and electromagnetic interferences. The former feature makes the probability of flaw detection less critically dependent on the flaw-signal illumination angle and allows use of the reflected signal amplitude for limited flaw sizing and characterization. The second feature has only recently become economically feasible due to advances in digital-computer hardware.

Digital techniques were used extensively to improve the quality of the ultrasonic signals. They partially compensate for the loss of ultrasonic beam collimation occurring when wavelengths are large with respect to transducer size. In addition, extensive digital signal processing allows the use of very effective algorithms for signal averaging in the time domain and filtering in the frequency domain. This capability is very important in welding environments dominated by electromagnetic interferences.

The present SH-wave EMAT system has somewhat limited transverse and longitudinal resolution, as determined primarily by the wavelength and EMAT linear dimensions. The wavelength is physically limited by the size of the samarium-cobalt permanent magnets used in the construction of the transducers. It is believed that the present operating frequency (454 kHz) represents the state-of-the-art for systems using the periodic-permanent-magnet EMA transducer. Therefore, if better resolution is necessary, alternative methods for generating and detecting SH-waves will be necessary.

The main accomplishment of the present work was the demonstration of the SH-wave EMAT technology in the context of inspecting thick weldments.

Previously, ultrasonic systems using SH-waves were demonstrated in thin-plate geometries where the propagation of the signals was more appropriately described in terms of guided wave formalisms. In the present case, freely diffracting ultrasonic signals were used.

This program was viewed as a technology demonstration. Therefore, a relatively flexible "brassboard" was developed to serve as a test vehicle to evaluate the system's inherent sensitivity limits with respect to surface flaws modeled by thin electrical-discharge-machined notches. The "brassboard" was designed primarily to investigate performance limits in estimating flaw size. Although the construction was robust, the design needs critical review before selecting a configuration for a field-ready prototype. Certain subsystems should be substantially redesigned. For example, the present "brassboard" system carries out digital signal processing using decidedly less-than-optimal hardware and software. Using array-processor technology and more efficient software driver routines can readily correct this deficiency. In addition, it is recommended that the transmitter-amplifiers, which currently use bipolar transistor technology, be redesigned to incorporate elements of the new high-power FET (field-effect transistor) technology. This change would result in stronger ultrasonic signals and higher reliability.

The "brassboard" system established a number of important performance parameters. In particular, it was found that thin surface notches > 0.5-mm deep and 25-mm long could be positively detected at 454 kHz in 25-mm thick plates made of standard HY-80 steel. This result is similar to that observed experimentally in thinner plates (16 mm) (Fortunko and Schramm, 1983). However, it is believed that this similarity is probably coincidental because, in the former case, the sensitivity was limited by ultrasonic-multipath and transducer-sidelobe effects. In the latter case, it was limited by an ultrasonic background generated by the weld reinforcement, weld root, and other surface irregularities.

This investigation did not include sensitivity limits with respect to sharp and blunt interior flaws because suitable calibration specimens were lacking. However, such limits can be extrapolated from the surface flaw results on the basis of theory (Datta, Shah, and Fortunko, 1982). Closure effects on the detectability of sharp flaws were not investigated. Also, because of the inherent limitations in the "brassboard" system, performance parameters with respect to transverse weld flaws were not established.

Among the major accomplishments of the present project is the development of a new SH-wave EMAT. The new EMAT design reduces susceptibility to electromagnetic interferences, an important factor in a welding environment. In addition, a thin metallic shield was found to protect the fragile parts of the EMAT from abrasion damage without significantly reducing transduction efficiencies. It was never found necessary to replace the EMATs during the project despite extensive use. It is believed that the new EMAT design is particularly suitable for ferromagnetic weldments, which are frequently covered with layers of rust or paint. Of course, further testing of the new EMAT design under realistic conditions is desirable.

In addition to physical reliability, the new EMATs have performed well in conjunction with synthetic-aperture signal processing. This requires good measurement repeatability in terms of signal phase and amplitude. In a related, but separately funded development, the new EMAT design was used successfully to determine residual stress distributions in plates locally subjected to non-linear deformation exceeding the yield point (King and Fortunko, 1983). In this case, sufficient phase repeatability was demonstrated to determine values of residual stress with approximately 10 MPa resolution. This level of resolution would not be routinely achievable using conventional, fluid or grease-coupled ultrasonic transducers.

It should be emphasized that much remains to be accomplished before SH-wave EMAT inspection systems can be adopted universally as either primary or back-up inspection tools for thick butt weldments. We recommend that the laboratory system developed under the present program be used as a test-bed system for further evaluations of the method's capabilities and weaknesses. In particular, before making a commitment to a field prototype, it will be necessary to evaluate system performance using flaw types representative of particular welding processes. Furthermore, performance limits should be independently confirmed by appropriate destructive testing procedures. The results of such a study should be compared with inspection records of the same weldment obtained with existing inspection techniques: conventional ultrasonics and radiography.

We believe that the low-frequency, SH-wave EMAT method is more advantageous for detecting elongated sharp and blunt flaws than radiography. However, because it uses long ultrasonic wavelengths, it may be less sensitive to certain categories of blunt flaws (porosity), than conventional ultrasonics and radiography. Consequently, it is recommended that a study be conducted to quantify the sensitivity limits of the low-frequency, SH-wave EMAT method to such flaws. In such work, the emphasis should be focused on an experimental plan that will make it possible to draw conclusions on the basis of statistics. In the present work, because of the limited number of calibration specimens and flaws, statistical methods could not be used.

Finally, it is recommended that a separate study be conducted on the performance characteristics of the present SH-wave EMATs when operated on ferromagnetic weldments exhibiting large internal residual and applied stresses. Influences of the material composition on the electromagnetic-acoustic transduction processes also need study. Past studies have shown that the presence of stress and compositional variations can significantly alter the characteristics of the transmitted and received ultrasonic signals (Thompson, 1978).

References

Datta, S. K., Shah, A. H., and Fortunko, C. M., 1982, Diffraction of medium and long wavelength horizontally polarized shear waves by edge cracks, J. Appl. Phys. 53:2895.

Fortunko, C. M. and Schramm. R. E., 1983, Evaluation of pipeline girth welds using low-frequency horizontally polarized waves, J. NDE, 3:155.

King, R. B. and Fortunko, C. M., 1983, Surface residual stress evaluation using horizontally polarized shear waves, to be published in J. Appl. Phys.

Thompson, R. B., 1978, A model for the electromagnetic generation and detection of guided waves in ferromagnetic metal crystals, IEEE Trans. Sonics-Ultrasonics, 25:7.

Appendix I

SOFTWARE LISTING

These computer programs are written in BASIC and executed on a system consisting of a CPU with 256 kbytes of memory, a dual floppy disk drive, video terminal, graphics printer, and an IEEE-488 interface bus. This bus permitted communication with a digital storage oscilloscope and carried transport information of a motion control interface card used with motion control indexer cards and synchronous/stepper motors and two lead screw positioners (almost 1.58 threads/mm or 40 threads/inch). With appropriate software changes, other types of equipment could be substituted for those used here. This software is divided into five parts only because of limitations on the size of the memory workspace.

SYN - Part 1

Always start here to enter the intial decision and parameters and to establish the physical position of the EMAT assembly.

```
100 REM  **  SYN  **
110 REM  ************************************************
120 REM  **  SYNTHETIC APERTURE BY PHASE SHIFT - PART 1  **
130 REM  ************************************************
140 REM  **  INITIALIZATION  **
150 REM  ***********************
160 COMMON P(20),I$,P$,A1,A2 \ DIM R(511),I(511),C$(5)
170 DIM #1,F(20) \ DIM #2,F1(511) \ DIM #3,F$(5)=255
180 DIM #5,R2(511) \ DIM #6,I2(511)
190 DISPLAY_CLEAR
200 PRINT 'NEW or OLD DATA? (N or O)  ';
210 GET_CHAR(V$)
220 IF V$='O' THEN 730
230 IF V$<>'N' THEN 210
240 PRINT  \ PRINT 'Are you going to USE THE SCANNER SYSTEM? (Y or N) ';
250 GET_CHAR(S1$) \ IF S1$='N' THEN 300
260 IF S1$<>'Y' THEN 250
300 REM  ******************
310 REM  **  PARAMETERS  **
320 REM  ******************
330 PRINT  \ PRINT  \ PRINT 'IDENTIFICATION (2 CHAR MAX) = '; \ INPUT I$
340 IF LEN(I$)>2 THEN 330
350 PRINT 'DATE: '; \ INPUT C$(0)
360 PRINT 'TRANSDUCERS: '; \ INPUT C$(1) \ C$(1)='TRANSDUCERS: '+C$(1)
370 PRINT 'PRF = '; \ INPUT C$(2) \ C$(2)='PRF = '+C$(2)
380 PRINT 'NUMBER OF CYCLES = '; \ INPUT C$(3) \ C$(3)=C$(3)+' CYCLES'
390 PRINT 'NOTES:  2 LINES AVAILABLE'
```

```
400 PRINT 'LINE 1:' \ LINPUT C$(4)
410 PRINT 'LINE 2:' \ LINPUT C$(5)
420 PRINT  \ PRINT 'NUMBER OF TRANSDUCER POSITIONS = '; \ INPUT P(0)
440 IF S1$='N' THEN P(19)=-1 \ GO TO 460
450 PRINT 'NUMBER OF SCAN SETS = '; \ INPUT P(19)
460 PRINT  \ PRINT 'DISTANCES IN MM:'
470 PRINT '   BETWEEN POSITIONS = '; \ INPUT P(1)
480 IF P(19)<2 THEN 510
490 PRINT '   BETWEEN SCAN SETS = '; \ INPUT P(20)
510 PRINT '   BETWEEN TRANSMITTER & RECEIVER = '; \ INPUT P(3)
520 PRINT '   PLATE THICKNESS = '; \ INPUT P(4)
530 PRINT '   FOCAL SPOT LOCATION:'
532 PRINT '      HORIZONTAL (from initial transmitter position) = ';
534 INPUT P(2)
536 PRINT '      VERTICAL DEPTH (from transducer side) = '; \ INPUT P(5)
540 PRINT  \ PRINT '# OF REFLECTIONS IN ACOUSTIC PATH = '; \ INPUT P(6)
560 PRINT  \ PRINT 'FORWARD OR BACKWARD SHIFT? (F OR B)  ';
570 GET_CHAR(D$) \ IF D$='B' THEN 620
580 IF D$<>'F' THEN 570
610 P(7)=1 \ PRINT 'ORWARD' \ GO TO 630
620 P(7)=-1 \ PRINT 'ACKWARD'
630 PRINT  \ PRINT 'FREQUENCY (KHZ) = '; \ INPUT P(8)
640 PRINT  \ PRINT 'SOUND VELOCITY (KM/SEC) = '; \ INPUT P(9)
650 PRINT  \ PRINT 'NUMBER OF AVERAGES DONE ON SCOPE = '; \ INPUT P(10)
660 Z$='SY1:'+I$ \ OPEN Z$ FOR OUTPUT AS FILE #1
670 BLOCK_MOVE(P(0),F(0),21) \ CLOSE
680 Z$=Z$+'N' \ OPEN Z$ FOR OUTPUT AS FILE #3
690 FOR K=0 TO 5 \ F$(K)=C$(K) \ NEXT K \ CLOSE
700 GOSUB 3000 \ PRINT  \ IF V$='O' THEN 720
710 IF P(19)<0 THEN 715
711 PRINT 'Do you want to INITIALIZE TRANSDUCER POSITION? (Y or N)  ';
713 GET_CHAR(M$) \ IF M$='Y' THEN 5000
714 IF M$<>'N' THEN 713
715 CHAIN 'SY0:TEKIN'
720 PRINT 'Do you want to REPROCESS THE DATA? (Y or N)  ';
722 GET_CHAR(E$) \ IF E$='Y' THEN PRINT  \ CHAIN 'SY0:CALC1'
723 IF E$<>'N' THEN 722
725 PRINT  \ IF P(19)<2 THEN J=1 \ GO TO 727
726 PRINT 'Which SCAN SET of ';P(19); \ INPUT J
727 I$=I$+STR$(J) \ CHAIN 'SY0:GRAPH'
730 REM  ***********************
740 REM  **  HANDLE OLD DATA  **
750 REM  ***********************
760 PRINT  \ PRINT 'OLD DATA PARAMETERS:'
770 PRINT 'IDENTIFICATION (2 CHAR MAX) = '; \ INPUT I$
780 IF LEN(I$)>3 THEN 770
790 W$='SY1:'+I$ \ OPEN W$ FOR INPUT AS FILE #1
800 BLOCK_MOVE(F(0),P(0),21) \ CLOSE
810 W$='SY1:'+I$+'N' \ OPEN W$ FOR INPUT AS FILE #3
820 FOR K=0 TO 5 \ C$(K)=F$(K) \ NEXT K \ CLOSE
830 GOSUB 2000
890 PRINT  \ PRINT 'Do you want to CHANGE THESE PARAMETERS? (Y or N)  ';
900 GET_CHAR(W$) \ IF W$='N' THEN 700
910 IF W$='Y' THEN 460
930 GO TO 900
2000 REM  **********************
2010 REM  **  PARAMETER LIST  **
2020 REM  **********************
2030 PRINT  \ PRINT 'ID:  ';I$ \ PRINT
2040 FOR K=0 TO 5 \ PRINT C$(K) \ NEXT K \ PRINT
2050 IF P(19)<0 THEN 2080
2060 PRINT P(19);' SCAN SETS'
2065 IF P(19)=1 THEN 2080
2070 PRINT P(20);' MM BETWEEN SETS'
2080 PRINT P(0);' TRANSDUCER POSITIONS'
2090 PRINT P(1);' MM BETWEEN POSITIONS'
2110 PRINT P(3);' MM BETWEEN TRANSMITTER & RECEIVER'
2120 PRINT P(4);' MM PLATE THICKNESS'
2130 PRINT 'FOCAL SPOT LOCATION:'
```

```
2132 PRINT '  ';P(2);' MM HORIZONTAL (from initial transmitter position)'
2134 PRINT '  ';P(5);' MM VERTICAL DEPTH (from transducer side)'
2140 PRINT P(6);' REFLECTIONS IN ACOUSTIC PATH'
2150 IF P(7)=1 THEN PRINT 'FORWARD SHIFT'
2160 IF P(7)=-1 THEN PRINT 'BACKWARD SHIFT'
2170 PRINT P(8);' KHZ FREQUENCY'
2180 PRINT P(9);' KM/SEC SOUND VELOCITY'
2190 PRINT P(10);' AVERAGES DONE ON SCOPE'
2200 RETURN
3000 REM  *********************
3010 REM  **  HARD COPY LIST  **
3020 REM  *********************
3030 PRINT  \ PRINT 'Do you want a HARD COPY OF THE PARAMETER LIST? (Y or N) ';
3040 GET_CHAR(W$) \ IF W$='N' THEN 3090
3050 IF W$<>'Y' THEN 3040
3080 PRINT CHR$(27),'[5i' \ GOSUB 2000 \ PRINT CHR$(27),'[4i'
3090 PRINT  \ RETURN
5000 REM  *************************************
5010 REM  **  INITIALIZE TRANSDUCER POSITION  **
5020 REM  *************************************
5030 PRINT  \ PRINT 'When system is READY push "R"';
5040 GET_CHAR(H$) \ IF H$<>'R' THEN 5040
5060 REM **  INITIALIZE MOTOR CONTROL  **
5070 T$=CHR$(13)+CHR$(10)
5090 SEND('XEYE'+T$,11) \ REM  **  MOTOR CURRENT OFF  **
5120 REM **  INPUT PARAMETERS  **
5130 PRINT  \ PRINT 'X or Y coordinate:  ';
5140 GET_CHAR(C$) \ IF C$='X' THEN 5160
5150 IF C$<>'Y' THEN 5140
5160 PRINT  \ PRINT 'DIRECTION? (+ OR -)  ';
5170 GET_CHAR(D$) \ IF D$='+' THEN 5210
5190 IF D$<>'-' THEN 5170
5210 PRINT  \ PRINT 'MM OF TRAVEL = '; \ INPUT D
5220 P=INT(D*16000/25.4+.5)
5230 PRINT  \ PRINT 'Push "E" to EXECUTE  ';
5240 GET_CHAR(E$) \ IF E$<>'E' THEN 5240
5260 R$='*'+T$ \ REM **  EXECUTE COMMAND  **
5270 C$='['+C$+'D;'+C$+'M'+D$+STR$(P)+'G;'+C$+'E]'+T$
5280 SEND(C$,11) \ SEND(R$,11)
5290 PRINT  \ PRINT 'Do you want to MOVE FURTHER? (Y or N)  ';
5300 GET_CHAR(G$) \ IF G$='Y' THEN 5130
5320 IF G$<>'N' THEN 5300
5330 PRINT  \ CHAIN 'SY0:TEKIN'
```

TEKIN - Part 2

This reads the digital data from the oscilloscope, stores it, and moves the EMATs in the designated pattern.

```
100 REM  **  TEKIN  **
110 REM  ************************************************
120 REM  **  SYNTHETIC APERTURE BY PHASE SHIFT - PART 2  **
130 REM  ************************************************
140 COMMON P(20),I$,P$,A1,A2 \ DIM R(511),I(511)
150 DIM #1,F(20) \ DIM #2,F1(511)
160 DIM #5,R2(511) \ DIM #6,I2(511)
170 DISPLAY_CLEAR
171 PRINT 'Press "E" to begin EXECUTION ';
172 GET_CHAR(V$) \ IF V$<>'E' THEN 172
173 PRINT
180 IF P(19)>=0 THEN  GOSUB 5000
190 REM  ***********************
200 REM  **  START COLLECTION  **
210 REM  ***********************
220 S=P(19)-1 \ IF S<0 THEN S=0
230 FOR J1=0 TO S \ PRINT  \ PRINT
```

```
240 PRINT 'Scan ';J1+1;' of ';S+1;' at ';J1*P(20);' mm'
250 FOR J=0 TO P(0)-1
260 PRINT 'Collecting position ';J+1;' of ';P(0);' at ';J*P(1);' mm'
265 IF J>0 THEN 890
270 FOR K=1 TO 5
280 RECEIVE(V$,1,6) \ IF V$<>',' THEN 280
300 NEXT K
310 FOR K=1 TO 6 \ RECEIVE(V$,1,6) \ NEXT K
340 REM  *************************
350 REM  **  GET TIME INCREMENT  **
360 REM  *************************
370 GOSUB 4000 \ P(11)=VAL(V$)/(10^3)
390 FOR K=1 TO 6 \ RECEIVE(V$,1,6) \ NEXT K
400 REM  *****************
410 REM  **  GET X ZERO  **
420 REM  *****************
430 GOSUB 4000 \ P(12)=VAL(V$)
450 FOR K=1 TO 7 \ RECEIVE(V$,1,6) \ NEXT K
460 REM  *************************
470 REM  **  GET X POINT OFFSET  **
480 REM  *************************
490 GOSUB 4000 \ P(13)=VAL(V$)
510 FOR K=1 TO 6 \ RECEIVE(V$,1,6) \ NEXT K
520 REM  *******************************************
530 REM  **  DETERMINE DECIMAL FOR TIME INCREMENT  **
540 REM  *******************************************
550 RECEIVE(X$,1,6)
560 IF X$='S' THEN P(14)=3
570 IF X$='M' THEN P(14)=0
580 IF X$='U' THEN P(14)=-3
590 IF X$='N' THEN P(14)=-6
600 RECEIVE(V$,1,6) \ IF V$<>':' THEN 600
610 REM  ***********************
620 REM  **  GET Y MULTIPLIER  **
630 REM  ***********************
640 GOSUB 4000 \ P(15)=VAL(V$)/(10^3)
660 FOR K=1 TO 6 \ RECEIVE(V$,1,6) \ NEXT K
670 REM  *****************
680 REM  **  GET Y ZERO  **
690 REM  *****************
700 GOSUB 4000
710 P(16)=VAL(V$)
720 RECEIVE(V$,1,6) \ IF V$<>':' THEN 720
730 REM  *******************
740 REM  **  GET Y OFFSET  **
750 REM  *******************
760 GOSUB 4000 \ P(17)=VAL(V$)/(10^3)
780 RECEIVE(V$,1,6) \ IF V$<>':' THEN 780
790 REM  *****************
800 REM  **  GET Y UNIT  **
810 REM  *****************
820 RECEIVE(V$,1,6)
830 IF V$='V' THEN P(18)=1
840 IF V$='M' THEN P(18)=2
850 IF V$='U' THEN P(18)=3
870 V$='SY1:'+I$ \ OPEN V$ FOR OUTPUT AS FILE #1
880 BLOCK_MOVE(P(0),F(0),21) \ CLOSE
890 RECEIVE(V$,1,6)
900 IF ASC(V$)<>1 THEN 890
910 REM  **********************
920 REM  **  READ SCOPE DATA  **
930 REM  **********************
940 FOR K=0 TO 511 \ RECEIVE(V$,1,6)
950 R(K)=ASC(V$) \ NEXT K
960 RECEIVE(V$,,6)
965 IF J<P(0)-1 THEN  GOSUB 6000
970 G$='SY1:'+I$+STR$(J1+1)+STR$(J+1) \ OPEN G$ FOR OUTPUT AS FILE #2
980 BLOCK_MOVE(R(0),F1(0),512) \ CLOSE
1000 NEXT J
1010 IF J1<S THEN  GOSUB 7000
```

```
1020 NEXT J1
1030 CHAIN 'SYO:CALC1'
4000 REM  ******************
4010 REM  **  READ NUMBER  **
4020 REM  ******************
4030 V$=''
4040 RECEIVE(X$,1,6)
4050 IF X$=',' THEN RETURN
4060 V$=V$+X$ \ GO TO 4040
5000 REM  ********************************
5010 REM  **  INITIALIZE MOTOR CONTROLS  **
5020 REM  ********************************
5030 IF P(19)<0 THEN RETURN
5040 T$=CHR$(13)+CHR$(10)
5050 SEND('XEYE'+T$,11) \ REM  **  MOTOR CURRENT OFF  **
5060 P$=STR$(INT(P(1)*16000/25.4+.5))
5070 C$='[XD;XM+'+P$+'G;XE;'+T$ \ SEND(C$,11) \ REM  **  X MOTION  **
5080 P$=STR$(INT((P(0)-1)*P(1)*16000/25.4+.5))
5090 C$='XD;XM-'+P$+'G;XE;'+T$ \ SEND(C$,11) \ REM  **  RETURN X MOTION  **
5100 P$=STR$(INT(P(20)*16000/25.4+.5))
5110 C$='YD;YM+'+P$+'G;YE;'+T$ \ SEND(C$,11) \ REM  **  Y MOTION  **
5112 P$=STR$(INT(32000/25.4+.5))
5114 C$='XD;XM-'+P$+'G;XM+'+P$+'G;XE;]'+T$ \ SEND(C$,11)
5116 SEND('#4/'+T$,11) \ PAUSE(3) \ REM  **  OVERSHOOT & RETURN  **
5120 R1$='#1/'+T$ \ R2$='#2*'+T$ \ RETURN
6000 REM  ***************************************************
6010 REM  **  MOVE TO NEXT TRANSDUCER POSITION [X DIRECTION]  **
6020 REM  ***************************************************
6025 IF P(19)<0 THEN 6040
6030 SEND(R1$,11) \ RETURN
6040 PRINT 'PUSH "G" AFTER MOVING TRANSDUCERS TO NEXT POSITION'
6050 GET_CHAR(G$) \ IF G$<>'G' THEN 6050
6060 PRINT  \ RETURN
7000 REM  ****************************
7010 REM  **  MOVE TO NEXT SCAN LINE  **
7020 REM  ****************************
7040 SEND(R2$,11) \ PAUSE(15) \ RETURN
```

CALC1 - Part 3

This asks for some decisions on the calculations to be done and starts this process. It includes signal averaging and subtraction, Fourier transformation, frequency windowing, and power calculations for the individual data sets.

```
100 REM  **  CALC1  **
110 REM  ************************************************
120 REM  **  SYNTHETIC APERTURE BY PHASE SHIFT - PART 3  **
130 REM  ************************************************
140 COMMON P(20),I$,P$,A1,A2
145 DIM R(511),I(511),W(511),R%(511),I%(511)
150 DIM #2,F1(511) \ DIM #3,F$(4)=255
160 IF P(19)<2 THEN I$=I$+'1' \ GO TO 205
170 PRINT  \ PRINT 'Perform calculations on WHICH DATA SET (of ';P(19);
180 PRINT ')'; \ INPUT I1$ \ I$=I$+I1$
205 PRINT  \ PRINT  \ PRINT 'Window choice:' \ PRINT '   1. NONE'
210 PRINT '   2. BARTLETT' \ PRINT '   3. HANNING'
220 GET_CHAR(D$)
230 IF D$='1' THEN I1$='NO WINDOW' \ GO TO 270
240 IF D$='2' THEN I1$='BARTLETT WINDOW' \ GO TO 270
250 IF D$<>'3' THEN 220
260 I1$='HANNING WINDOW'
```

```
270 D=VAL(D$)
272 PRINT  \ PRINT 'Perform calculations on WHICH POSITIONS? (1 to ';P(0);')'
274 PRINT 'Start with position # '; \ INPUT A1
276 PRINT '  End with position # '; \ INPUT A2
278 I2$='POSITIONS #'+STR$(A1)+' TO #'+STR$(A2)
280 PRINT  \ PRINT  \ PRINT 'Do you want to SUBTRACT THE AVERAGE? (Y or N)  ';
290 GET_CHAR(D$) \ IF D$='Y' THEN I3$='AVERAGE SUBTRACTED' \ GO TO 322
300 IF D$<>'N' THEN 290
310 I3$='NO AVERAGE SUBTRACTION'
322 PRINT  \ PRINT 'Do you want to CALCULATE POWER SPECTRUM? (Y or N)  ';
324 GET_CHAR(P$) \ IF P$='Y' THEN I4$='POWER CALCULATIONS DONE' \ GO TO 328
326 IF P$<>'N' THEN 324
327 I4$='NO POWER CALCULATIONS'
328 PRINT  \ OPEN 'SY1:ID' FOR OUTPUT AS FILE #3 \ F$(0)=I$ \ F$(1)=I1$
329 F$(2)=I2$ \ F$(3)=I3$ \ F$(4)=I4$ \ CLOSE
330 PRINT  \ PRINT  \ PRINT "I'M THINKING ABOUT YOUR PROBLEM NOW!"
340 PRINT 'START ';CLK$
350 REM  ************************
360 REM  **  CALCULATE AVERAGE  **
370 REM  ************************
380 FOR K=0 TO 511 \ W(K)=0 \ NEXT K
390 IF D$='N' THEN 470
400 FOR J=A1 TO A2
410 V$='SY1:'+I$+STR$(J) \ OPEN V$ FOR INPUT AS FILE #2
420 BLOCK_MOVE(F1(0),R(0),512) \ CLOSE
430 FOR K=0 TO 511 \ W(K)=W(K)+R(K)/(A2-A1+1) \ NEXT K
440 NEXT J
450 OPEN 'SY1:AVG' FOR OUTPUT AS FILE #2
460 BLOCK_MOVE(W(0),F1(0),512) \ CLOSE
470 PRINT 'AVG   ';CLK$
480 REM  *****************************************
490 REM  **  SUBTRACT AVERAGE & CALCULATE FFT'S  **
500 REM  *****************************************
510 M1=INT(P(8)*(10^3)*512*P(11)*(10^P(14))+.5)
520 REM  **  M1 IS THE POINT # AT THE CENTER OF THE WINDOW  **
530 W=45 \ REM  **  WIDTH OF WINDOW [# OF POINTS] = 2*W=1  **
540 IF W>M1 THEN W=M1
550 FOR J=A1 TO A2
560 V$='SY1:'+I$+STR$(J) \ OPEN V$ FOR INPUT AS FILE #2
570 BLOCK_MOVE(F1(0),R(0),512) \ CLOSE
580 FOR K=0 TO 511 \ R%(K)=R(K)-W(K) \ I%(K)=0 \ NEXT K
590 FFT(,512,R%(0),I%(0),S%)
600 R%(0)=0 \ REM  REMOVE DC LEVEL
610 GOSUB 700 \ GOSUB 1000
620 FOR K=0 TO 255 \ R(K)=R%(K)*2^S% \ I(K)=I%(K)*2^S% \ NEXT K
630 V$='SY1:FFT'+STR$(J)+'R' \ OPEN V$ FOR OUTPUT AS FILE #2
640 BLOCK_MOVE(R(0),F1(0),256) \ CLOSE
650 V$='SY1:FFT'+STR$(J)+'I' \ OPEN V$ FOR OUTPUT AS FILE #2
660 BLOCK_MOVE(I(0),F1(0),256) \ CLOSE
670 NEXT J
680 PRINT 'FFT   ';CLK$
690 CHAIN 'SY0:CALC2'
700 REM  **********************
710 REM  **  WINDOW POSITION  **
720 REM  **********************
730 IF D=1 THEN RETURN
740 FOR K=0 TO 255
750 IF K<M1-W THEN 780
760 IF K>M1+W THEN 780
770 GOSUB 830 \ GO TO 790
780 W1=0
790 R%(K)=R%(K)*W1
800 I%(K)=I%(K)*W1
810 NEXT K
820 RETURN
830 REM  ***************************
840 REM  **  CALCULATE WINDOW SIZE  **
850 REM  ***************************
860 N=K-(M1-W)
```

```
870 IF D=3 THEN 910
880 REM **  BARTLETT WINDOW  **
890 IF N<=W THEN W1=N/W \ RETURN
900 IF N>W THEN W1=2-N/W \ RETURN
910 REM  **  HANNING WINDOW  **
920 W1=.5*(1-COS(PI*N/W)) \ RETURN
1000 REM  ***********************
1010 REM  **  POWER CALCULATION  **
1020 REM  ***********************
1030 IF P$='N' THEN RETURN
1040 POWER(256,R%(),I%(),R())
1050 FOR K=0 TO 255 \ R(K)=SQR(R(K))*2^S% \ NEXT K
1060 V$='SY1:PWR'+STR$(J) \ OPEN V$ FOR OUTPUT AS FILE #2
1070 BLOCK_MOVE(R(0),F1(0),256) \ CLOSE  \ RETURN
```

CALC2 - Part 4

This continues the previous part and includes phase shifting, coefficient averaging, reverse Fourier transformation, and power calculations for the result.

```
100 REM  **  CALC2  **
110 REM  ************************************************
120 REM  **  SYNTHETIC APERTURE BY PHASE SHIFT - PART 4  **
130 REM  ************************************************
140 COMMON P(20),I$,P$,A1,A2
145 DIM R(511),I(511),W(255),T(255),R%(511),I%(511)
150 DIM #2,F1(511)
160 REM  ******************
170 REM  **  PHASE SHIFT  **
180 REM  ******************
185 IF INT(P(6)/2)=P(6)/2 THEN 195
190 T=((P(6)+1)*P(4)-P(5))^2 \ GO TO 200
195 T=(P(6)*P(4)+P(5))^2
200 IF P(7)=1 THEN 230
210 D0=SQR((P(2)+(A2-A1)*P(1))^2+T)+SQR((P(2)+P(3)+(A2-A1)*P(1))^2+T)
220 GO TO 240
230 D0=SQR(P(2)^2+T)+SQR((P(2)+P(3))^2+T)
240 FOR J=A1 TO A2
250 D=SQR((P(2)+J*P(1))^2+T)+SQR((P(2)+P(3)+J*P(1))^2+T)-D0
260 Z=2*PI*D/512/(P(11)*10^P(14))/(P(9)*10^6)
270 V$='SY1:FFT'+STR$(J)+'R' \ OPEN V$ FOR INPUT AS FILE #2
280 BLOCK_MOVE(F1(0),R(0),256) \ CLOSE
290 V$='SY1:FFT'+STR$(J)+'I' \ OPEN V$ FOR INPUT AS FILE #2
300 BLOCK_MOVE(F1(0),I(0),256) \ CLOSE
310 FOR K=0 TO 255
320 R=R(K) \ I=I(K)
330 X=K*Z \ C=COS(X) \ S=SIN(X)
340 REM  **  DIV BY 2 HERE, THEN ADD 1 TO S% IN 770-780  **
350 R(K)=(R*C-I*S)/2 \ I(K)=(I*C+R*S)/2
360 NEXT K
370 V$='SY1:SFT'+STR$(J)+'R' \ OPEN V$ FOR OUTPUT AS FILE #2
380 BLOCK_MOVE(R(0),F1(0),256) \ CLOSE
390 V$='SY1:SFT'+STR$(J)+'I' \ OPEN V$ FOR OUTPUT AS FILE #2
400 BLOCK_MOVE(I(0),F1(0),256) \ CLOSE
410 NEXT J
420 PRINT 'SHIFT ';CLK$
430 REM  ************************************
440 REM  **  SUM COEFFICIENTS & REVERSE FFT  **
450 REM  ************************************
460 FOR K=0 TO 511 \ R(K)=0 \ I(K)=0 \ NEXT K
470 FOR J=A1 TO A2
480 V$='SY1:SFT'+STR$(J)+'R' \ OPEN V$ FOR INPUT AS FILE #2
490 BLOCK_MOVE(F1(0),W(0),256) \ CLOSE
```

```
500 FOR K=0 TO 255 \ R(K)=R(K)+W(K) \ NEXT K
530 V$='SY1:SFT'+STR$(J)+'I' \ OPEN V$ FOR INPUT AS FILE #2
540 BLOCK_MOVE(F1(0),W(0),256) \ CLOSE
550 FOR K=0 TO 255 \ I(K)=I(K)+W(K) \ NEXT K
560 NEXT J
570 FOR K=0 TO 255 \ R%(K)=R(K)/(A2-A1+1) \ I%(K)=I(K)/(A2-A1+1) \ NEXT K
680 REM  **  NOW FOLD COEFFICIENTS  **
690 FOR K=256 TO 511 \ R%(K)=R%(512-K) \ I%(K)=-I%(512-K) \ NEXT K
700 FOR K=0 TO 511 \ R(K)=R%(K) \ I(K)=I%(K) \ NEXT K
710 V$='SY1:CF'+I$+'R' \ OPEN V$ FOR OUTPUT AS FILE #2
720 BLOCK_MOVE(R(0),F1(0),512) \ CLOSE
730 V$='SY1:CF'+I$+'I' \ OPEN V$ FOR OUTPUT AS FILE #2
740 BLOCK_MOVE(I(0),F1(0),512) \ CLOSE
745 GOSUB 1000
750 FFT('REVERSE',512,R%(0),I%(0),S1%)
760 REM  **  SEE 340 ABOVE  **
770 FOR K=0 TO 511 \ R(K)=R%(K)*(2^(S1%+1))/512
780 I(K)=I%(K)*(2^(S1%+1))/512/1000 \ NEXT K
790 OPEN 'SY1:RESULT' FOR OUTPUT AS FILE #2
800 BLOCK_MOVE(R(0),F1(0),512) \ CLOSE
830 PRINT 'PHASE ';CLK$
840 CHAIN 'SY0:GRAPH'
1000 REM  *************************
1010 REM  **  POWER CALCULATIONS  **
1020 REM  *************************
1030 IF P$='N' THEN RETURN
1040 POWER(256,R%(),I%(),T())
1050 FOR K=0 TO 255 \ T(K)=SQR(T(K))*2 \ NEXT K
1060 OPEN 'SY1:PWRF' FOR OUTPUT AS FILE #2
1070 BLOCK_MOVE(T(0),F1(0),256) \ CLOSE  \ RETURN
```

GRAPH - Part 5

This is for data display and output. It produces graphs and peak-to-peak amplitudes for the raw, average, and final data, Fourier coefficients, and power spectrum. It also calculates the total power within a selected frequency range.

```
100 REM  **  GRAPH  **
110 REM  **************************************************
120 REM  **  SYNTHETIC APERTURE BY PHASE SHIFT - PART 5  **
130 REM  **************************************************
140 REM  *************************
150 REM  **  GRAPHICAL DISPLAY  **
160 REM  *************************
170 COMMON P(20),I$,P$,A1,A2
175 DIM R(511),X(511) \ DIM #2,F1(511) \ DIM #3,F$(4)=255
180 OPEN 'SY1:ID' FOR INPUT AS FILE #3 \ J$=F$(0)
184 K$='***********************************' \ PRINT  \ PRINT
185 PRINT K$ \ PRINT 'All calculated files done on ';J$ \ PRINT K$
187 FOR K=1 TO 4 \ J$=F$(K) \ PRINT J$ \ NEXT K \ CLOSE
190 PRINT  \ PRINT  \ PRINT  \ PRINT
200 L3$=''
210 PRINT 'Display choice:'
220 PRINT '   1. RAW DATA          2. COEFFICIENTS or POWER'
230 PRINT '   3. AVERAGE DATA      4. FINAL DATA'
240 PRINT '   5. INTEGRATE POWER   6. TERMINATE  ';
250 GET_CHAR(A$)
260 IF A$='2' THEN 6200
270 IF A$='3' THEN 360
280 IF A$='4' THEN 380
```

```
300 IF A$='5' THEN 7000
305 IF A$='6' THEN 8000
310 IF A$<>'1' THEN 250
320 DISPLAY_CLEAR \ L3$='RAW DATA' \ PRINT  \ PRINT L3$
330 PRINT 'Which INDIVIDUAL RUN (of ';P(0);')';
340 INPUT I \ L3$=L3$+'  #'+STR$(I)
350 V$='SY1:'+I$+STR$(I) \ GO TO 470
360 DISPLAY_CLEAR \ L3$='AVERAGE DATA' \ PRINT  \ PRINT L3$
370 V$='SY1:AVG' \ GO TO 470
380 DISPLAY_CLEAR \ L3$='FINAL DATA' \ PRINT  \ PRINT L3$
390 V$='SY1:RESULT' \ GO TO 470
400 PRINT 'REAL or IMAGINARY? (R or I)  ';
410 GET_CHAR(C$) \ IF C$='R' THEN 440
430 IF C$<>'I' THEN 410
440 PRINT  \ V$=V$+C$
450 IF C$='I' THEN L3$=L3$+' IMAG'
460 IF C$='R' THEN L3$=L3$+' REAL'
470 OPEN V$ FOR INPUT AS FILE #2
480 BLOCK_MOVE(F1(0),R(0),512) \ CLOSE
500 PRINT 'Do you want to SCALE COORDINATES? (Y or N)  ';
510 GET_CHAR(S$) \ IF S$='N' THEN 580
530 IF S$<>'Y' THEN 510
540 PRINT  \ PRINT 'X MIN = '; \ INPUT X1
550 PRINT 'X MAX = '; \ INPUT X2
560 PRINT 'Y MIN = '; \ INPUT Y1
570 PRINT 'Y MAX = '; \ INPUT Y2
580 PRINT  \ GOSUB 4000 \ GOSUB 5000 \ GO TO 190
4000 REM  *******************************************
4010 REM  **  CALCULATE X's, GRAPH LIMITS, LABELS  **
4020 REM  *******************************************
4030 IF A$='2' THEN 4240
4040 FOR K=0 TO 511 \ X(K)=K*P(11) \ NEXT K
4044 FOR K=0 TO 511 \ R(K)=R(K)*P(15) \ NEXT K
4050 IF P(18)=1 THEN L2$='KILOVOLTS'
4060 IF P(18)=2 THEN L2$='VOLTS'
4070 IF P(18)=3 THEN L2$='MILLIVOLTS'
4080 IF P(14)=3 THEN L1$='10^3 SECONDS'
4090 IF P(14)=0 THEN L1$='SECONDS'
4100 IF P(14)=-3 THEN L1$='MILLISECONDS'
4110 IF P(14)=-6 THEN L1$='MICROSECONDS'
4112 IF S$='Y' THEN 4170
4120 IF A$='1' THEN 4140
4130 IF A$<>'3' THEN 4150
4140 Y1=0 \ Y2=300*P(15) \ GO TO 4160
4150 Y1=-150*P(15) \ Y2=-Y1 \ REM  **  FOR A$= 4 & 5  **
4160 X1=0 \ X2=600*P(11)
4170 X1$=STR$(X1) \ X2$=STR$(X1+(X2-X1)/4)
4180 X3$=STR$(X1+(X2-X1)/2) \ X4$=STR$(X1+3*(X2-X1)/4)
4190 Y1$=STR$(Y1) \ Y2$=STR$(Y1+(Y2-Y1)/4) \ Y3$=STR$(Y1+(Y2-Y1)/2)
4200 Y4$=STR$(Y1+3*(Y2-Y1)/4) \ Y5$=STR$(Y2)
4210 WINDOW("EXACT",X1,Y1,X2,Y2)
4220 GRAPH(,512,X(0),R(0))
4230 GO TO 4340
4240 FOR K=0 TO 511 \ X(K)=K/512/P(11) \ NEXT K
4250 IF P$='N' THEN L2$='COEFFICIENTS' \ GO TO 4260
4252 IF B$='C' THEN L2$='COEFFICIENTS' \ GO TO 4260
4254 L2$='POWER'
4260 IF P(14)=3 THEN L1$='FREQUENCY, mHz'
4270 IF P(14)=0 THEN L1$='FREQUENCY, Hz'
4280 IF P(14)=-3 THEN L1$='FREQUENCY, kHz'
4290 IF P(14)=-6 THEN L1$='FREQUENCY, MHz'
4300 IF S$='Y' THEN 4170
4310 X1=0 \ X2=250/500/P(11)
4320 X1$='0' \ X2$=STR$(X2/4) \ X3$=STR$(X2/2) \ X4$=STR$(3*X2/4)
4330 GRAPH(,256,X(0),R(0))
4340 PRINT  \ PRINT 'Do you want to calculate the MAXIMUM, MINIMUM, and';
4350 PRINT ' SPAN of the graph?  ';
4360 GET_CHAR(H$) \ IF H$='N' THEN PRINT  \ RETURN
4380 IF H$<>'Y' THEN 4360
```

```
4390 PRINT  \ PRINT 'Within what RANGE?'
4400 PRINT 'MINIMUM X is '; \ INPUT X3
4410 PRINT 'MAXIMUM X is '; \ INPUT X4
4420 REM    Y3 IS MINIMUM Y, Y4 IS MAXIMUM Y
4430 Y3=R(0) \ Y4=R(0) \ I=0
4440 IF X(I)<X3 THEN I=I+1 \ GO TO 4440
4450 IF X(I)>X4 THEN 4490
4460 IF R(I)<Y3 THEN Y3=R(I)
4470 IF R(I)>Y4 THEN Y4=R(I)
4480 I=I+1 \ GO TO 4450
4490 PRINT CHR$(27),'[5i'
4492 PRINT I$ \ PRINT L3$ \ PRINT
4497 PRINT 'Between ';X3;' and ';X4;' ';L1$
4500 PRINT 'The MINIMUM VALUE is ';Y3
4510 PRINT 'The MAXIMUM VALUE is ';Y4
4530 PRINT 'The SPAN is ';Y4-Y3 \ PRINT CHR$(27),'[4i' \ RETURN
5000 REM  SUBROUTINE TO ADD UNITS AND AXIS LABELS TO GRAPHICS
5010 REM
5020 REM  **** THE LABELS FOR THE X-AXIS AND Y-AXIS MUST BE PASSED TO THIS
5030 REM       ROUTINE VIA:
5040 REM
5050 REM                X-AXIS -- L1$
5060 REM                Y-AXIS -- L2$
5070 REM
5080 B$=CHR$(27)+'P1p'
5090 E$=CHR$(27)+'\'
5100 K$='S(A[0,479][767,0])'
5110 PRINT B$+K$+E$
5120 PRINT B$+'P[51,479]V[]V[51,101]P[711,479]V[]V[711,101]'+E$
5130 IF A$<>'2' THEN 5250
5140 IF S$='Y' THEN 5250
5190 PRINT  \ PRINT 'TYPE IN THE Y-ORIGIN AND Y-MAX UNITS'
5200 PRINT 'LIMIT EACH ENTRY TO FIVE CHARACTERS INCLUDING DECIMAL POINT.'
5210 PRINT  \ PRINT 'ORIGIN   '; \ INPUT Y1
5220 PRINT 'MAX      '; \ INPUT Y2
5230 Y1$=STR$(Y1) \ Y2$=STR$(Y1+(Y2-Y1)/4) \ Y3$=STR$(Y1+(Y2-Y1)/2)
5240 Y4$=STR$(Y1+3*(Y2-Y1)/4) \ Y5$=STR$(Y2)
5250 L1=LEN(L1$) \ T1%=385-L1/2*20
5260 L2=LEN(L2$) \ T2%=294-L2/2*20
5270 ERASE_TEXT
5280 PRINT B$+'T(S[9,15])'+E$;
5290 PRINT B$+"P[0,479]T'"+Y5$+"'"+E$;
5300 PRINT B$+"P[0,389]T'"+Y4$+"'"+E$;
5310 PRINT B$+"P[0,299]T'"+Y3$+"'"+E$;
5320 PRINT B$+"P[0,209]T'"+Y2$+"'"+E$;
5330 PRINT B$+"P[0,119]T'"+Y1$+"'"+E$;
5340 \
5350 PRINT B$+"P[70,97]T'"+X1$+"'"+E$;
5360 PRINT B$+"P[228,97]T'"+X2$+"'"+E$;
5370 PRINT B$+"P[388,97]T'"+X3$+"'"+E$;
5380 PRINT B$+"P[548,97]T'"+X4$+"'"+E$;
5390 \
5400 PRINT B$+"P["+STR$(T1%)+",69]T[+20,+0](D0S2S2H2)'"+L1$+"'"+E$;
5410 PRINT B$+"P[716,"+STR$(T2%)+"]T[+0,+20](D90S2S2H2)'"+L2$+"'"+E$;
5420 \
5430 PRINT B$+'T[+9,+0](S1,H2,S[9,20],M[1,2],D0,I0)'+E$
5450 PRINT 'Do you want to make a HARD COPY? (Y or N)  ';
5460 GET_CHAR(V$) \ IF V$='N' THEN RETURN
5480 IF V$<>'Y' THEN 5460
5490 PRINT  \ PRINT CHR$(27),'[5i' \ PRINT  \ PRINT I$ \ PRINT L3$
5500 PRINT  \ PRINT  \ PRINT CHR$(27),'[4i'
5510 DISPLAY_COPY
5550 RETURN
6200 REM  ***************************
6210 REM  **  HANDLE COEFFICIENTS  **
6220 REM  ***************************
6225 DISPLAY_CLEAR
6230 PRINT  \ IF P$='N' THEN 6290
6240 PRINT 'COEFFICIENTS or POWER? (C or P) ';
```

```
6250 GET_CHAR(B$) \ IF B$='C' THEN 6290
6260 IF B$<>'P' THEN 6250
6270 PRINT  \ PRINT  \ L3$='POWER' \ PRINT  \ PRINT L3$
6280 GOSUB 6500 \ GO TO 470
6290 PRINT  \ L3$=' COEFFICIENTS' \ PRINT  \ PRINT L3$
6300 PRINT 'RAW, SHIFTED, or FINAL? (R, S, or F) ';
6310 GET_CHAR(C$) \ IF C$='R' THEN 6360
6320 IF C$='S' THEN 6350
6330 IF C$<>'F' THEN 6310
6340 PRINT  \ V$='SY1:CF'+I$ \ L3$='FINAL'+L3$ \ GO TO 6380
6350 PRINT  \ V$='SY1:SFT' \ L3$='SHIFTED'+L3$ \ GO TO 6370
6360 PRINT  \ V$='SY1:FFT' \ L3$='RAW'+L3$
6370 GOSUB 6600
6380 PRINT 'REAL or IMAGINARY? (R or I) ';
6390 GET_CHAR(C$) \ IF C$='R' THEN 6410
6400 IF C$<>'I' THEN 6390
6410 PRINT  \ V$=V$+C$
6420 IF C$='I' THEN L3$=L3$+' IMAG'
6430 IF C$='R' THEN L3$=L3$+' REAL'
6440 GO TO 470
6500 PRINT 'INDIVIDUAL or FINAL? (I or F) ';
6510 GET_CHAR(C$) \ IF C$='I' THEN  GOSUB 6600 \ RETURN
6520 IF C$<>'F' THEN 6510
6530 V$='SY1:PWRF' \ L3$=L3$+' FINAL' \ PRINT  \ RETURN
6600 PRINT  \ PRINT 'Which INDIVIDUAL RUN (of ';P(0);')';
6610 INPUT I \ L3$=L3$+' - #'+STR$(I)
6615 IF B$='C' THEN V$=V$+STR$(I) \ RETURN
6620 V$='SY1:PWR'+STR$(I) \ RETURN
7000 REM *************************
7010 REM **  POWER INTEGRATION  **
7020 REM *************************
7030 F0=0 \ F2=0 \ A$="" \ B$=""
7050 PRINT  \ PRINT 'INTEGRATED POWER'
7060 PRINT 'INDIVIDUAL OR FINAL (I or F)  ';
7070 GET_CHAR(A$) \ IF A$='F' THEN 7100
7080 IF A$<>'I' THEN 7070
7090 PRINT  \ PRINT 'Which INDIVIDUAL RUN (of ';P(0);')'; \ INPUT I
7100 IF P(14)=3 THEN L1$='mHz'
7110 IF P(14)=0 THEN L1$='Hz'
7120 IF P(14)=-3 THEN L1$='kHz'
7130 IF P(14)=-6 THEN L1$='MHz'
7140 PRINT  \ PRINT 'What are the LIMITING FREQUENCIES, in ';L1$;'?'
7150 PRINT 'STARTING FREQUENCY'; \ INPUT F0
7160 PRINT 'FINAL FREQUENCY'; \ INPUT F2
7170 K1=F0*512*P(11) \ K2=F2*512*P(11)
7180 IF A$='I' THEN 7200
7190 V$='SY1:PWRF' \ GO TO 7210
7200 V$='SY1:PWR'+STR$(I)
7210 OPEN V$ FOR INPUT AS FILE #2 \ BLOCK_MOVE(F1(0),X(0),256) \ CLOSE
7220 FOR K=K1 TO K2 \ P0=P0+X(K) \ NEXT K
7230 PRINT CHR$(27),'[5i' \ PRINT
7240 IF A$='I' THEN 7260
7250 PRINT  \ PRINT 'The FINAL INTEGRATED POWER for ';I$;' is ';P0; \ GO TO 7270
7260 PRINT  \ PRINT 'The INTEGRATED POWER for position #';I;' is ';P0;
7270 PRINT ' between ';F0;' and ';F2;L1$
7280 PRINT  \ PRINT CHR$(27),'[4i'
7290 GO TO 190
8000 DISPLAY_CLEAR \ END
```

Appendix II

SOFTWARE SAMPLE RUN

The following represents a typical session of data collection, analysis, and output. All keyboard entries are circled, and printer output is delineated by the square brackets ([). All other prompts and information appear on the screen of the video display terminal (VDT). Those entries marked by * are used for information recording only and do not enter into any calculations. Other entries are used for decision making, scanner control, and data processing.

```
RUN SYN
NEW or OLD DATA? (N or O) N
Are you going to USE THE SCANNER SYSTEM? (Y or N) Y

IDENTIFICATION (2 CHAR MAX) = ?YZ
* DATE: ?9-6-83
* TRANSDUCERS: ?GIMBAL
* PRF = ?999
* NUMBER OF CYCLES = ?4
  NOTES:  2 LINES AVAILABLE
  LINE 1:
* ?THIS IS A SAMPLE PRINTOUT
  LINE 2:
* ?EDM NOTCH ON SAME SIDE OF PLATE AS EMATS

  NUMBER OF TRANSDUCER POSITIONS = ?5
  NUMBER OF SCAN SETS = ?1

  DISTANCES IN MM:
     BETWEEN POSITIONS = ?2
     BETWEEN TRANSMITTER & RECEIVER = ?32.5
     PLATE THICKNESS = ?25
     FOCAL SPOT LOCATION:
       HORIZONTAL (from initial transmitter position) = ?40
       VERTICAL DEPTH (from transducer side) = ?0

  # OF REFLECTIONS IN ACOUSTIC PATH = ?0

  FORWARD OR BACKWARD SHIFT? (F OR B) FORWARD

* FREQUENCY (KHZ) = ?454

  SOUND VELOCITY (KM/SEC) = ?3.2

* NUMBER OF AVERAGES DONE ON SCOPE = ?16
```

```
Do you want a HARD COPY OF THE PARAMETER LIST? (Y or N) Y
ID:  YZ

9-6-83
TRANSDUCERS: GIMBAL
PRF = 999
4 CYCLES
THIS IS A SAMPLE PRINTOUT
EDM NOTCH ON SAME SIDE OF PLATE AS EMATS

 1   SCAN SETS
 5   TRANSDUCER POSITIONS
 2   MM BETWEEN POSITIONS
 32.5   MM BETWEEN TRANSMITTER & RECEIVER
 25   MM PLATE THICKNESS
FOCAL SPOT LOCATION:
   40   MM HORIZONTAL (from initial transmitter position)
    0   MM VERTICAL DEPTH (from transducer side)
 0   REFLECTIONS IN ACOUSTIC PATH
FORWARD SHIFT
 454   KHZ FREQUENCY
 3.2   KM/SEC SOUND VELOCITY
 16   AVERAGES DONE ON SCOPE

Do you want to INITIALIZE TRANSDUCER POSITION? (Y or N) Y
When system is READY push "R" R
X or Y coordinate: X
DIRECTION? (+ OR -) -
MM OF TRAVEL = ? 18
Push "E" to EXECUTE E
Do you want to MOVE FURTHER? (Y or N) N
Press "E" to begin EXECUTION E


Scan  1  of  1  at  0  mm
Collecting position  1  of  5  at  0  mm
Collecting position  2  of  5  at  2  mm
Collecting position  3  of  5  at  4  mm
Collecting position  4  of  5  at  6  mm
Collecting position  5  of  5  at  8  mm


Window choice:
   1. NONE
   2. BARTLETT
   3. HANNING
1
Perform calculations on WHICH POSITIONS? (1 to  5 )
Start with position # ? 1
  End with position # ? 5


Do you want to SUBTRACT THE AVERAGE? (Y or N) Y
Do you want to CALCULATE POWER SPECTRUM? (Y or N) Y


I'M THINKING ABOUT YOUR PROBLEM NOW!
START 14:13:27
AVG   14:13:58
FFT   14:15:20
SHIFT 14:16:24
PHASE 14:17:20
```

```
**********************************
All calculated files done on YZ1
**********************************
NO WINDOW
POSITIONS #1 TO #5
AVERAGE SUBTRACTED
POWER CALCULATIONS DONE

Display choice:
   1. RAW DATA           2. COEFFICIENTS or POWER
   3. AVERAGE DATA       4. FINAL DATA
   5. INTEGRATE POWER    6. TERMINATE  1
RAW DATA
Which INDIVIDUAL RUN (of  5 )? 1
Do you want to SCALE COORDINATES? (Y or N)  N
```

(Data plotted on VDT)

```
Do you want to calculate the MAXIMUM, MINIMUM, and SPAN of the graph? Y
Within what RANGE?
MINIMUM X is ? 0
MAXIMUM X is ? 30

YZ1
RAW DATA  #1

Between  0  and  30  MICROSECONDS
The MINIMUM VALUE is  .172
The MAXIMUM VALUE is  .382
The SPAN is  .21

Do you want to make a HARD COPY? (Y or N)  Y
```

YZ1
RAW DATA #1

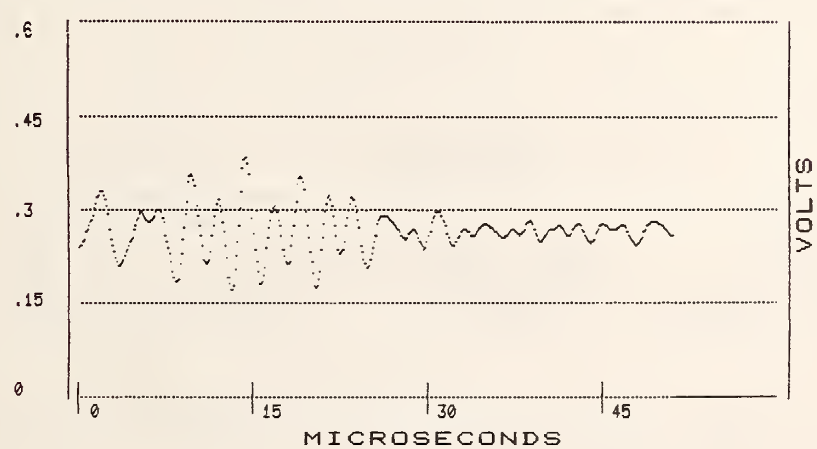

```
Display choice:
    1. RAW DATA           2. COEFFICIENTS or POWER
    3. AVERAGE DATA       4. FINAL DATA
    5. INTEGRATE POWER    6. TERMINATE  4
FINAL DATA
Do you want to SCALE COORDINATES? (Y or N)  N
```

(Data plotted on VDT)

```
Do you want to calculate the MAXIMUM, MINIMUM, and SPAN of the graph?  Y
Within what RANGE?
MINIMUM X is ? 0
MAXIMUM X is ? 30
```

```
YZ1
FINAL DATA

Between  0  and  30  MICROSECONDS
The MINIMUM VALUE is -.0777266
The MAXIMUM VALUE is  .0753516
The SPAN is  .153078
```

```
Do you want to make a HARD COPY? (Y or N)  Y
```

```
YZ1
FINAL DATA
```

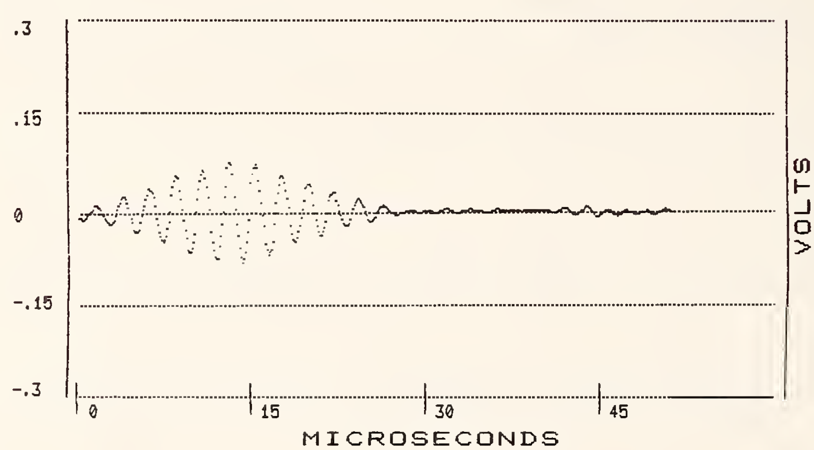


```
Display choice:
    1. RAW DATA           2. COEFFICIENTS or POWER
    3. AVERAGE DATA       4. FINAL DATA
    5. INTEGRATE POWER    6. TERMINATE  2
COEFFICIENTS or POWER? (C or P) P


POWER
INDIVIDUAL or FINAL? (I or F) F
Do you want to SCALE COORDINATES? (Y or N)  N
```

(Data plotted on VDT)

```
Do you want to calculate the MAXIMUM, MINIMUM, and SPAN of the graph? Y
Within what RANGE?
MINIMUM X is ?0
MAXIMUM X is ?1

YZ1
POWER FINAL

Between  0  and  1  FREQUENCY, MHz
The MINIMUM VALUE is  0
The MAXIMUM VALUE is  2709.79
The SPAN is  2709.79

TYPE IN THE Y-ORIGIN AND Y-MAX UNITS
LIMIT EACH ENTRY TO FIVE CHARACTERS INCLUDING DECIMAL POINT.

ORIGIN  ?0
MAX     ?3000

Do you want to make a HARD COPY? (Y or N)  Y

YZ1
POWER FINAL
```

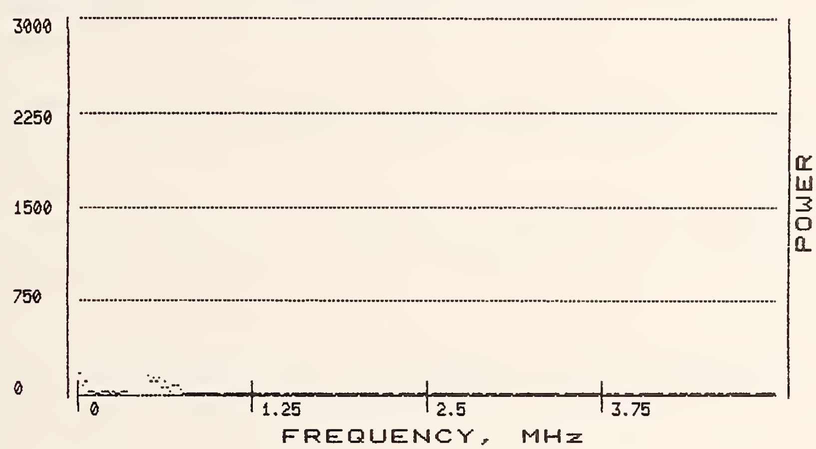


```
Display choice:
   1. RAW DATA           2. COEFFICIENTS or POWER
   3. AVERAGE DATA       4. FINAL DATA
   5. INTEGRATE POWER    6. TERMINATE  5
INTEGRATED POWER
INDIVIDUAL OR FINAL (I or F)  F
What are the LIMITING FREQUENCIES, in MHz?
STARTING FREQUENCY?0
FINAL FREQUENCY?1

The FINAL INTEGRATED POWER for YZ1 is  11627.9  between  0  and  1 MHz
```

APPENDIX III

TECHNICAL PAPERS RESULTING FROM THIS PROGRAM

Several papers based on various aspects of this work or using equipment and ideas developed in the course of the program have been published.

Fortunko, C. M., and Schramm, R. E., 1983, An analysis of electromagnetic-acoustic transducer arrays for nondestructive evaluation of thick metal sections and weldments, in: "Review of Progress in Quantitative Nondestruction Evaluation, Vol. 2A," D. O. Thompson and D. E. Chimenti, eds., Plenum Press, New York, p. 283.

King, R. B., and Fortunko, C. M., 1983, Evaluation of residual stress states using horizontally polarized shear waves, in: "Review of Progress in Quantitative Nondestructive Evaluation, Vol. 2B," D. O. Thompson and D. E. Chimenti, eds., Plenum Press, New York, p. 1327.

King, R. B., and Fortunko, C. M., 1983, Determination of in-plane residual stress states in plates using horizontally polarized shear waves, J. Appl. Phys., 54:3027.

King, R. B., and Fortunko, C. M., 1983, Acoustoelastic evaluation of arbitrary plane residual stress states in non-homogeneous, anisotropic plates, Ultrasonics 21:256.

King, R. B., and Fortunko, C. M., 1984, Evaluation of surface residual stresses using horizontally polarized shear waves at grazing incidence, to be published in J. Appl. Phys.

Schramm, R. E., Fortunko, C. M., and Moulder, J. C., 1984, Advanced methods for noncontact inspection of welds using electromagnetic-acoustic transducers, submitted to: "Review of Progress in Quantitative Nondestructive Evaluation, Vol. 3," D. O. Thompson and D. E. Chimenti, eds., Plenum Press, New York.

Schramm, R. E., Moulder, J. C., and Fortunko, C. M., 1984, Nondestructive evaluation of thick austenitic stainless steel weldments by shear horizontal acoustic waves, in: "Advances in Cryogenic Engineering, Vol. 30," A. F. Clark and R. P. Reed, eds., Plenum Press, New York, p. 119.

APPENDIX IV

ACKNOWLEDGMENTS

The authors are grateful for the sponsorship of the U.S. Department of Defense, Department of the Navy, Naval Sea Systems Command through the Energy and Minerals Resources Research Institute, Ames Laboratory, Iowa State University. We wish especially to thank our Navy monitor, Dr. Hans Vanderveldt, for his thoughtful interest.

Many people in our laboratory have contributed to various aspects of this work and we wish to acknowledge their considerable efforts. Dr. Richard King provided insights into the vagaries of ultrasonic propagation and diffraction. Earl Ballinger, Dave Brannon, Al Bennett, Jim Newman, and Shelly Dalton aided in various parts of equipment design and construction or testing and data collection. Nick Sanchez managed to make our artwork intelligible and readable. Diane Shields, JoAnne Wilken, and Peggy Vigliotti led us through the myraid administrative details and survived our many text revisions. To all these, and yet more, we offer our gratitude and thanks.

NBS-114A (REV. 2-80)

U.S. DEPT. OF COMM. **BIBLIOGRAPHIC DATA SHEET** *(See instructions)*	1. PUBLICATION OR REPORT NO. NBS TN-1075	2. Performing Organ. Report No.	3. Publication Date May 1984

4. TITLE AND SUBTITLE

Electromagnetic-Acoustic-Transducer/Synthetic-Aperture System for Thick-Weld Inspection

5. AUTHOR(S)

C. M. Fortunko, R. E. Schramm, J. C. Moulder, J. D. McColskey

6. PERFORMING ORGANIZATION *(If joint or other than NBS, see instructions)*

NATIONAL BUREAU OF STANDARDS
DEPARTMENT OF COMMERCE
WASHINGTON, D.C. 20234

7. Contract/Grant No. A1-4572 A2-1699, SC-83-051

8. Type of Report & Period Covered Final 7-1-81 to 12-31-83

9. SPONSORING ORGANIZATION NAME AND COMPLETE ADDRESS *(Street, City, State, ZIP)*

Ames Laboratory
Energy & Mineral Resources Research Institute
Iowa State University
Ames, Iowa 50011

10. SUPPLEMENTARY NOTES

☐ Document describes a computer program; SF-185, FIPS Software Summary, is attached.

11. ABSTRACT *(A 200-word or less factual summary of most significant information. If document includes a significant bibliography or literature survey, mention it here)*

This report describes a system based on electromagnetic-acoustic transducers (EMATs) as an approach to automated nondestructive evaluation of thick weldments ($\geq$25 mm). Good signal-to-noise ratios, often a problem with EMATs, were possible through careful design of the transducers and associated electronic circuits and the use of signal averaging. At 454 kHz, the transducers produce shear-horizontal waves of approximately 7-mm wavelength in steel. The long wavelength permits determination of through-thickness flaw depth from the amplitudes of scattered ultrasonic waves. A minicomputer controlled transducer positioning and acquired the digitized ultrasonic waveforms for synthetic aperture processing. The synthetic aperture technique further improved signal quality and yielded flaw localization through the weld thickness. Measurements on artificial flaws demonstrated a detectability threshold of 0.5 mm (through thickness) and sizing ability up to 2.5 mm, in agreement with theoretical predictions. Details include the design of the transducers and electronics, as well as the mechanical positioner, signal processing algorithms, and complete computer program listings.

12. KEY WORDS *(Six to twelve entries; alphabetical order; capitalize only proper names; and separate key words by semicolons)*

electromagnetic-acoustic transducer; flaw detection; nondestructive evaluation; S-H waves; synthetic aperture; ultrasonics; weld inspection

13. AVAILABILITY

[X] Unlimited
☐ For Official Distribution. Do Not Release to NTIS
[X] Order From Superintendent of Documents, U.S. Government Printing Office, Washington, D.C. 20402.
☐ Order From National Technical Information Service (NTIS), Springfield, VA. 22161

14. NO. OF PRINTED PAGES 130

15. Price

U.S. GOVERNMENT PRINTING OFFICE: 1984—779-422 9337 REGION NO. 8

NBS TECHNICAL PUBLICATIONS

PERIODICALS

JOURNAL OF RESEARCH—The Journal of Research of the National Bureau of Standards reports NBS research and development in those disciplines of the physical and engineering sciences in which the Bureau is active. These include physics, chemistry, engineering, mathematics, and computer sciences. Papers cover a broad range of subjects, with major emphasis on measurement methodology and the basic technology underlying standardization. Also included from time to time are survey articles on topics closely related to the Bureau's technical and scientific programs. As a special service to subscribers each issue contains complete citations to all recent Bureau publications in both NBS and non-NBS media. Issued six times a year. Annual subscription: domestic $18; foreign $22.50. Single copy, $5.50 domestic; $6.90 foreign.

NONPERIODICALS

Monographs—Major contributions to the technical literature on various subjects related to the Bureau's scientific and technical activities.

Handbooks—Recommended codes of engineering and industrial practice (including safety codes) developed in cooperation with interested industries, professional organizations, and regulatory bodies.

Special Publications—Include proceedings of conferences sponsored by NBS, NBS annual reports, and other special publications appropriate to this grouping such as wall charts, pocket cards, and bibliographies.

Applied Mathematics Series—Mathematical tables, manuals, and studies of special interest to physicists, engineers, chemists, biologists, mathematicians, computer programmers, and others engaged in scientific and technical work.

National Standard Reference Data Series—Provides quantitative data on the physical and chemical properties of materials, compiled from the world's literature and critically evaluated. Developed under a worldwide program coordinated by NBS under the authority of the National Standard Data Act (Public Law 90-396).

NOTE: The principal publication outlet for the foregoing data is the Journal of Physical and Chemical Reference Data (JPCRD) published quarterly for NBS by the American Chemical Society (ACS) and the American Institute of Physics (AIP). Subscriptions, reprints, and supplements available from ACS, 1155 Sixteenth St., NW, Washington, DC 20056.

Building Science Series—Disseminates technical information developed at the Bureau on building materials, components, systems, and whole structures. The series presents research results, test methods, and performance criteria related to the structural and environmental functions and the durability and safety characteristics of building elements and systems.

Technical Notes—Studies or reports which are complete in themselves but restrictive in their treatment of a subject. Analogous to monographs but not so comprehensive in scope or definitive in treatment of the subject area. Often serve as a vehicle for final reports of work performed at NBS under the sponsorship of other government agencies.

Voluntary Product Standards—Developed under procedures published by the Department of Commerce in Part 10, Title 15, of the Code of Federal Regulations. The standards establish nationally recognized requirements for products, and provide all concerned interests with a basis for common understanding of the characteristics of the products. NBS administers this program as a supplement to the activities of the private sector standardizing organizations.

Consumer Information Series—Practical information, based on NBS research and experience, covering areas of interest to the consumer. Easily understandable language and illustrations provide useful background knowledge for shopping in today's technological marketplace.

Order the **above** *NBS publications from: Superintendent of Documents, Government Printing Office, Washington, DC 20402.*

Order the **following** *NBS publications—FIPS and NBSIR's—from the National Technical Information Service, Springfield, VA 22161.*

Federal Information Processing Standards Publications (FIPS PUB)—Publications in this series collectively constitute the Federal Information Processing Standards Register. The Register serves as the official source of information in the Federal Government regarding standards issued by NBS pursuant to the Federal Property and Administrative Services Act of 1949 as amended, Public Law 89-306 (79 Stat. 1127), and as implemented by Executive Order 11717 (38 FR 12315, dated May 11, 1973) and Part 6 of Title 15 CFR (Code of Federal Regulations).

NBS Interagency Reports (NBSIR)—A special series of interim or final reports on work performed by NBS for outside sponsors (both government and non-government). In general, initial distribution is handled by the sponsor; public distribution is by the National Technical Information Service, Springfield, VA 22161, in paper copy or microfiche form.

U.S. Department of Commerce
National Bureau of Standards

Washington, D.C. 20234
Official Business
Penalty for Private Use $300

U.S.MAIL

POSTAGE AND FEES PAID
U S DEPARTMENT OF COMMERCE
COM-215

SPECIAL FOURTH-CLASS RATE
BOOK